NASA
SPACE VEHICLE
DESIGN CRITERIA
(CHEMICAL PROPULSION)

NASA SP-8073

SOLID PROPELLANT GRAIN

STRUCTURAL INTEGRITY ANALYSIS
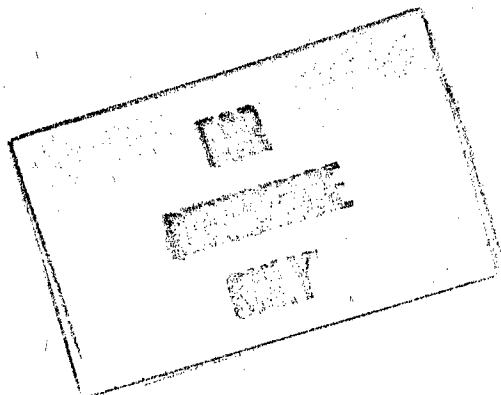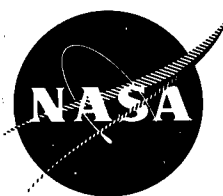
JUNE 1973

NATIONAL AERONAUTICS AND SPACE ADMINISTRATION

FOREWORD

NASA experience has indicated a need for uniform criteria for the design of space vehicles. Accordingly, criteria are being developed in the following areas of technology:

> Environment
> Structures
> Guidance and Control
> Chemical Propulsion

Individual components of this work will be issued as separate monographs as soon as they are completed. This document, part of the series on Chemical Propulsion, is one such monograph. A list of all monographs issued prior to this one can be found on the final pages of this document.

These monographs are to be regarded as guides to design and not as NASA requirements, except as may be specified in formal project specifications. It is expected, however, that these documents, revised as experience may indicate to be desirable, eventually will provide uniform design practices for NASA space vehicles.

This monograph, "Solid Propellant Grain Structural Integrity Analysis," was prepared under the direction of Howard W. Douglass, Chief, Design Criteria Office, Lewis Research Center; project management was by John H. Collins, Jr. The monograph was written by Dr. James S. Noel of Rocketdyne-McGregor, Rockwell International Corporation, and was edited by Russell B. Keller, Jr., of Lewis. Dr. L. D. Webb of Texas A&M University prepared the monograph dossier. To assure technical accuracy of this document, scientists and engineers throughout the technical community participated in interviews, consultations, and critical review of the text. In particular, Dr. R. F. Landel of the Jet Propulsion Laboratory, California Institute of Technology; Prof. R. A. Schapery of Texas A&M University; R. L. Carroll of Lockheed Propulsion Co., Lockheed Aircraft Corporation; and R. H. Wall of Thiokol Chemical Corporation reviewed the monograph in detail.

Comments concerning the technical content of this monograph will be welcomed by the National Aeronautics and Space Administration, Lewis Research Center (Design Criteria Office), Cleveland, Ohio 44135.

June 1973

GUIDE TO THE USE OF THIS MONOGRAPH

The purpose of this monograph is to organize and present, for effective use in design, the significant experience and knowledge accumulated in development and operational programs to date. It reviews and assesses current design practices, and from them establishes firm guidance for achieving greater consistency in design, increased reliability in the end product, and greater efficiency in the design effort. The monograph is organized into two major sections that are preceded by a brief introduction and complemented by a set of references.

The State of the Art, section 2, reviews and discusses the total design problem, and identifies which design elements are involved in successful design. It describes succinctly the current technology pertaining to these elements. When detailed information is required, the best available references are cited. This section serves as a survey of the subject that provides background material and prepares a proper technological base for the *Design Criteria* and Recommended Practices.

The *Design Criteria*, shown in italics in section 3, state clearly and briefly what rule, guide, limitation, or standard must be imposed on each essential design element to assure successful design. The *Design Criteria* can serve effectively as a checklist of rules for the project manager to use in guiding a design or in assessing its adequacy.

The Recommended Practices, also in section 3, state how to satisfy each of the criteria. Whenever possible, the best procedure is described; when this cannot be done concisely, appropriate references are provided. The Recommended Practices, in conjunction with the *Design Criteria,* provide positive guidance to the practicing designer on how to achieve successful design.

Both sections have been organized into decimally numbered subsections so that the subjects within similarly numbered subsections correspond from section to section. The format for the Contents displays this continuity of subject in such a way that a particular aspect of design can be followed through both sections as a discrete subject.

The design criteria monograph is not intended to be a design handbook, a set of specifications, or a design manual. It is a summary and a systematic ordering of the large and loosely organized body of existing successful design techniques and practices. Its value and its merit should be judged on how effectively it makes that material available to and useful to the designer.

CONTENTS

LIST OF FIGURES

vii

LIST OF TABLES

SOLID PROPELLANT GRAIN STRUCTURAL INTEGRITY ANALYSIS

1. INTRODUCTION

Grain design for a solid propellant rocket motor frequently necessitates compromises among the conflicting requirements of ballistic performance, structural integrity, mission reliability, and geometric constraints. Consequently, there must be a coordinated exchange of information among several technical disciplines, with inevitable iterations and redesign before a satisfactory motor can be produced. The study of the structural properties of the propellant, its response to loads, and its resistance to failure is one of these vital disciplines. This study, the structural integrity analysis, may be repeated several times, each time to a different degree of scope, detail, and sophistication, before the grain design is complete. Every motor design program is different in the details and ordering of the activities that lead ultimately to a successful motor. The principles on which a structural integrity analysis is performed, however, are independent of the specific application. The formulation and statement of these principles in a form useful to the designer and analyst is the subject of this monograph.

From the time a solid propellant rocket grain is cast until it has burned away in the performance of its mission, it is subjected to an array of stress-inducing environments: the continuing forces of gravity, loads arising from propellant curing and temperature excursion, shocks and vibrations due to handling and captive flight, and finally the pressurizations and accelerations that accompany ignition, launch, and flight. Characteristically, these loads induce displacements, strains, and stresses in the grain and may cause generation of internal heat. If the loading condition is severe, it can lead to catastrophic cracking, debonding, creep, or autoignition. Ballistic performance is dependent on grain geometry, and excessive dimensional changes (especially changes in the burning surface area) usually mean that specified motor performance and vehicle mission objectives cannot be achieved. Restraint to grain dilatation and distortion provided by the motor case or other supporting structure is a major parameter available to change the propellant response to loads. Either the amount of surface area or the stiffness of the restraint may be varied. Optimum resolution of the conflicting requirements for inertial and pressurization loads (severe constraint) and those for thermally induced loads (moderate constraint) is the task of the designer. The structural integrity analysis provides the insight and quantitative substantiations for this resolution. Successful grain design, therefore, depends upon a comprehensive assessment of the grain's structural integrity in close coordination with the other members of the design team.

For this assessment, the analyst must take the prescribed (or expected) environments, sometimes singly but usually in combination, and calculate the temperatures, stresses, strains, and deformations that result. This calculation requires realistic values for the thermal and mechanical properties of the propellant. From these solutions, he determines, frequently on the basis of experience and judgment, the most severe environments and the corresponding critical locations within the grain. A failure analysis must be performed for each critical condition. For this analysis to be significant, the failure properties of the propellant must be known.

Evaluation of the structural integrity of a solid propellant grain is particularly difficult because the behavior of propellant material deviates from many of the assumptions inherent in conventional methods of analysis. These deviations arise from the strong time- and temperature-dependence of propellants, the high degree of structural constraints placed upon the nearly incompressible grains, and the lack of adequate instrumentation for meaningful sensing of structural responses. Thus, a much larger degree of uncertainty is associated with the predictions of propellant behavior than is the case with more conventional materials. This monograph recognizes the increased uncertainty by emphasizing the value of analogue and prototype testing and the beneficial use of intuitive problem sense developed by experience with propellant behavior.

2. STATE OF THE ART

The number of approaches to the detailed structural integrity analysis of a solid propellant grain is nearly as great as the number of practicing analysts. This variety is attributable to (1) the many kinds of loads and environments a propellant grain must survive, (2) the wide spectrum of mechanical and failure properties exhibited by the various propellants, (3) the differences among available test and computing facilities, and (4) the inability to demonstrate one approach as superior to another. Definition of a state-of-the-art procedure is further obscured by the personalized nature of the information exchanges and iterations that occur among the structural analyst, ballistician, chemist, and designer in a motor design program. Summary descriptions of useful concepts and techniques have been published and have proven historically to be of great help to the analyst. Such articles include the classical work of Williams, Blatz, and Schapery (ref. 1); the engineering-oriented report published by Lockheed Propulsion Co. (ref. 2); the more recent seminar notes by Hoekle (ref. 3); and the treatises on large solid rocket grain designs by Bollard and Dill (ref. 4) and by Leeming (ref. 5). Also, the parametric design curves in the appendix of the report on propellant properties published by Aerojet-General Corp. (ref. 6) and the continuously updated Solid Propellant Mechanical Behavior Manual (ref. 7) containing descriptions of many of the mechanical property tests are day-to-day references for most grain analysts. The most recent additions to this list of generally helpful literature is the exhaustive review and discussion in reference 8 and the review of measurement techniques in reference 9.

The analytical procedure described below, therefore, is only an example, at best; however, it provides an orderly basis for the discussions that follow. Four basic steps are included in a typical grain structural integrity analysis:

(1) Obtain grain case geometry, material characterizations, and specified environments and loads.
(2) Calculate mechanical states throughout the grain resulting from the cure process, environments, and loads.
(3) Select the potential failure sites and applicable failure criteria. Solve for margin of safety or probability the grain will survive to accomplish its mission.
(4) When appropriate, suggest courses of action available to the designer to improve structural reliability of the grain.

The analyst typically works within the constraints of a design load and test specification derived from the mission requirements and a propellant and grain case geometry dictated by ballistic and processing considerations. The structural integrity of the grain is a later, though not necessarily secondary, consideration. Usually, the variety of modifications available for improving the structural reliability of a grain is limited by conflicting requirements. Possible alternatives and their relative effectiveness often are apparent after the analyses of steps (2) and (3) have been performed. Because of the difficulties caused by the variations in the behavior of propellant from that assumed for analyses, however, an alternate approach often

is used to replace steps (2) and (3), particularly in the final design stages when only slight additional changes in configuration are expected. This alternative is to build and test representative motor models (either full-scale or subscale) carefully instrumented to monitor stresses (forces), strains, displacements, and temperatures. The resulting data can then be used to adjust or correct the calculated solutions of step (2), thus increasing their accuracy and usefulness for further analyses. Similarly, the test motor can be subjected to loads or environments severe enough to cause failure, a procedure that provides the information required to evaluate the actual margin of safety or probability of survival of the given design. Such a model constructed for the purpose of evaluating the structural integrity of a design is commonly known as a structural test motor (STM).

2.1 GRAIN GEOMETRY

Solid propellant motors generally are composite structures of two unlike materials: (1) propellant, a compliant viscoelastic material, and (2) a shell or pressure vessel of comparatively stiff material in which the propellant is encased. The grain geometry is designed primarily on the basis of the ballistic requirements, but the design is also influenced by processing and economic factors. Typically, the magnitudes of thrust, chamber pressure, and duration of burning needed to accomplish the intended mission are specified. Additional design constraints usually are imposed by the dimensions specified for the envelope, the type of mission the rocket is expected to perform, the fabrication techniques available, and the type of propellant to be used. To optimize case and grain design within these constraints, several parameters may be varied; web dimensions, burning rate, burning-surface area, and the case and nozzle characteristics are the chief variables.

The wide range of sizes, shapes, and designs that have resulted from satisfying varied mission requirements can be seen in reference 10, which contains a listing of all solid propellant motors made in this country together with related performance data. Figure 1 shows some typical solid propellant grain geometries. Grain design procedures, ballistic considerations, and performance analyses that enter into the selection and final evaluation of these configurations are discussed in references 11 and 12.

The internal-burning grain (fig. 1(a)) currently is the most widely used. It is usually the least expensive and permits a variety of port shapes and sizes, thereby giving wide latitude for varying the ballistic characteristics. Experience has proven the internal burner to be relatively rugged and easy to fabricate. Structural failures in these grains generally are either cracks originating at high-strain regions of the free port surface or bond failures along the grain case interface.

Early applications of end-burning grains (fig. 1(b)) were limited to short geometries (low length-to-diameter ratios). However, the development of compliant grain case suspension systems and high-burning-rate propellants has permitted fabrication of larger end-burning

4
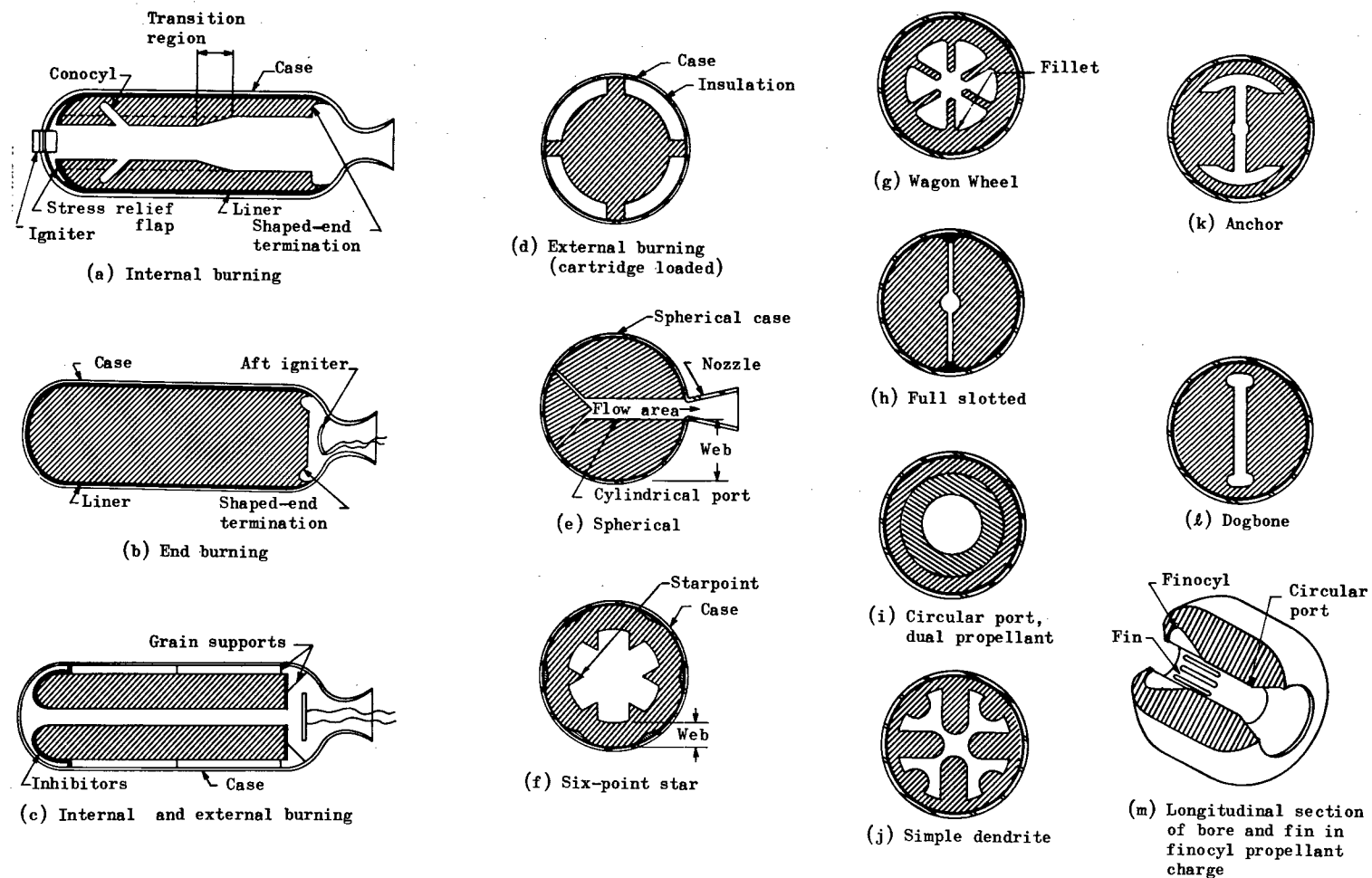
Figure 1. – Representative solid propellant grain geometries.

(a) Internal burning

(b) End burning

(c) Internal and external burning

(d) External burning (cartridge loaded)

(e) Spherical

(f) Six-point star

(g) Wagon Wheel

(h) Full slotted

(i) Circular port, dual propellant

(j) Simple dendrite

(k) Anchor

(l) Dogbone

(m) Longitudinal section of bore and fin in finocyl propellant charge

grains with length-to-diameter ratios comparable to those of the internal-burning grains. Analyses of these unported grains when they are subjected to severe constraints require a more precise definition for the bulk properties (coefficient of thermal expansion and bulk modulus) than do the analyses of grains with greater ratios of free surface area to volume.

The external- and internal-burning grain, schematically illustrated in figure 1(c), greatly increases the burning surface area that can be exposed for a given volume of propellant. This characteristic can be used to simplify the shape required for the port; e.g., the port can be made circular. However, these grains usually require a complex supporting structure capable of enduring exposure to hot gases for the duration of the firing. This consideration has greatly retarded the development of new motors with grains having the internal- and external-burning feature.

Other configurations of practical value include cartridge-loaded grains (fig. 1(d)), so-called because the propellant is not cast and cured within the case but rather in a mold outside the case; and spherical grains (fig. 1(e)). Each of these geometries presents a slightly different problem to the analyst and may require slightly different analytical techniques. Cartridge-loaded grains, if bonded to the case, require special attention because of postcure bonding. Frequently they are left free-standing, i.e., bonded only at the ends. In this instance the grain may be susceptible to damage from dynamic loadings. Spherical grains require special attention because there is no cylindrical section where a plane-strain analysis can be used with confidence.

Examples of grain cross sections are shown in figures 1(f) through 1(l). The wagon-wheel and dendrite configurations typically expose a large burning surface, while the full-slotted and dogbone grains give high volumetric loadings. The cantilevered star points of the wagon-wheel and dendrite shapes require special attention because of their vulnerability to the effects of lateral accelerations. Both free-surface crack failures and bondline failures are major considerations for the full-slotted and dogbone grains. Usually, special insulation designs are required at the case on the axis of the slot to protect the case during firing and to resist initiation of bond cracks. Dual-propellant grains, which are often used to generate two-level (boost-sustain) thrusts, can also be used to place propellant with enhanced structural properties in regions of duress. Consideration of the strength of the interface is always necessary.

Often, special geometrical features can be added to the grain to help maintain the structural integrity during the motor service life. Such features include fillets, stress relief flaps (floaters), conocyls and finocyls (fig. 1(m)), contoured end terminations, and transition regions between differing cross sections. Although final evaluation of structural integrity is not made until the grain design has been completed, the analyst is required to advise and consent while the geometrical layout is being made. This early support is based on experience, judgment, and rapid approximate analyses.

2.2 PROPELLANT PROPERTY CHARACTERIZATION

The material properties required for a structural analysis of a solid propellant grain fall into three groups:

(1) Thermal properties. — The properties necessary to compute the temperatures and thermally induced volume changes everywhere in the motor.

(2) Mechanical properties. — The properties necessary to compute the body forces due to accelerations and to define the interrelationships among stresses, strains, and temperatures.

(3) Failure properties. — The properties necessary to characterize conditions at which failure will occur and to evaluate susceptibility to failure.

The analytical techniques inevitably are based on restrictive assumptions regarding the behavior of the material. The most significant of these assumptions are that (1) the coefficient of thermal expansion is constant, (2) the responses to superposed loads also can be superposed (linearity), and (3) the effects of temperature on the mechanical and failure properties can be characterized by uniform extensions or contractions of the time scale (thermorheological simplicity). An early and decisive step in any given testing program is one that establishes the degree to which the propellant deviates from these assumptions. Alternative techniques must be employed when the assumptions do not hold.

2.2.1 Thermal Properties

The prediction of the mechanical state of a grain when deformation is the result of temperature change requires that certain thermal properties be known: (1) coefficient of thermal expansion, (2) specific heat per unit initial volume, and (3) thermal conductivity or thermal diffusivity. These parameters are necessary for the calculation of motor grain temperatures, times required to reach states of thermal equilibrium, and the volumetric responses to temperature changes. Thermal properties usually are obtained by methods specified by the ASTM (refs. 13 through 17) or by the ICRPG (ref. 7), the method being modified as necessary for the study of propellant properties.

For measuring coefficient of thermal expansion α[1], the Mechanical Behavior Manual (ref. 7, sec. 4.9.1) specifies a quartz-tube dilatometer similar to the one prescribed by ASTM Method D 696-70 (ref. 13). The technique described in the Manual is more accurate than the ASTM method because of refinements in temperature control and in the way linear measurements are taken. The procedure in the Manual was established, in part, to provide

---

[1] Symbols and abbreviations are defined in the Glossary.

the additional data required to determine the glassy transition temperature T_g, a value that is helpful in establishing a baseline for the time-temperature correspondence that is discussed in later sections.

An "empirical" method for determining effective values for α with the propellant under realistic motor-like conditions is described in section 2.3.4.1. This method employs small circular-port grains in tubular cases subjected to slow changes in temperature. This kind of structural test motor (STM) is sometimes referred to as a strain evaluation cylinder (ref. 7, sec. 4.8.2).

The differential scanning calorimeter (DSC) is now used for most measurements of the mean specific heat c. The device measures the energy per unit time necessary to maintain a constant heating rate on the sample and on the empty sample holder. The data are recorded in millicalories per second; from the data, the specific heat of the sample at all temperatures can be calculated. Agreement of measured values within ±3 percent has been reported (ref. 18).

Partly because solid propellants are poor conductors of heat, an adequate method for measuring thermal conductivity k or thermal diffusivity X has not yet been established. Three ASTM methods (refs. 15 through 17) have been adapted for use with solid propellants. A modification of the method described in reference 17, used in a large number of tests with RTV-60 silicone rubber, demonstrated reproducibility of results within ± 4 percent (ref. 19).

2.2.2 Mechanical Properties

The prediction of the stress-strain response of a body to external loads or to temperature changes requires constitutive equations, i.e., equations that relate the stresses, strains, and temperatures. For linearly elastic materials, these equations are algebraic and involve simple constants of proportionality (stiffnesses and coefficients of thermal expansion). For solid propellants, however, the relationships between the stresses and strains are more complicated and involve stiffnesses, or moduli, that are not constant but are extremely variable. The moduli are known to vary with both time and temperature and may well depend on other influences such as the strain state, strain history, and strain magnitude. Thus, the measurement of the moduli for propellants is considerably more difficult than is a similar measurement for elastic materials.

As discussed in later sections, there are several types of grain analyses that can be performed. These analyses can be broadly categorized in levels of increasing complexity. Each category has many subdivisions descriptive of the more specific techniques and

8

assumptions used. Analyses based on gross assumptions are relatively simple but often lead to unacceptable errors. The more common of these assumptions concern

- Material compressibility
- Effects of time
- Effects of temperature

In the attempt to enable the practicing analyst to obtain needed engineering information at reasonable time and cost, simplifying assumptions in each of these areas have become common practice throughout the industry. A systematic and thorough study of the implications of the more important assumptions on the accuracy of predicted grain stresses and strains (ref. 20) found that for many, if not most, practical problems the customary analytical practices may give predicted quantities greatly different from those that actually occur. The variation sometimes is so large that the analytical solution has limited engineering value. Clearly, stress analyses of such doubtful validity may be of more harm to the decision-making analyst or designer than no analyses at all. However, the more general nonlinear characterization and analytical techniques suggested in reference 20 are neither developed nor practiced to the extent required to classify them as state of the art. In this monograph, therefore, the customary methods will be described, and frequent comments about their shortcomings and suggestions for evaluating possible errors and alternative calculations or measurements will be made.

The more common loading histories used for laboratory characterization tests include the stepped stress or strain, the constant-rate increase in the stress or strain, and the cyclic application of the stress or strain. In the stepped test, the force or displacement is imposed on the specimen as abruptly as possible and then is maintained constant while the data are collected. In the constant-rate test, the force or displacement on the specimen is increased linearly in time. In the cyclic tests, the imposed force or displacement typically is sinusoidal. Each of these histories can be imposed on any type of specimen, but the method of data reduction depends on the specimen geometry.

The more common laboratory test specimens include the JANAF uniaxial tensile specimen (the "dogbone"), the shear chevron, the biaxial tensile strip, and the triaxial tensile specimen (the "poker chip"); less well known are the microbone uniaxial, hollow sphere, pressurized cylinder, and grain-sector specimens. Each specimen has advantages and disadvantages, the primary difference among them being the inherent state of stress (or strain). The interpretation of the resulting data often depends on the assumptions or analyses used to establish the stress or strain state. Often these interpretations will depend upon the material properties one is attempting to measure. Costs, testing facilities, and schedule requirements also may influence the selection of test specimens. The techniques required to reduce the data collected with the common specimen shapes are described in reference 7.

The inherently simple uniaxial tensile test is appealing because one can be certain about both the state of stress (uniaxial tension) and its magnitude. For a linearly viscoelastic

9

material, data from this test alone are sufficient to determine both the time-dependent tensile modulus and Poisson's ratio (or both the shear and bulk moduli). The desirable simplicity and economy of the uniaxial test provide strong motivation for its continued use, whenever possible, as a primary characterization tool. A variety of loading histories can be applied to the uniaxial specimen, and the responses monitored. However, this statement can also be made for most of the other specimens. The most important difficulty with the specimen is that the uniaxial stress state is representative of only a small part, if any, of the stressed propellant in most rocket grains. Because of the strong dependence of the material properties on the stress (or strain) state, the uniaxial specimen has lost its position as the primary characterization specimen. It does continue as the primary test method for guiding propellant development activities and for quality control.

Regardless of the specimen or loading history chosen, the parameters that are evaluated from the resulting data, the moduli and time-temperature interrelationships, are the same. A method for reducing the data to obtain a time-dependent modulus is described in reference 7, from which the illustrative curves of figures 2 and 3 were adapted. Figure 2 shows the data collected from identical relaxation (constant strain level) tests of uniaxial specimens at 11 different temperatures. Typically, the colder specimens are stiffer. For most materials of this type, the temperature effect can be absorbed into the time variable. With one curve (usually the one at $70°$ or $77°F$ [294 or $298°K$][1]) held unchanged, the other curves are shifted horizontally in time as required to superpose onto a single curve. The time shift required for each temperature provides the so-called time-temperature shift factor $\log a_T$.

The inset on figure 3 shows the shift factor $\log a_T$ required at each test temperature to cause the modulus curves to superpose. Figure 3 shows the resulting plot of the tensile relaxation modulus as a function of time and temperature reflected in the variable t/a_T (usually referred to as the reduced time). Regardless of the specimen used or the type of modulus being evaluated, the procedure is essentially the same.

When a steady-state sinusoidal loading history is imposed, a dynamic modulus can be determined by appropriate data reduction. The dynamic modulus E^* is a complex number; the real part is called the storage modulus, E', and the imaginary part the loss modulus, E''. Typically, these quantities are also considered to be interrelated with temperature through a logarithmic shift factor denoted as for the relaxation data by $\log a_T$. Both components are usually shown on the same graph plotted against the reduced frequency ωa_T, where ω is the frequency (rad/sec) of the sinusoidal strain (or stress) input.

One mechanical property other than a stiffness required to predict grain responses is the density ρ. Most commonly, ρ is used for the calculation of weights, centers of gravity, and moments of inertia. It is required, however, for the determination of the body forces of the equilibrium equations when the grain is subjected to inertial load, e.g., gravity during

---

[1] Parenthetical units here and elsewhere in the monograph are in the International System of Units (SI units). See Mechtly, E. A.: The International System of Units. Physical Constants and Conversion Factors, Revised, NASA SP-7012, 1969.

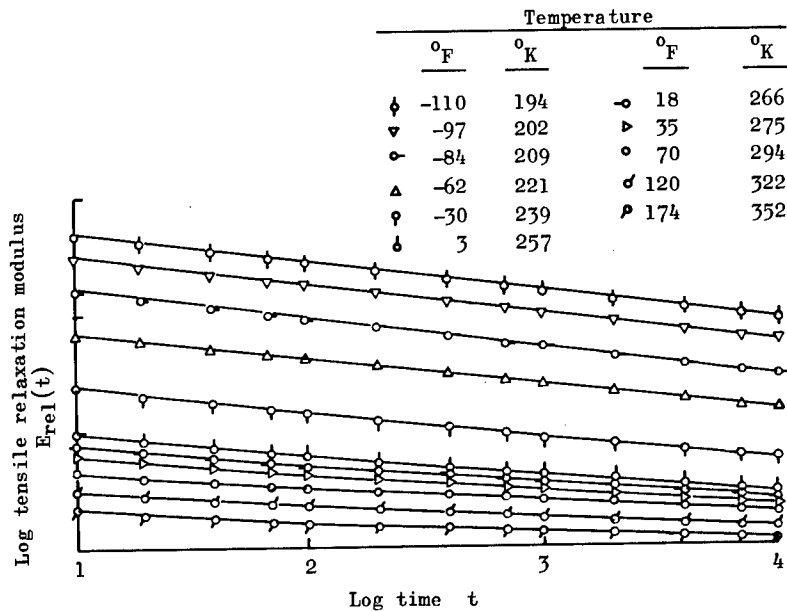| Temperature				
	°F	°K	°F	°K
ϕ	-110	194	-o 18	266
▽	-97	202	▷ 35	275
o-	-84	209	o 70	294
△	-62	221	d 120	322
ϙ	-30	239	ρ 174	352
♦	3	257		

Figure 2. — Stress relaxation data measured at different temperatures for a typical propellant (adapted from ref. 7).
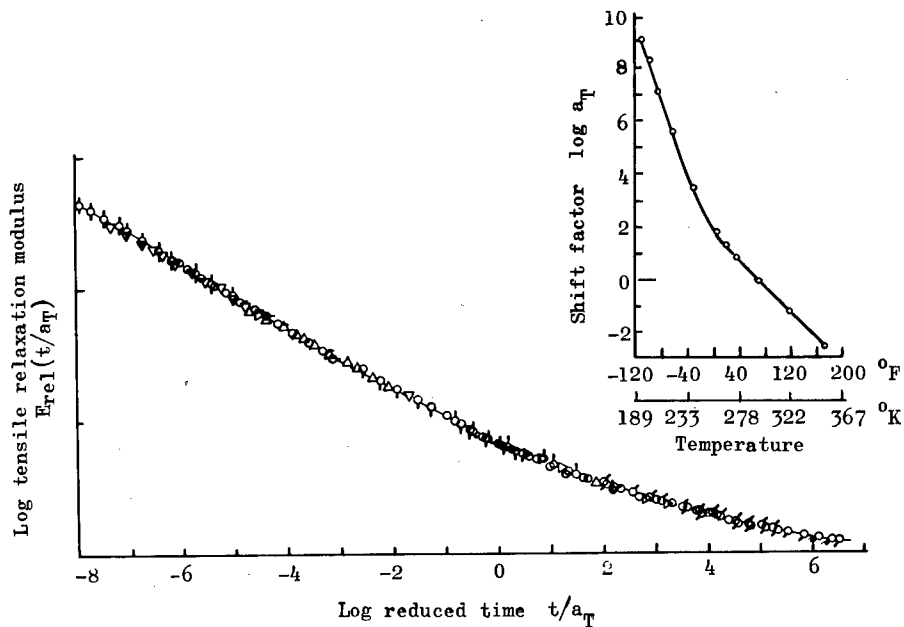
Figure 3. — Stress relaxation moduli in figure 2 shifted to T = 70° F (294°K) (adapted from ref. 7).

11

storage, uniform acceleration, shock, and vibration. Typically, density has been determined by a liquid displacement test such as that described in ASTM D 297-68 (ref. 21), but it can be measured simply by weighing large-dimension blocks of propellant (ref. 6).

2.2.3 Failure Properties

The purpose of a failure theory is to provide an analytical expression by which conditions at failure observed in laboratory tests can be used to predict failure in other, more realistic circumstances. No failure theory has been shown to be universally applicable to the prediction of cracking in solid propellants. This is not surprising when one considers the difficulties that have been experienced in attempting to formulate universal theories applicable to other, more homogeneous material.

It is clear that such a theory for propellant must at least include state of stress (or strain), loading history, temperature, and surface condition (machined, cast, or other) as parameters.

The failure prediction for propellant is further complicated by the possibility of either excessive deformation or autoignition. The grain deformations are calculated during the stress-analysis phase of a structural integrity study and can be used, with the advice of a ballistician, to decide if a failure due to restricted gas flow is possible. The large deformations that are apt to lead to such failures, often termed slump, are usually the result of accelerations and are exaggerated in the presence of high temperatures. Autoignition, on the other hand, results when the propellant is allowed to reach or dwell at a temperature required for ignition. As implied by this statement, the ignition temperature decreases slightly as the dwell time increases. The prediction that such temperature will occur must be based on a thermal or thermo-mechanical analysis.

But slump and autoignition are relatively insignificant modes of failure that occur only rarely in comparison with the frequency of propellant cracking. Cracks can expose additional burning surface to the extent that gas pressures greater than those for which the hardware was designed can be generated, and the motor will fail. Even small or submerged cracks can precipitate failures by growing, during ignition, to expose too much burning surface. An extensive study to define just which cracks may lead to motor failures and which may not recently was completed (ref. 22).

As noted in the detailed discussion of fracture in section 2.5.1, cracking failures are divided into two groups: failures that originate at existing flaws, and those that do not (ref. 23). The necessity for such a division is obvious when one considers that, even though the calculated stress at the tip of a sharp crack, no matter how small, will be infinite, there exists a crack size (flaw size) below which this "infinite" stress will not be physically significant. For the

12

prediction of failure under this condition, a failure theory is required. A universal theory including the effects of all or most of the significant parameters for "unflawed" material does not exist, and therefore it is necessary to design laboratory failure tests to simulate the state and history of the propellant at the point in the motor where cracking is expected to occur. Because this necessity is equally real for the mechanical as well as the failure characterization, one specimen and test sequence is usually used for both purposes.

When the crack size is significant, the susceptibility to growth when loads are applied must be evaluated. An energy-balance criterion analogous to that used by fracture-mechanics theory to predict crack instability in other engineering materials has been found to be the best approach to this problem.

2.2.4 Property Variability

The inherent variability of mechanical and especially failure properties is larger for solid propellants than for most structural materials because of the sensitivity of these properties to variations in ingredients, processing, temperatures, and to environmental effects (principally aging). If the probability of survival (satisfactory mission completion) for a grain is to be computed, the influence of property variabilities on calculated stresses, strains, and displacements must be taken into account.

The degree to which statistical distributions are established depends on the mission of the given motor and on the resources available for its analysis. In some instances, it is sufficient to assume both the characteristic shape and spread of the statistical data on properties based on experience with similar propellants. In others, the characteristic shape is assumed, usually normal (Gaussian), and the spread determined by a relatively small number of replicate tests. Because the properties are variable with time, a linear regression analysis as described in reference 24 is used to obtain the regression line (mean) and standard error of the estimate (spread). Variations in the loading histories may be assumed on the basis of experience with similar motors, or actual ignition pressurization histories may be used as they become available during the motor testing program.

Once the properties are established, a distribution of the margin of safety can be calculated. One method is the technique of selecting random numbers from which related random properties and loads can be chosen within the constraints of observed property statistics. An example of the use of this procedure is reported in reference 24. Margin-of-safety calculations are discussed in section 2.5.5.

2.2.4.1 PROCESSING EFFECTS

Mechanical properties of propellant are sensitive to specific, definable processing variables (refs. 6 and 25) and also to many unknown intra- and inter-batch variations. Frequently the steps followed in actually manufacturing the motor and grain may cause the mechanical and failure properties of the *in situ* propellant to differ markedly from the properties measured in the laboratory. Property variations between batches typically are larger than those within a given batch. Causes of these batch-to-batch variations are differences in raw-material properties, mixing times, times of cast, and cure histories. When possible, the cause of a variation is isolated; the affected parameters are adjusted and taken into account in the structural integrity analyses. Otherwise, variations due to processing are simply considered as a part of the inherent property variations characteristic of the propellant.

2.2.4.2 ENVIRONMENTAL EFFECTS

Environmental conditions and storage time during the service life of a motor may result in changes to the propellant characteristics that, in turn, affect stress levels and ultimate capabilities. For example, aging normally results in a significant change in the properties even in a controlled environment (ref. 26); some formulations, however, show little effect. The effects of aging may include significant changes in both the stiffness and strength.

Aging effects often are simulated in an accelerated manner by holding the propellant at high temperature. With this procedure, a time-temperature shift factor, similar to the time-temperature shift for mechanical properties, sometimes can be used to calculate the amount of real time simulated by the test time and temperature (ref. 27). The validity of this technique is usually checked by a surveillance program that includes laboratory tests of the propellant following real-time aging and service.

Most propellants are sensitive to humidity: exposure over a period of time to a moist atmosphere tends to degrade the properties. When it is suspected that humidity may cause significant variations in the properties, these changes may be evaluated by tests (ref. 28).

Propellant may be contaminated when volatiles are released from other motor components or when chemicals inadvertently are introduced (ref. 29). In some instances, the contamination may enhance one property (e.g., strength) at the expense of another property (e.g., elongation). Contamination by chemicals that attack polymer chains may result in decreased structural capabilities at the propellant surfaces. Again, the magnitude of any such degradation is assessed by material property tests of the affected material. Another kind of propellant contamination occurs when radiation energy is absorbed by the propellant. Possible energy sources include electromagnetic waves and subatomic particles. Metal cases provide a fairly effective screen for these forms of radiation.

2.3 LOAD ANALYSIS

Loads for propellant grains include specified loads (prescribed loads that simulate the most severe service conditions anticipated) and motor operational loads (loads not prescribed but occurring as a characteristic of the given motor design; e.g., ignition pressurization). So the magnitude of the operational loads are not known until the grain design is complete. The basic standards for specifying test loads are MIL-STD-810B and MIL-STD-167 (refs. 30 and 31). A general discussion of the typical requirements for a solid rocket motor is given in reference 32 and an evaluation of their relevance to actual service experience is given in reference 33.

Thermally induced structural loads are of major importance. These loads arise from the differing dimensional responses of motor components (grain, liner, case) to a temperature change. The dimensional changes, characterized by the coefficient of thermal expansion, differ by an order of magnitude; the case materials change much less than do liner materials and propellants. Thus, following cooldown from cure, the grain and liner alone normally would shrink to a much greater degree than the case. The stiff case, however, bonded to the propellant, tends to restrain the grain shrinkage, resulting in significant tensile tractions. Grain failures due to thermal loads, developing either as cracks in the grain or as "unbonds" along the grain/liner/case interface, permit the grain to come nearer its natural (reduced) volume state. Aerodynamic heating of a cold motor case may impose additional tractions. Under aeroheating, the case heats rapidly because of its relatively high conductivity; the temperature change in the poorly conducting liner and propellant is far more sluggish. So the case tends to expand but is restrained by the grain; thus, increased tractions are exerted across the propellant/liner and liner/case bonds. The possibility of failure is further heightened by the fact that the increasing temperature is simultaneously lowering the bond surface strength.

Another important classification of structural loads are those imposed by the accelerations due to ground handling, transportation, and actual flight. When the time variations of an acceleration are slow compared to the natural frequencies of a grain, they can be treated as static loads or as superpositions of static loads. Otherwise, the variations are treated either as vibrations, when repetitive, or as shock, when not repetitive. Dropping the motor results in rapid deceleration forces applied to relatively concentrated areas of the case external surface. Such a load is classified as impulse or shock. Uniform accelerations are generated by storage (1 g), flight initiation, flight maneuvers, and in some instances flight decelerations. Nearly all forms of transportation, including captive and free vehicle flight, result in a broad spectrum of vibratory loads that vary in magnitude and frequency.

The final structural load imposed on a propellant grain results from internal pressurization that occurs during ignition and continues until burnout. The pressure usually builds up at a relatively high rate and, for center-perforated grains, provides additive (to thermal strains)

tensile strains at the inner bore. After ignition, the pressurization problem becomes somewhat more complex because of the continuously changing geometry of the ablating grain. In general, however, the bore strain level decreases because the web is growing thinner and initial points of stress concentration caused by geometry are deteriorating. An additional problem may arise, however, in the form of oscillatory combustion, in which the internal pressure variations become rhythmic. Loads arising from oscillatory combustion are, at best, extremely difficult to analyze and require modifications in motor design or propellant formulation to minimize their importance.

Complicating the analytical treatment of loads is the fact that they often occur in combination or prescribed sequences. Since most methods of analyses are limited to one or, at most, two combinations of load types, methods of superposing the individual effects must be considered carefully. Because behavior of a propellant is dependent on its stress and strain history, the magnitudes and sequences of previous loads must be taken into account, especially in predicting failure. Current stress-analysis practice is to disregard the effects of previous loadings and, when loads are imposed simultaneously, to combine the failure properties for the loads in proportion to the predicted stress or strain magnitudes resulting from each load.

2.4 STRESS, STRAIN, AND DISPLACEMENT ANALYSES

A primary part of grain structural integrity analysis is the prediction of the stresses, strains, and displacements that occur in a particular grain geometry in response to the specified and operational loads. To make this prediction, the analyst must have available a valid characterization of the thermal and mechanical properties. The significance of deviations of the material behavior from that assumed must be assessed, and there must exist good judgment concerning use of possible corrective, alternate, or supplementary analyses. Current analytical methods usually are based on the assumption that the propellant behaves as a linearly viscoelastic material. Numerical elasticity solutions, using the finite-element stiffness approach, provide a powerful method that is used almost universally for analyzing all but the simplest grain geometries. Methods of experimental stress analysis and the instrumented analogue motors known as structural test motors (STM's) are employed to provide solutions when "all else fails." The method or combination of methods of analyses employed depends on the nature of the loads expected, the grain geometry, and the results of the material property characterization.

2.4.1 Deviations from Assumptions

Several simplifying assumptions are inherent in the derivation of the equations used to predict the response of a grain to loads. In many instances, actual propellant behavior has

been found to differ from that implied by these assumptions; and, as a consequence, validity of the resulting predictions is questionable. Thus, the analyst must be able to (1) deduce from the laboratory characterization the significance that can be placed on his calculations and (2) select appropriate courses of action when the deductions are discouraging. These alternates may include making rule-of-thumb modifications of the analyses, comparing calculated solutions with other calculated solutions for grain responses with which the analyst has experience, or using STM's to obtain required data. Satisfactory theoretical treatments of the observed erratic behavior of propellants have not yet been developed or accepted. It should be noted, however, that several approaches have been proposed (refs. 34, 35, 36, and 37, p. 68).

Variations of as much as 30 percent have been observed in the value for coefficient of thermal expansion as a function of temperature in solid propellants. Variations of this coefficient as a function of strain level have been suspected, but their ranges are unknown.

Deviation from the assumption of a linear relationship between stress and strain is even more significant. Modern high-energy, high-solids (86 to 90 weight percent) propellants exhibit nonlinearities even at very low strains (refs. 36, 38, and 39). Geometrical nonlinearities are expected at large strains even for an idealized material. The non-linearities observed in propellants, however, are much greater than those due to geometrical effects alone. They have been found to be dependent on the state of strain (or stress) as well as on the strain history and strain level. Primary causes for these nonlinearities are believed to be particle dewetting[1] and, for small strains, molecular chain scission. For this reason, characterization tests that define the modulus and its degree of nonlinearity as a function of the controlling variables are necessary. In addition, these characterization tests provide data from which the magnitude of the error in the analysis may be estimated.

Deviations from the behavior implicit in the assumption of "thermorheological simplicity" also lead to significant errors. Thermorheological simplicity means that the effects of temperature on the relaxation modulus can be taken into account by expanding (for cold) or contracting (for hot) the time scale (sec. 2.2.2). Validity of the time-temperature shift factor a_T for practical applications, however, is established by the tests employing simultaneous straining and cooling. If a_T derived from constant-temperature tests is a continuous function of temperature as assumed, the force calculated to maintain the strain rate (eq. (29), sec. 2.4.2.2) will be the same as the force measured during the simultaneous straining and cooling test. In practice, even at small strain levels there are gross differences between the predicted and measured values for many propellants (refs. 36, pp. 191-193, and 37).

---

[1] The binder (fuel) breaks free from the embedded oxidizer and metal particles.

17

2.4.2 Theoretical Stress Analyses

The equations of the theory of linear viscoelasticity and those of linear elasticity are similar. The strain-displacement equations and equilibrium equations are identical; only the stress-strain relationships are different. The assumptions basic to elasticity (homogeneity, isotropy, small displacements, and linearity) continue to be required; and deviations from the assumptions lead to erroneous solutions. The main difference is that in viscoelastic analyses the stress-strain relationship must be characterized by another parameter on which the relationship depends: time. Various simple models such as elementary combinations of springs and dash pots can be used to visualize the time-dependent relationship. However, rocket propellants have broad transition regions (on the order of 20 orders of magnitude) and require many spring/dash-pot combinations if the actual behavior is to be simulated realistically.

Although practical techniques (especially computer programs) for the viscoelastic analyses are being developed rapidly, the present practice almost invariably is to perform only elastic analyses. When the loading history is known, an "effective" modulus can be used to give the responses directly. In other instances, the elastic solutions are used to devise the response to a step load (the quasi-elastic solution), which then can be used with the convolution integral to determine the responses to any arbitrary (in time) load. So, typically, a decisive judgment required during an analysis is the selection of the appropriate stiffness(es) to use in the elastic analyses.

2.4.2.1 ANALYSES BASED ON ELASTICITY

The stress-strain law of classical elasticity can be written with two sets of independent equations, each involving only a single material constant. The first, the relationship between the dilatational (volume change) components, is written

$$e = \frac{\Theta}{3K} + 3 \, \alpha \, \Delta \, T \qquad (1a)$$

or

$$\frac{\Theta}{3} = K \, (e - 3 \, \alpha \, \Delta \, T) \qquad (1b)$$

18

where

K = bulk modulus

$\Theta = \sigma_{ii}$ = sum of the normal stresses

$e = \epsilon_{ii}$ = sum of the normal strains

(Following the usual summation convention, repeated indices indicate summation over the range of the index).

The other, the relationship between the deviatoric (shape change) components, is written, in double-index notation, as

$$s_{ij} = 2Ge_{ij} \qquad (2a)$$

or

$$e_{ij} = s_{ij}/2G \qquad (2b)$$

where G is the shear modulus and the subscripted s's and e's are defined in terms of the corresponding dilatational components as

$$s_{ij} = \sigma_{ij} - \frac{\Theta}{3} \delta_{ij} \qquad (3a)$$

$$e_{ij} = \epsilon_{ij} - \frac{e}{3} \delta_{ij} \qquad (3b)$$

Here, s_{ij} and e_{ij} are the components of the deviatoric stress and strain tensors, respectively; σ_{ij} and ϵ_{ij} are the components of the stress and strain tensors, respectively; and δ_{ij} is the Kronecker delta

$$\delta_{ij} = 0, i \neq j \qquad (4)$$

$$= 1, i = j$$

Five elastic material constants normally are used by the stress analyst: E, ν, K, G, and λ (Lamé's constant). Equations (1) and (2) reflect the physical significance of the G and K. The other constants are related to G and K by the equations

19

$$\lambda = \frac{3K - 2G}{3} \tag{5}$$

$$E = \frac{9KG}{3K + G} \tag{6}$$

$$\nu = \frac{3K - 2G}{2(3K + G)} \tag{7}$$

These three equations are equally valid for linearly viscoelastic materials when they are written in terms of the Laplace transforms of the time-dependent properties with p-multipliers. However, the quasi-elastic method can be used to show that equations (5) through (7) are approximately true for viscoelastic materials even when the properties are expressed directly as functions of time.

For polymeric materials, two simplifying assumptions concerning the bulk modulus K sometimes are used. The more common one is to assume that K is infinitely large (i.e., the material is incompressible); so, from equations (6) and (7), E = 3G and ν = 0.5. For loads and geometries that produce primarily deviatoric strains (eq. (2)), this assumption results in relatively small errors in predicted stresses. But when dilatational components are significant, as when a highly constrained grain is subjected to uniform thermal cooling, the errors will be much larger.

The second simplifying assumption is that K can be treated as a constant, independent of time. The bulk modulus of unfilled materials has been found to decay in magnitude only about one logarithmic decade while simultaneously the shear modulus falls off three or more decades. The assumption of a constant bulk modulus is equivalent to assuming Poisson's ratio is given by

$$\nu(t) = \frac{3K - 2G(t)}{2\left[3K + G(t)\right]} \tag{8}$$

where the quasi-elastic approximation has been used. In problems where the temperature does not vary with time and the strain histories are known, effective elastic moduli are calculated with the use of the convolution integral as discussed in the following section.

2.4.2.2 ANALYSES BASED ON VISCOELASTICITY

Several expressions are used to represent the responses of linearly viscoelastic materials. These include two analytical representations of the relaxation modulus and creep

compliance: the modified power law, and the Prony series. The modified-power-law representation of the relaxation modulus commonly is written as

$$E_{rel}(t/a_T) = E_e + \frac{E_g - E_e}{\left[1 + \left(\dfrac{t/a_T}{\tau_o}\right)\right]^n} \qquad (9)$$

where

$E_{rel}(t/a_T)$ = tensile relaxation modulus as a function of reduced time

E_e = rubbery (or long-time) modulus

E_g = glassy (or instantaneous) modulus

τ_o = time constant providing the horizontal location of the transition region on a log/log plot of the modulus vs time

n = slope of the log/log relaxation curve

The creep compliance is expressed as

$$D_{crp}(t/a_T) = D_e + \frac{D_g - D_e}{\left[1 + \left(\dfrac{t/a_T}{\tau_o'}\right)\right]^{n'}} \qquad (10)$$

where

$D_{crp}(t/a_T)$ = tensile creep compliance as a function of reduced time

D_g = glassy compliance

D_e = rubbery compliance

τ_o' = time constant to give best horizontal position for the log/log curve

n' = slope of the log/log compliance curve

If the material is linearly viscoelastic, it is usually assumed that $1/D_e = E_e$ and $1/D_g = E_g$; and the exponent n has the same value in both the expression for compliance and that for relaxation.

21

In an analysis of a viscoelastic material, it often is necessary to perform Laplace transformations and inversions (ref. 1). Such manipulations are difficult with the modified-power-law representation. Primarily to avoid this difficulty, the Prony (or Dirichlet) series representation has been suggested (ref. 40)[1]. The series for the relaxation modulus

$$E_{rel}(t/a_T) = E_e + \sum_{k=1}^{n} E_k \exp(-t/a_T \tau_k) \tag{11}$$

is based on a mechanical model, consisting of springs and dash pots, called the generalized Maxwell model. Approximately 15 to 20 terms in this summation normally are needed to characterize propellant behavior. The τ_k's, which determine the time span during which the varying nature of the kth term is influential, usually are chosen in advance. For ease of computation, a τ_k is chosen for each decade of time through the transition region. The coefficients E_k then are selected, by collocation or hand curve fitting, to best fit the experimental data (ref. 41). Again E_e is the rubbery or long-time modulus. The corresponding series for the creep compliance, also a spring and dash-pot model, called the Kelvin model, is

$$D_{crp}(t/a_T) = D_g + \sum_{k=1}^{n} D_k [1 - \exp(-t/a_T \tau_k)] \tag{12}$$

where the τ_k's are selected in advance as with the relaxation modulus. The coefficients D_k then are picked to give the best fit to the measured compliance curve.

Experience has shown that a dynamic modulus E^* derived directly from a relaxation or creep test is of questionable validity (ref. 44). Therefore, this modulus must be determined from vibration tests where the state of stress approximates that in the propellant where the modulus is to be used. Once measured, it can be fit to a series representation of the form

$$E'(\omega) = E_e + \sum_{k=1}^{n} \frac{E_k \omega^2 \tau_k^2}{1 + \omega^2 \tau_k^2} \tag{13}$$

and

$$E''(\omega) = \sum_{k=1}^{n} \frac{E_k \omega \tau_k}{1 + \omega^2 \tau_k^2} \tag{14}$$

---

[1]Specific situations where the Prony series has proven to be especially helpful include (1) use of the axisymmetric, thermoviscoelastic numerical analysis described in ref. 42; (2) calculations of the dynamic moduli from the static relaxation modulus or creep compliance or vice versa (technique assumes linear material behavior [ref. 41]); and (3) solution of wave propagation problems with the Laplace transform as described in reference 43.

where again the τ_k's are chosen at approximately one-decade intervals on the logarithmic time scale.

The concept of convolution (fig. 4) is based on the premise that the response $R_s\,(t - \tau)$ to a unit step function $H_s\,(t - \tau)$

$$
\begin{aligned}
H_s(t - \tau) &= 0 & (t - \tau) &< 0 \\
&= 1 & (t - \tau) &> 0
\end{aligned}
\tag{15}
$$

is known (fig. 4(a)). So if linearity can be assumed, a step input $I_s = k\,H_s\,(t -\tau)$ will generate a proportional response $k\,R_s\,(t - \tau)$ (fig. 4(b)). By superposing step inputs, one can represent effectively any arbitrary time-dependent input; individual responses also can be superposed to find the gross response to the time-varying input. This concept, frequently referred to as Boltzmann superposition, is illustrated in figure 4(c). The gross response is written as

$$
\begin{aligned}
R &= \Delta I_1\,R(t - \tau_1) & \tau_1 &< t < \tau_2 \\
&= \Delta I_1\,R(t - \tau_1) + \Delta I_2\,R(t - \tau_2) & \tau_2 &< t < \tau_3
\end{aligned}
\tag{16}
$$

etc.

or

$$
R = \sum_{j=1}^{n} \Delta I_j\,R(t - \tau_j) \qquad \tau_n < t < \tau_{n+1}
\tag{17}
$$

In the limit, as $\Delta I_j \to 0$ and $n \to \infty$, the summation can be written in integral form (the convolution integral):

$$
R = \int_0^t R(t - \tau)\,\frac{\partial I}{\partial \tau}\,d\tau
\tag{18}
$$

Expression (18) can be used to evaluate the response of any linear system to any input when the response to a step function is known. Thus, if the time response of a viscoelastic body to a step load (e.g., surface tractions or displacements) is known, the response to any time-varying loading can be calculated. This derivation makes the requirement for linearity appear very clear. Note that there are two conditions that must be met (as emphasized in ref. 45, p. 165) for the material to be considered linear: (1) the response $R_s\,(t - \tau)$ that results from the unit step input $H_s\,(t - \tau)$ will be $kR_s\,(t - \tau)$ when the input is $kH_s\,(t - \tau)$;

23
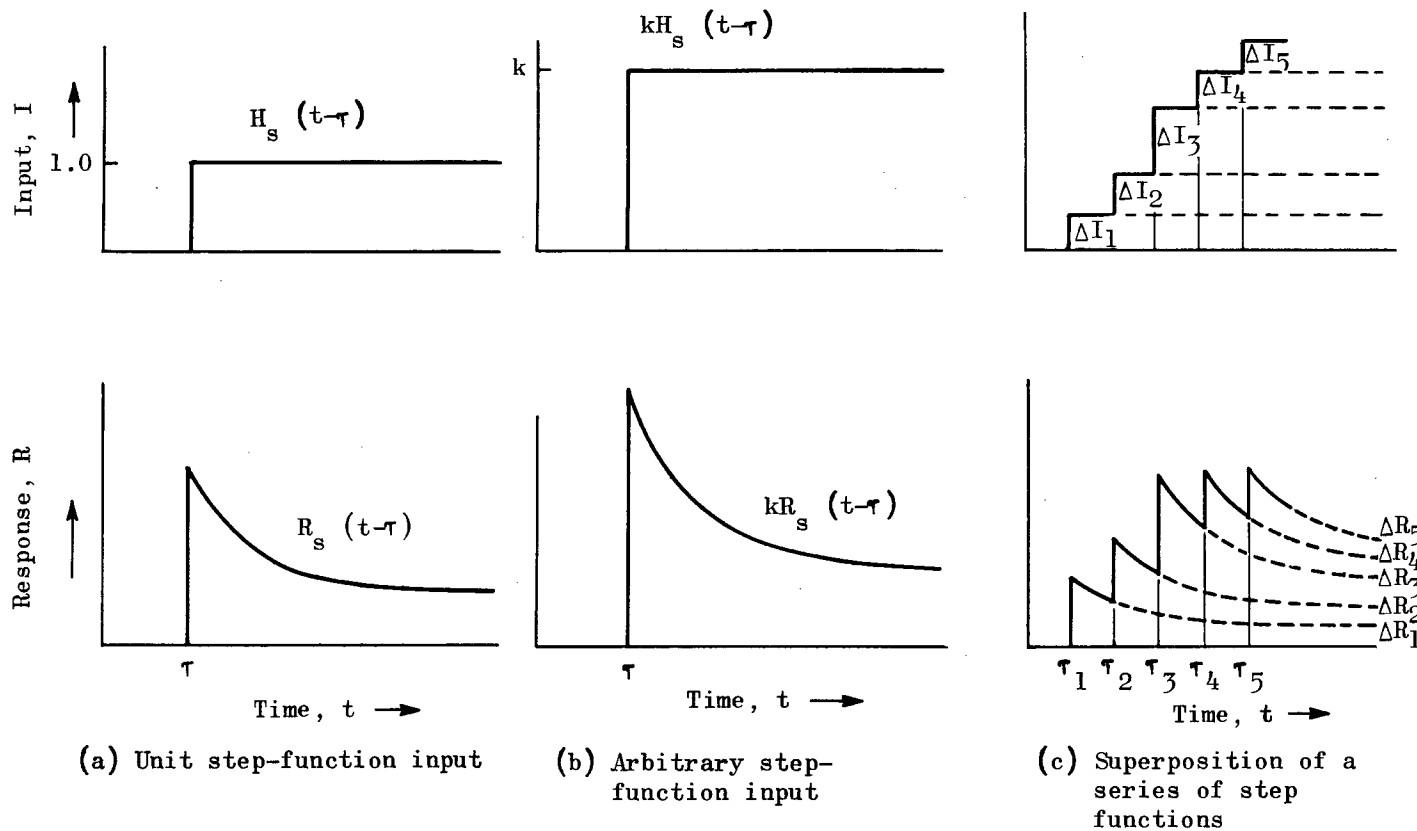
Figure 4. – Graphical representation of the concept of convolution

and (2) individual responses $R_1 (t - \tau)$, $R_2 (t - \tau)$, etc., to individual step inputs can be superposed, when the inputs act in combination, to give the resulting, or total, response.

The convolution concept conventionally is used for analyses of propellant. For the simple example of a time-dependent strain $\epsilon(t)$ being imposed on a uniaxial specimen, the stress is

$$\sigma (t) = \int_0^t E_{rel} (t - \tau) \frac{\partial \epsilon}{\partial \tau} \, d\tau \tag{19}$$

or, for a time-dependent stress $\sigma(t)$, the strain is

$$\epsilon (t) = \int_0^t D_{crp} (t - \tau) \frac{\partial \sigma}{\partial \tau} \, d\tau \tag{20}$$

If it is assumed that the bulk modulus K is a constant and the temperature does not change, the stress-strain law for a three-dimensional problem in a viscoelastic material is written, in notation like that in equations (1), (2), and (3),

$$\Theta/3 = Ke \tag{21}$$

$$s_{ij} = 2 \int_0^t G_{rel} (t - \tau) \frac{\partial e_{ij}}{\partial \tau} \, d\tau \tag{22}$$

As before, the subscripts i and j are indexed to the three orthogonal axes.

For a temperature change ΔT, if the material is thermorheologically simple, equations (21) and (22) become

$$\Theta/3 = K (e - 3\alpha\Delta T) \tag{23}$$

(which is identical to eq. (1b) for elastic materials) and

$$s_{ij} = 2 \int_0^\zeta G_{rel} (\zeta - \zeta') \frac{\partial e_{ij}}{\partial \zeta'} \, d\zeta' \tag{24}$$

where ζ and ζ' are reduced times defined as

$$\zeta = \int_0^t \frac{dt'}{a_T} \; ; \; \zeta' = \int_0^\tau \frac{dt'}{a_T} \tag{25}$$

25

Several important manipulations of equations (21) through (24) are possible when they are Laplace transformed by use of the so-called correspondence principle. This principle, as first advanced by Alfrey (ref. 46), says simply that if the stresses, strains, and displacements in an elastic body are known then the corresponding stresses, strains, and displacements in an incompressible viscoelastic body can be expressed in terms of the transform variable p. Indeed, the two expressions will be the same except that each time-varying term will have a transformed counterpart. Each counterpart will vary with p, the transform variable, rather than with real time t. Each elastic modulus will be replaced by p multiplied by the transformed viscoelastic modulus. The resulting expression, when inverted, gives the correct solution as a function of the time t. When the temperature varies with time but is the same at all points in the grain, the same operations can be performed using the reduced time ζ.

If the time-varying functions have "small" curvature when plotted against log time (the meaning of small curvature is defined in ref. 47), a simplified method may be used. Several elastic responses to a unit step load are calculated with use of elastic moduli that correspond to values for the relaxation modulus at various values of t/a_T. These individual elastic solutions are approximations to the viscoelastic grain responses at the corresponding t/a_T's. This approximate solution for a step load then is used as the response portion of the integrand to an arbitrary (in time) load. This procedure, probably utilized to solve more solid propellant grain problems than any other, is termed the quasi-elastic technique (refs. 1 and 47).

An even simpler approach, commonly employed, is based on the use of the relaxation modulus E_{rel} (t/a_T) as an "effective" elastic modulus. Equations (23) and (24) rewritten for a uniaxial state of stress and assuming incompressibility become

$$\sigma = \int_0^\zeta E_{rel}(\zeta - \zeta') \frac{d}{d\zeta'} (\epsilon - \alpha\Delta T) d\zeta' \tag{26a}$$

or when consideration is given to the definition of ζ and ζ'

$$\sigma = \int_0^t E_{rel}(\zeta - \zeta') \frac{d}{d\tau} (\epsilon - \alpha\Delta T) d\tau \tag{26b}$$

For a constant rate of change of $(\epsilon - \alpha\Delta T)$, this equation reduces to

$$\sigma = \left[\frac{1}{t} \int_0^t E(\zeta - \zeta')d\tau \right] (\epsilon - \alpha\Delta T) \tag{27}$$

26

where the quantity in the brackets can be considered an "effective" modulus (in this case the secant modulus) and thus

$$\sigma(t) = E_{eff} (\epsilon - \alpha \Delta T) \tag{28}$$

This exact approach is often cumbersome to use; moreover, experimental data has indicated that the predicted stresses are relatively inaccurate. Therefore, it has been suggested that the approximation

$$\sigma(t/a_T) = \left[E_{rel} (t/a_T) \right] (\epsilon - \alpha \Delta T) \tag{29}$$

be used.

Equation (28) is, of course, exact under the stated assumptions. On the other hand, equation (29) predicts a different and always greater stress. This observation follows from the fact that equation (29) is actually the stress in a thermorheologically simple bar that is first cooled to a given temperature and then strained. Thus, there are two points that justify the use of equation (29): (1) it is easier to use than equation (28), and (2) it yields a conservative stress (i.e., a high value compared to that calculated on the basis of simultaneous straining and cooling).

2.4.3 Experimental Stress Analyses

Particular grain design problems may extend beyond the capabilities of the analytical techniques described. The behavior of many solid propellants is exceedingly complex and in many instances is not amenable to conventional analyses. In addition, certain loading conditions, particularly those involving transient heating caused by vibration, at present cannot be analyzed. Deviations from the assumption of thermorheological simplicity also will lead to errors in the predicted responses to changing temperatures.

When the analytical techniques have been found to give questionable results, experimental techniques must be used. Reference 48 describes most of the special techniques that are especially adaptable to the requirements unique to rocket motor grains; reference 49 is more fundamental and probably is the best general treatment of the subject available. The techniques most successful for propellant grains are instrumented structural test motors (STM's) and photoelasticity, both two- and three-dimensional. Other methods include the use of brittle coatings (ref. 49) and Moire fringes (refs. 48 and 50), but these are of secondary importance. Experimental motors provide valuable stress-strain and failure data. Development and refinement of instruments and devices for measuring forces, displacements, accelerations, and temperatures have added considerably to the value of the STM approach. The final report of an exploratory study of the use of STM's (ref. 51) and the resulting compilation of techniques (ref. 9) probably are the best guides to the effective use of instrumented analogue motors.

2.4.3.1 STRUCTURAL TEST MOTORS

The term "structural test motor" implies a motor fabricated for purposes of load testing and applies to small circular ported grains with little or no integral instrumentation as well as to full size, carefully instrumented prototypes. To prevent scaling difficulties, full-scale motors are used as STM's where possible. Scaled models are used when propellant grains are too large to serve economically and effectively for tests.

During design and development programs, several representative test motors usually are required to survive specified loading sequences (qualification and pre-flight rating tests). By instrumenting these motors to measure stresses, strains, temperatures, and accelerations, the validity of theoretical analyses can be checked. The propellants for the motors can be processed in a manner similar to that for production motors and can be exposed to like environments. Material compatibility can be evaluated, as can the curing and aging characteristics. Loads for which analytical solutions are not available can be imposed on a grain, and the effects can be observed and measured.

Propellant behavior predicted on the basis of properties measured in the laboratory and behavior observed in STM's have been compared (refs. 29, 37, and 52). These comparisons show clearly that for some loads, especially thermal and vibration, the differences between predicted and experimentally measured stresses are large. The discrepancies increase when the loads are repeated. For highly constrained incompressible materials, rather accurate strain distributions often can be calculated directly for given displacement boundary conditions without reference to or a knowledge of constitutive relations. Hence, greater reliance is placed on the calculated deflections and the corresponding strains than on the stresses for the evaluation of grain structural integrity; so it is particularly important that STM instrumentation be capable of monitoring the displacements. However, under acceleration loadings, greater reliance can be placed on the calculated stresses; hence, for this condition, the importance of force (stress) gages is emphasized.

The advent of improved instrumentation for measuring surface displacements and internal deformations has enabled the experimentalist to reduce the number of STM's required for the compilation of meaningful data. Instruments available for use in measuring displacements include the following:

    (1) Linear potentiometers. — Displacements induce electrical resistance changes that can be measured (ref. 53).

    (2) Linear variable differential transformers (LVDT). — Displacements induce electrical voltage changes that can be measured (ref. 53).

    (3) Moire grids. — Visual comparisons of strained and unstrained graphical grids reveal vernier-type fringes, from which strains may be calculated (refs. 48 and 50).

    (4) Compliant high-elongation strain gages. — Strains induce measurable changes in gage electrical resistance (ref. 9).

(5) Photocell devices. — Displacements can be followed by measuring the shift in a beam of light.

Linear potentiometers and LVDT's, frequently used to measure grain bore dimensional changes and slump, also are suitable for measuring average surface strains over the length of the instrument. Surface-strain measurements over smaller areas may be made using Moire grids (ref. 50) and compliant, high-elongation strain gages (ref. 9). Such surface-displacement measuring devices, applied directly to solid propellant rocket motors, may be removed, and the motors subsequently fired. Thus, these techniques may be considered nondestructive.

Recent advances also have been made in measuring deformation in propellant grain interiors with embedded shear gages and in measuring interfacial tractions along bond surfaces with load cells (ref. 9). With these instruments, it is difficult not to violate the cardinal rule that the instrument must not disturb the quantity to be measured; the instrument/ propellant-grain interaction must be known. Reference 52 presents data on this problem. Continuing development of instruments and techniques makes deformation measurement a rapidly changing area of investigation.

Instrumented subscale models can be used to obtain basic mechanical property data. For example, measurement of the bore diameter of circular-bore STM's at various temperatures provides information for the calculation of Poisson's ratio ν and the coefficient of thermal expansion α. From reference 54, it is seen that in thermal equilibrium (plane strain)

$$2 \left[\frac{u}{a} - (1 + \nu_c) \, \alpha_c \, \Delta T \right] \nu + (\alpha \, \Delta T) \left[\left(\frac{a}{b} \right)^2 - 1 \right] (1 + \nu)$$
$$- \left\{ \frac{u}{a} \left[\left(\frac{a}{b} \right)^2 + 1 \right] - 2 \, (1 + \nu_c) \, \alpha_c \, \Delta T \right\} = 0 \tag{30}$$

where

a = radius of port (inside radius of grain)

b = outside radius of grain

u = change in radius a

c (subscript) = case property

29

Thus, the change in the port radius with temperature for a particular web fraction provides a relationship between the effective Poisson's ratio and coefficient of thermal expansion. If a second STM having a different web fraction is similarly tested, the two sets of data are sufficient to determine uniquely the effective values for the two properties. Should the two web fractions bracket that of the actual motor, the properties thus determined can be considered as average values suitable for subsequent calculations.

2.4.3.2 PHOTOELASTICITY

Photoelastic material selectively retards polarized light in such a manner that fringes appear; the fringes are proportional to any shear strains that are present. Photoelastic materials may be applied as external coatings on bodies to be studied or may be used to construct two-dimensional and three-dimensional models of arbitrary geometry.

Two-dimensional modeling of grain cross sections that reproduces the strain distributions occurring in long (plane-strain) grains is the most frequently used of the photoelastic techniques. Parametric studies (refs. 55 and 56), conducted over a wide range of geometries simulating cross sections of case-bonded solid propellant grains, provide valuable information for initial design evaluations. Models used in these studies were plane stress, loaded by a uniformly distributed pressure around the periphery. They have been demonstrated analytically to be applicable to plane-strain, elastic propellant grains subjected to both ignition pressurization and to steady-state loads resulting from restrained thermal shrinkage. Studies of thermal transient loadings in both photoelastic and photoviscoelastic models demonstrate that linear-elastic-model results may be extended through the viscoelastic correspondence principle to linearly viscoelastic, thermorheologically simple materials.

The most useful information made available to the working analyst by photoelastic model studies is in the form of stress-concentration factors. These factors relate the stresses in the grain at the port free surface to the stresses applied on the outer boundary by the case. References 57 and 58 describe improvements in the technique for estimating the applied stresses. Reference 55 contains data for numerous port shapes such as those shown in figure 1. One significant point of this reference, made also in reference 58, is the general benefit derived from use of an elliptical fillet (fig. 1(l)) rather than a circular fillet at the star root. Parmerter's work (ref. 55) suggests that the optimal ellipticity (ratio of major to minor axes) will lie between 1.25:1 and 2.5:1; however, Sampson (ref. 58) more specifically states that a 2:1 ellipse will give the lowest concentration factors. The 2:1 ratio seems to be a good rule of thumb for design purposes.

By means of transmitted light, three-dimensional models can be examined for internal strain distributions. Either the scattered-light techniques (ref. 59) or the "frozen-stress" techniques (ref. 48) may be used. The development of the scattered-light technique, which uses a pencil of collimated polarized light, has been enhanced by the advent of lasers. The

30

column of light is passed through a point in photoelastic models at various angles, and the resulting fringes are observed and recorded. The stresses may be calculated (ref. 60) and the observations repeated for as many points as is necessary. Strains may be "frozen" in a loaded model by appropriate excursions in temperature, and the model subsequently can be sliced for examination. This freezing phenomenon occurs in certain polymeric materials categorized as diphase polymers. The deformations and accompanying birefringence resulting from an imposed load are locked in by cooling the specimen below the T_g of the material (ref. 48). Slices of the "frozen" model then can be examined using conventional two-dimensional photoelastic techniques, i.e., normal incidence and oblique incidence of the transmitted polarized light for the separation of the stress components.

Still another method for photoelastic analysis involves the use of birefringent coatings on free surfaces. The photoelastic coatings can be analyzed, using reflected polarized light, for surface strain distributions. The coating materials must be carefully selected and applied so that they do not reinforce the propellant. Because the coatings must be calibrated over a wide range of temperatures, the deduced strains are subject to question. As a consequence, this method has not gained wide acceptance.

2.4.4 Analyses for Specific Loads

The analysis used to obtain stress-and-strain solutions must be appropriate for the type of load involved. The more important loads include those resulting from (1) uniform cooling (no thermal gradients in space); (2) internal pressurization; and (3) axial, lateral, and spin-type accelerations. The influence of the motor case can be included in most solutions.

2.4.4.1 UNIFORM COOLING

Because the coefficient of thermal expansion for a solid propellant is almost always greater than that for case material (approximately 10 times greater when the case material is steel), natural shrinkages during cooling are different. To the degree that the case and grain are bonded together, this differential shrinkage will generate strains and, in turn, stresses. As the requirements for mass fraction increase (larger propellant volumetric loading) and the specified temperature excursions become greater, the necessity for more detailed thermal analyses become obvious.

The term "uniform cooling" implies cooling under conditions such that the temperature throughout the grain stays in continuing equilibrium, i.e., there are no temperature gradients in space. For this condition to occur, the diffusivity χ must be very large or the cooling rate very small. In practice, cold-environment test specifications usually require that a motor be kept in the low-temperature environment until it is near thermal equilibrium. In most

31

instances, the thermal stresses will be larger at the end of such a test than at any intermediate time. This condition does not imply, however, that the smallest margin of safety will occur at the lowest, or final, temperature during the test.

A comprehensive discussion of the practical implications of the assumption of uniform cooling (ref. 61) reports that the approximate time required for the port surface of a grain to reach 90% of a step temperature change imposed on the outer surface can be expressed as

$$t_{90} \cong \frac{(b-a)^2}{\chi} \tag{31}$$

For $\chi = 7.5$ cm^2/hr $= 0.0194$ in^2./min (a typical measured value for a PBAA[1] propellant), t_{90} was computed for three sizes of solid rocket grains:

Motor Size	Diameter		Web (b—a)		t_{90}, min
	in.	cm	in.	cm	
Small	4	10	1	2½	60
Medium	36	92	10	25	6000 (4 days)
Large	156	396	50	127	150 000 (3+ months)

Cooling (or cold soak) times much shorter than those above result in gradients that violate the assumption of uniform temperatures.

Calculations involving the closed-form solutions based on the assumption of plane strain are used for making preliminary judgments and decisions in problems involving thermal stresses. Table I, derived from the more complete listings of reference 1, gives equations for determining the stresses and strains in a uniformly cooled linearly elastic grain with a circular port. Plane strain and a thin case were both basic assumptions.

Parametric curves and formulas resulting from photoelastic studies (refs. 55 and 58) and from published numerical analyses (refs. 6 and 57) are useful for early decisions regarding the port shape. The curves presented in reference 8, pp. 5-41 to 5-46, reflect the influence the free ends have on the stresses and strains calculated from plane-strain equations.

For preliminary calculations, $E(t/a_T)$ is used as the effective modulus, the time required for the grain to achieve thermal equilibrium being taken into account. The temperature change ΔT typically is not measured from the cure temperature but rather from the so-called strain-free temperature, which is determined from STM studies. A characteristic port dimension (e.g., the diameter) is measured during slow cooling; the measurements are plotted against temperature. The temperature at which the diameter equals that of the mandrel is considered the strain-free temperature.

---

[1]Polybutadiene/acrylic-acid-based composite.

Table I. – Stress–Strain Equations for Restrained Thermal Shrinkage

Uniform Temperature Change

$T(r,\theta)$ = Constant

Plane strain:

$\epsilon_{zz}(t) = 0$

Boundary condition:

$\sigma_{rr}(a) = 0$

Stresses in the grain:

$$\sigma_{rr}(r) = - E \, \alpha \, \Delta T \, \left(\frac{b}{a}\right)^2 \left[\frac{1 - \dfrac{\alpha_c(1+\nu_c)}{\alpha(1+\nu)}}{\Omega}\right]\left[1 - \left(\frac{a}{r}\right)^2\right]$$

$$\sigma_{\theta\theta}(r) = - E \, \alpha \, \Delta T \, \left(\frac{b}{a}\right)^2 \left[\frac{1 - \dfrac{\alpha_c(1+\nu_c)}{\alpha(1+\nu)}}{\Omega}\right]\left[1 + \left(\frac{a}{r}\right)^2\right]$$

$$\text{where} \quad \Omega = \left[(1-2\nu)\left(\frac{b}{a}\right)^2 + 1\right] + \frac{\left[\left(\frac{b}{a}\right)^2 - 1\right](1-\nu_c^2)\,bE}{(1+\nu)\,hE_c}$$

Strains in the grain:

$$\epsilon_{rr}(r) = - (1+\nu)\,\alpha\,\Delta T \left\{\left[\frac{1 - \dfrac{\alpha_c(1+\nu_c)}{\alpha(1+\nu)}}{\Omega}\right]\left[1-2\nu - \left(\frac{a}{r}\right)^2\left(\frac{b}{a}\right)^2\right] + 1\right\}$$

$$\epsilon_{\theta\theta}(r) = - (1+\nu)\,\alpha\,\Delta T \left\{\left[\frac{1 - \dfrac{\alpha_c(1+\nu_c)}{\alpha(1+\nu)}}{\Omega}\right]\left[1-2\nu + \left(\frac{a}{r}\right)^2\left(\frac{b}{a}\right)^2\right] - 1\right\}$$

(The subscript c indicates a case property.)
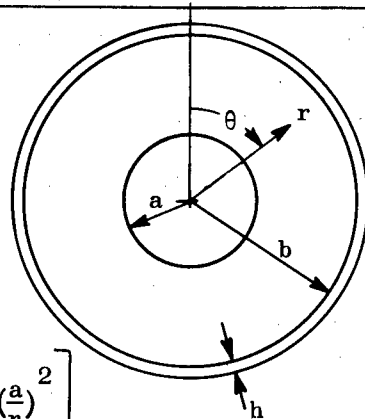
Viscoelastic stress-strain equations, e.g., equations (23) and (24), applicable to simple grain geometries (those that can be handled as one-dimensional problems) can be evaluated for most cooling histories (ref. 47). However, because the improvement in the resulting prediction is questionable, the calculation seldom is made.

The more precise calculations afforded by the finite-element programs for linearly elastic materials can be brought into use for evaluating the stresses and strains at or near conocyls, end reliefs, star valleys, and other geometrical features. Some attempts to develop numerical programs for solving for the thermal stresses in viscoelastic, thermorheologically simple materials have been made (refs. 37 and 62). However, because of the observed disparity between theoretical and actual propellant behavior, the value of such refined solutions continues to be questionable.

Another important thermal loading condition arises when a cold motor is subjected to aeroheating due to skin friction with the atmosphere. Because the thermal conductivity of the propellant is low compared with that of a metal case, the critical stresses can be conservatively approximated by assuming the grain to be uniformly cold and the case uniformly hot. This means that the case is subjected to a thermal expansion that increases the bond surface tractions. For failure analyses, a reaonsable temperature gradient through the case and liner is calculated or assumed, and the allowable bond stresses are established therefrom.

There is a great deal of evidence that propellants do not exhibit the property of thermorheological simplicity under simultaneous mechanical straining and thermal cooling. Reference 37, for example, describes an experiment in which a circular cylinder of propellant (2-in. (5.1 cm) diameter x 3-in. (7.6 cm) length) was cooled slowly from +140°F to -75°F (333°K to 214°K) with the flat ends restrained from relative displacement. The total force required to maintain the length was predicted with use of the classical analyses that have been described; the results are shown in figure 5. The required forces were three to four times those predicted. Similar test data in reference 20 shows quite different trends but further substantiates the nonlinear character of propellants. When propellants exhibit such behavior, STM's must be used to obtain meaningful property data. If predictions are needed prior to the qualification and preflight rating tests, the analyst must combine judgment and the laboratory characterization results to estimate the grain responses. At least one simultaneous-straining-and-cooling test is required in the laboratory characterization. The accuracy with which the force (stress) that is measured during such tests can be predicted is a measure of the value of conventional approach. Further, the differences between measured and predicted forces can be used as a guide for modification of the analyses to make them more meaningful.
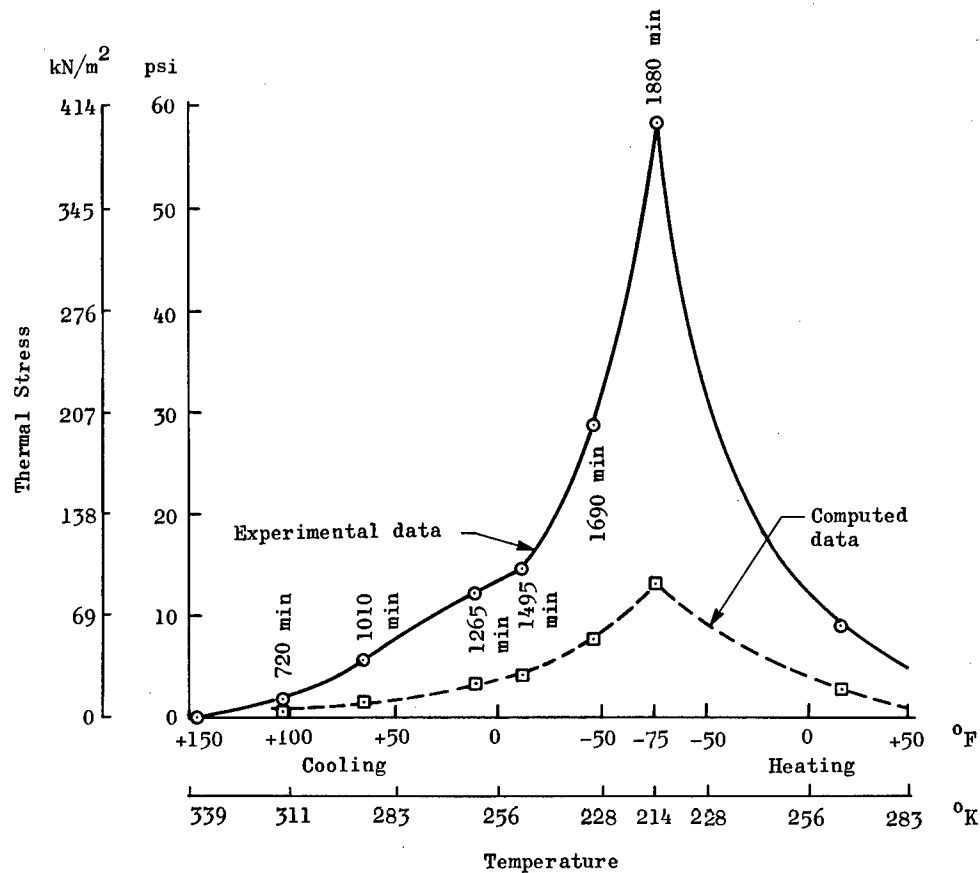
Figure 5. – Comparison of predicted and measured tensile stresses at
the platen of a cylindrical test specimen during cooling
and subsequent warming (adapted from ref. 37).

2.4.4.2 PRESSURIZATION

Pressurization during and after ignition is a critical load in many motors, especially when the thermal requirements are not severe and the case is relatively compliant. This loading condition usually is not prescribed by specification, and its characteristics depend on the temperature, ignition system, grain geometry, and many other factors. Rise times for ignition pressurization vary from 0.005 to 0.5 second, and thus impose stress and strain rates within the propellant that, in turn, strongly affect propellant properties (ref. 11).

35

Grains are subjected primarily to compressive stresses during firing pressurization; and the assumption of incompressibility within a compression field is more justifiable than the same assumption for a tension field, especially for the composite propellants. This difference is at least partly due to tensile stresses resulting in particle dewetting. Internal voids develop, and the apparent volume changes. The tendency for the solid particles to dewet is greatly reduced when the stress state is primarily compressive. Further, the failure strains (note that a combination of compressive stresses and tensile strains is possible during pressurization) are higher when the stresses are primarily compressive (ref. 52).

Equations for the stresses and strains in a plane-strain, circular-port grain are shown in table II. These formulas, based on the assumptions of linear elasticity, reflect the influence of the web radius ratio, Poisson's ratio, and case stiffness on the resulting stresses and strains. References 8, 55, 56, and 58 describe how to account for end effects and star-shaped ports.

For grain geometries for which the equations of table II are not applicable, finite-element stiffness computer programs have been formulated to consider stress boundaries such as those imposed by pressurization. Both plane-strain and axially symmetric geometries can be treated, as can the effects of the case. The restraining influence the grain exerts on the case during pressurization is slight; a circular cylindrical case, even though it has been distorted out-of-round by the thermal shrinkage of a nonsymmetric grain, will become round again under pressurization. This fact is important when calculating the deformed shape and stresses in grains with slots or dogbones where the elastic superposition of internal pressure loads on the deformed geometry (due to cooling from cure) will lead to significant errors. The better procedure is to determine the case deformations due to pressure alone, without a grain, and impose these displacements on the outer boundary of the grain as the pressure is applied to the inner boundary.

The pressurization problem with viscoelastic materials is readily solvable using quasi-elastic solutions and the convolution integral (sec. 2.4.2.2). During firing, the inner boundary ablates as the propellant ignites. This ablation reduces the stresses and strains by lowering the web fraction and by reducing the intensity of the stress concentrations due to geometry. Hence, use of the rising portion of the pressure-time trace and the original geometry will be a conservative treatment for most motors with regressive and neutral-burning patterns.

In typical problems, the assumption of propellant incompressibility has slight, though unconservative, effect on the values calculated for strains.

2.4.4.3 ACCELERATION

When a rocket motor is accelerated, stresses, strains, and displacements occur within the grain. These dynamic effects are incorporated into the equations of elasticity by adding displacement acceleration terms to the equilibrium equations.

Table II. – Stress-Strain Equations for Internal Pressurization

Internal Pressurization

Plane strain:

$$\varepsilon_{zz}(r) = 0$$

Boundary conditions:

$$\sigma_{rr}(a) = -p$$

(p = internal pressure)

Stresses in the grain:

$$\sigma_{rr}(r) = \frac{p}{\left[\left(\frac{b}{a}\right)^2 - 1\right]} \left\{ \left[1 - \left(\frac{b}{r}\right)^2\right] - \frac{2(1-\nu)}{\Omega}\left[\left(\frac{b}{a}\right)^2 - \left(\frac{b}{r}\right)^2\right] \right\}$$

$$\sigma_{\theta\theta}(r) = \frac{p}{\left[\left(\frac{b}{a}\right)^2 - 1\right]} \left\{ \left[1 + \left(\frac{b}{r}\right)^2\right] - \frac{2(1-\nu)}{\Omega}\left[\left(\frac{b}{a}\right)^2 + \left(\frac{b}{r}\right)^2\right] \right\}$$

where

$$\Omega = \left\{ \left[1 + (1-2\nu)\left(\frac{b}{a}\right)^2\right] + \frac{\left[\left(\frac{b}{a}\right)^2 - 1\right](1-\nu_c^2)\, bE}{(1+\nu)\, hE_c} \right\}$$

Strains in the grain:

$$\varepsilon_{rr}(r) = \frac{(1+\nu)\, p}{\left[\left(\frac{b}{a}\right)^2 - 1\right]E} \left\{ \left[1-2\nu - \left(\frac{b}{r}\right)^2\right] + \frac{2(1-\nu)}{\Omega}\left[(1-2\nu)\left(\frac{b}{a}\right)^2 - \left(\frac{b}{r}\right)^2\right] \right\}$$

$$\varepsilon_{\theta\theta}(r) = \frac{(1+\nu)\, p}{\left[\left(\frac{b}{a}\right)^2 - 1\right]E} \left\{ \left[1-2\nu + \left(\frac{b}{r}\right)^2\right] - \frac{2(1-\nu)}{\Omega}\left[(1-2\nu)\left(\frac{b}{a}\right)^2 + \left(\frac{b}{r}\right)^2\right] \right\}$$
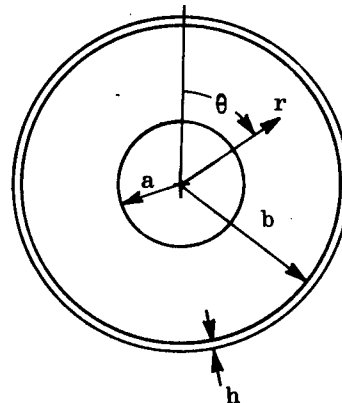
(The subscript c indicates a case property.)

37

The simplest acceleration load is that classed as uniform, i.e., the displacement acceleration terms entering the equilibrium equations can be considered as independent of time. This condition is not true for shock, where the acceleration terms are functions of time. Uniform accelerations range from 1 g (g = 32.2 ft/sec^2 [9.81 m/sec^2]) experienced by a motor at rest to hundreds of g's experienced by some specialized rockets during flight. Except for large motors, the effects of accelerations equal to or smaller than 1 g are unimportant unless the accelerations are continued over an extremely long time (e.g., storage). Some propellants and configurations under sustained loads have a tendency to take a permanent deformation that may influence ballistic performance significantly. During flight, longitudinal accelerations occur as a result of speed changes, and lateral accelerations occur as a result of directional maneuvers. Generally, spin-induced accelerations also can be classified as uniform and the resulting body forces treated as static loads or superpositions of static loads.

Shock is the rapid (nearly instantaneous) application of a force, usually to a localized region on the exterior of the motor case. This load arises primarily from dropping or other mishandling and seldom is a critical loading condition. Usually drop tests to establish the capability of the propellant to withstand shock are specified.

Another type of acceleration load occurs when the grain boundary is subjected to loads that may be characterized as oscillatory. Such loads occur during transportation of the motor and during free and captive flight. Because of the viscous nature of solid propellant, vibratory stresses and strains create heat, a corresponding increase in temperature, and a change in mechanical properties. This phenomenon in motor grains has not been satisfactorily modeled (mathematically), but the problem is minimized by providing sturdy grain support, eliminating possible points of friction, and utilizing a propellant formulation with a small loss modulus.

2.4.4.3.1 Uniform Acceleration

Because lateral accelerations are not axially symmetric, the finite-element computer programs cannot calculate the responses of finite-length grains. As a result, the curves and formulas derived for rather elementary models (refs. 3, 63, and 64) are used extensively as guides for evaluating the significance of this kind of load for a given grain design. Plane-strain bodies (long grains) with arbitrary cross sections, however, can be analyzed by the finite-element computer programs.

Because the loads usually are carried by the bending of the motor case and because the case walls are thin (i.e., compliant in the direction normal to their surface), the body forces in the grain usually are reacted by shear forces in the plane of the case wall. Such forces customarily are assumed to be distributed sinusoidally, with maximum shear flows 90° from the direction of the acceleration. The quasi-elastic technique then can be used to extend these elastic solutions, either closed-form or numerical, to give the viscoelastic responses.

38

A uniform axial (or longitudinal) acceleration may cause either large deformations affecting the motor ballistic properties or high stresses (primarily shear) tending to tear the grain from the case (refs. 65 and 66). For a long elastic grain with a circular port, the stresses, strains, and displacements are best calculated with closed-form solutions. These solutions are derived by noting that the shear at every radial coordinate must balance the body forces of the enclosed propellant. The most frequently used equations are given in table III. The more significant deflections and stresses due to axial accelerations, however, result from the end effects. These effects on the displacements for various grain geometries are shown by the curves presented in references 6 and 67.

The finite-element computer programs are appropriate for studying end effects, conocyls, and other axially symmetric geometric features. Again these solutions provide the quasi-elastic input necessary to evaluate the convolution integral (eq. (18)) for the particular acceleration prescribed.

2.4.4.3.2 Shock

Drop tests usually are required for small motors. Test requirements normally specify distance of free fall, orientation at impact, and material on which impact occurs. Typically, more than one orientation at impact is tested to produce both longitudinal and lateral accelerations. Some specifications require only that the grain not ignite on impact; others, with smaller drop distances, that the grain subsequently fire satisfactorily.

The shock problem is not amenable to analytical treatment because of the difficulty associated with defining the passage of stress waves through the irregularly shaped viscoelastic grain and the interaction of the waves with the case. The impact forces usually are applied at point locations on the motor case and tend to produce local damage of the case rather than the grain. Points with high stress concentrations on the grain port have been known to fail during shock, especially when the grain is cold. When the possibility for such failures is present, the only valid method of analysis is to conduct tests with instrumented STM's and measure the responses. Judgment coupled with static-body-force calculations provides the only indicators of continued structural integrity under this kind of load.

2.4.4.3.3 Vibration

Vibratory displacements may be characterized as axial, lateral, rotative, or combinations of these. However, specifications usually require test in only the first two of these modes. The analysis of solid propellant grains subjected to vibration has been covered by two extensive surveys (refs. 68 and 69). These surveys make it clear that a multitude of analytical solutions have been devised, the vast majority of them for elastic materials; but they also make it clear that correlations with the actual grain responses are sparse.

Table III. – Stress–Strain Equations for Longitudinal Accelerations

<u>Longitudinal Acceleration</u>

<u>Assumptions</u>:

1. Elastic grain

2. Rigid case

3. No end effects (or, equivalently, an infinitely long cylinder)

<u>Boundary conditions</u>:

$$\sigma_{rz}(r) = 0 \quad : \quad r = a$$

$$w \quad = 0 \quad : \quad r = b$$

<u>Stresses in the grain</u>:

$$\sigma_{rz}(r) = \frac{\rho \, N \, r}{2} \left[\left(\frac{a}{r}\right)^2 - 1 \right]$$

(N = number of g's acceleration)

<u>Strain and displacement in the grain</u>:

$$\varepsilon_{rz}(r) = \frac{\rho \, N \, r}{2} \left[\left(\frac{a}{r}\right)^2 - 1 \right]$$

$$w = \frac{\rho \, N}{2} \left[\frac{b^2 - r^2}{2} - a^2 \ln \frac{b}{r} \right]$$

Displacements
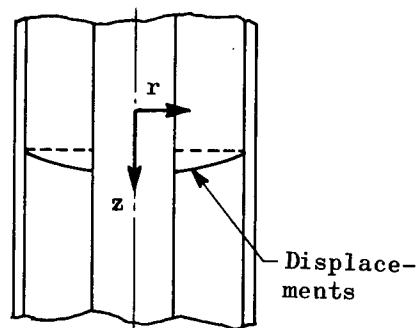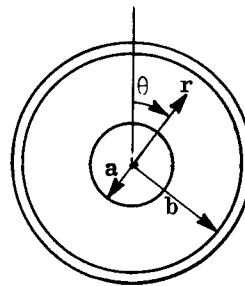
Failures of solid rocket motors during vibration tests have been observed and reported (ref. 5). Further, such failures have been duplicated in laboratories on various test models. Propellant-fatigue study programs on these models have been conducted (refs. 70 and 71). Results of a load-definition study of the correlation between actual service loads and vibratory loads specified for test are reported in reference 33. It was concluded that many of the test requirements, particularly those for continuous vibration at grain resonance, were overly severe.

The response of the entire system (case, grain, and attached hardware) to lateral vibration usually is analyzed by assuming that the system behaves as a beam. The dynamic analysis of such a simple model is straight-forward and is discussed in many textbooks, e.g., reference 72. Generally, bending and longitudinal stiffnesses of the grain are neglected relative to the case stiffness, but the mass of the propellant is taken into account (refs. 73 and 74). Other strength-of-materials solutions also provide for studying the influence of design variables and for supporting early design decisions on geometry. In reference 3, for example, the solution for the response of a weightless viscoelastic beam with a mass concentrated at the end is used to examine the behavior of star points. Plane-stress and plane-strain finite-element computer analyses for elastic materials subjected to steady-state vibratory loadings have been formulated (ref. 75). Figure 6 illustrates the kind of results that can be obtained when these programs are used to compute stresses and strains in a plane-strain motor cross section.

Axially symmetric responses to axially symmetric forcing functions on axially symmetric viscoelastic bodies can be handled by the finite-element program described in reference 76. This program provides for the effects of a dynamic modulus E^*, as illustrated in figure 7. For the geometry shown in figure 7(a), with storage and loss moduli as shown in figure 7(b), the responses shown in figure 7(c) were computed. The solid line in figure 7(c) presents the response as the ratio of maximum amplitude of the input to the amplitude of the response that would have been obtained had the body been rigid; the broken line shows the ratio of amplitude of the displacement at the far end of the case to that of the input.

A practical and ever-present difficulty in vibration testing is the inability to apply a pure axially symmetric excitation during a test. This deficiency results in other, coupled modes and an inability to correlate with the analytical predictions. In recent vibration tests of STM's (refs. 52 and 37), measured responses to vibration were radically different from those calculated.

Sustained vibration of a viscoelastic structure may lead to appreciable internal dissipative heating. Compounding the resulting thermal problem is the very low thermal conductivity of solid propellants, which inhibits transfer of thermal energy into the atmosphere. Dissipative heating is greatest in regions of strain concentration; and, unless the regions are near a cooled grain boundary, the local temperature rise can trigger ignition or weaken the grain to the point of fatigue failure or flow. The interaction between heating and dynamic response of viscoelastic bodies with temperature-dependent properties has been studied in
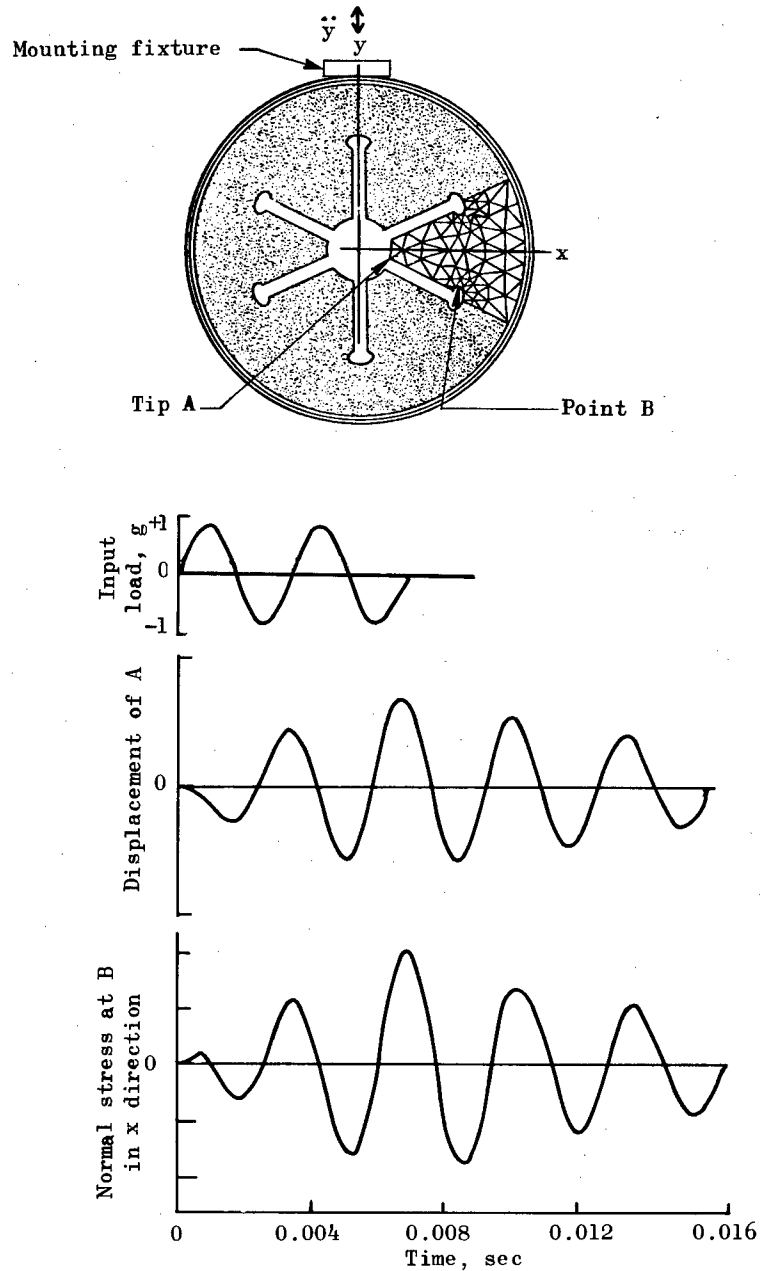
Figure 6. – Illustrative curves showing stresses and displacements in a motor cross section (calculated by finite-element computer techniques) (adapted from ref. 75).

42

(a) Schematic of two-layered cylinder

(b) Dynamic tensile modulus of core material

(c) Frequency response of two-layered cylinder with ends free
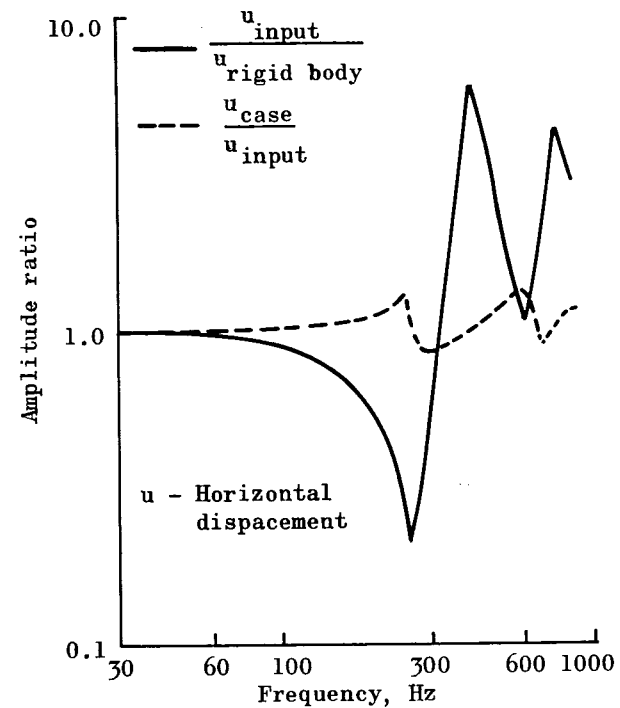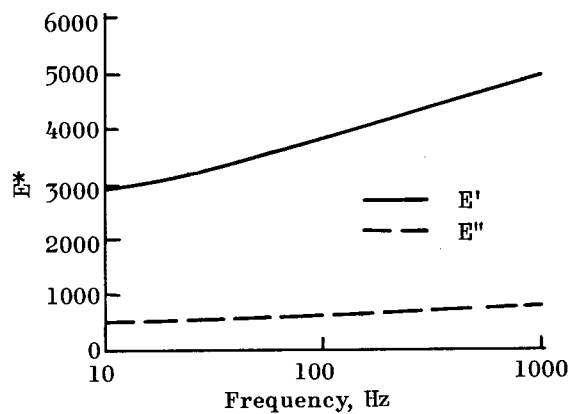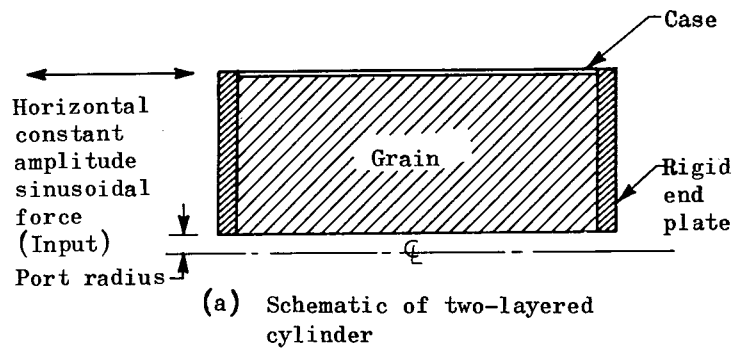
Figure 7. – Illustration of the use of a dynamic modulus in the finite-element stiffness method for analyzing steady-state sinusoidal-vibration problems (adapted from ref. 76).

43

simple geometries (refs. 77 and 78). However, solutions have not been devised for practical grain geometries. Typical practice is simply to locate regions of high strain and calculate q, the energy generated per cycle, from the expression

$$q = \pi(\epsilon^*)^2 \, |E^*| \, \sin\left(\tan^{-1}\frac{E''}{E'}\right) \tag{32}$$

where ϵ^* is the steady-state cyclic strain amplitude. The capability of the grain to dissipate this energy (heat) then can be evaluated; and, at any given point, the ΔT per cycle can be determined (ref. 1). Such calculations are crude estimates at best, and require skill and experience on the part of the analyst.

A motor in service usually experiences a random vibration rather than a steady-state harmonic vibration. Such random vibrations have become a test requirement for motor qualification; and they can be treated analytically if the responses to sinusoidal inputs can be calculated (ref. 79). In general, the load is defined in terms of the power spectral density as a function of the frequency, written as $G(\omega)$. For example, if the response to an input $I = I_o \exp(i\omega t)$ is $R = R_o \exp(i\omega t)$, then one can define the complex ratio

$$H(\omega) = \frac{R_o}{I_o} \tag{33}$$

The mean square value of the response $<R>^2$ to a prescribed random vibration can be expressed as

$$<R>^2 = 2 \int_0^\infty |H(\omega)|^2 \, G(\omega) \, d\omega \tag{34}$$

where

$|H(\omega)|$ = absolute amplitude of $H(\omega)$

$G(\omega)$ = input power spectral density

The response symbolized by R (usually a strain) is the quantity the analyst considers in evaluating the potential for heat buildup resulting from random vibration.

2.4.4.3.4 Spin

Some rockets are spun about the longitudinal axis to provide ballistic stability during flight. Spin rates may be high and the resulting body forces significant. There is little published

44

information concerning grain responses and failures that can result from this load. However, the stresses and strains at the inner port surface, at least for a steady-state angular velocity, are similar to those in uniform thermal cooling.

For a plane-strain motor with a circular center port and an incompressible propellant, formulas for the stresses and strains at selected locations (adapted from ref. 1) are

$$\sigma_{rr}(b) = \frac{-\left[\dfrac{\left(\left(\frac{b}{a}\right)^2 - 1\right)\omega^2}{6}\right]\left[3a^2\,\dfrac{\rho}{g} - \left(4b^2\,\dfrac{\rho_c}{g}\,(1-\nu_c^2)\,\dfrac{E}{E_c}\right)\right]}{1 + \dfrac{2}{3}\left(\left(\frac{b}{a}\right)^2 - 1\right)(1-\nu_c^2)\,\dfrac{bE}{hE_c}} \tag{35}$$

$$\sigma_{\theta\theta}(a) = \frac{\rho}{g}\,\omega^2 b^2 + \left[\frac{2\left(\frac{b}{a}\right)^2\,\sigma_r(b)}{\left(\frac{b}{a}\right)^2 - 1}\right] \tag{36}$$

$$\epsilon_{\theta\theta}(a) = \frac{0.75}{E}\left[\frac{\rho}{g}\,\omega^2 b^2 - \left(\frac{2\left(\frac{b}{a}\right)^2\,\sigma_r(b)}{\left(\frac{b}{a}\right)^2 - 1}\right)\right] \tag{37}$$

where, as before, a and b are the inside and outside grain radii, respectively, r and θ are the polar coordinates, and ω is the spin rate in rad/sec.

Note that both the stresses and strains are proportional to the square of the spin rate and that they are very nearly proportional to the square of the outer radius.

Plane-stress, plane-strain, and axially symmetric finite-element computer programs can be applied with equal facility to the solution of the spin problem. The quasi-elastic analysis is used to incorporate the time-dependent material properties into these solutions. However, time effects are not usually of consequence in spin responses, especially when the case is stiff (metal).

2.5 FAILURE ANALYSES

Failure of a rocket motor is defined as an unacceptable deviation in programmed performance or any change in the motor that ultimately will lead to such a deviation. The stress analyst normally is concerned with three forms of failure: fracture (cohesive and adhesive), excessive deformation, and autoignition due to grain heating. Once the temperatures, stresses, strains, and deformations have been calculated, they are compared with measured limit values that can be sustained without causing a failure. Specific techniques for each type of failure are used in making these comparisons.

2.5.1 Cohesive Fracture

Stress and strain states in critical areas of a propellant grain calculated for the prescribed and anticipated loadings are compared with measured failure data to determine whether or not the grain can survive to complete its mission. These comparisons cannot be based on a single parameter. Time, temperature, stress state, loading history, and geometry — all are important considerations.

As noted previously, fracture predictions fall into one of two groups (ref. 23) depending on the inherent or characteristic size of the flaw or crack pre-existing within the propellant: when the pre-existing cracks are not large enough to influence fracture (insignficant flaws), classical approaches are used; when the pre-existing cracks or other geometrical features will influence fracture (significant flaws), a fracture-mechanics approach is required. Figure 8 illustrates this concept.

Insignificant flaws. — A number of attempts have been made to establish a classical-type failure criterion for solid propellants (refs. 27, 80, 81, and 82). These attempts have had only a limited success, and at the present time a criterion valid for a reasonably general set of loading conditions is not available (ref. 83). Most of the investigations have sought to establish the criterion in a form of a failure surface constructed in principal-stress or principal-strain space. Various attempts have been made to correlate the failure surface with a suitable analytical criterion such as maximum tensile stress, maximum tensile strain, maximum shear stress or strain, or total strain energy (ref. 1). No particular analytical criterion has been found applicable for a wide range of propellant materials, but different criteria have been found to have limited or conditional ranges of validity. Sometimes two different criteria are needed to fit two different portions of an observed failure surface (ref. 80). The ability to calculate accurately the variable (either the stress or the strain) entering a criterion would indicate an inherent advantage of that criterion over a criterion in which the variable is not amenable to accurate computation.
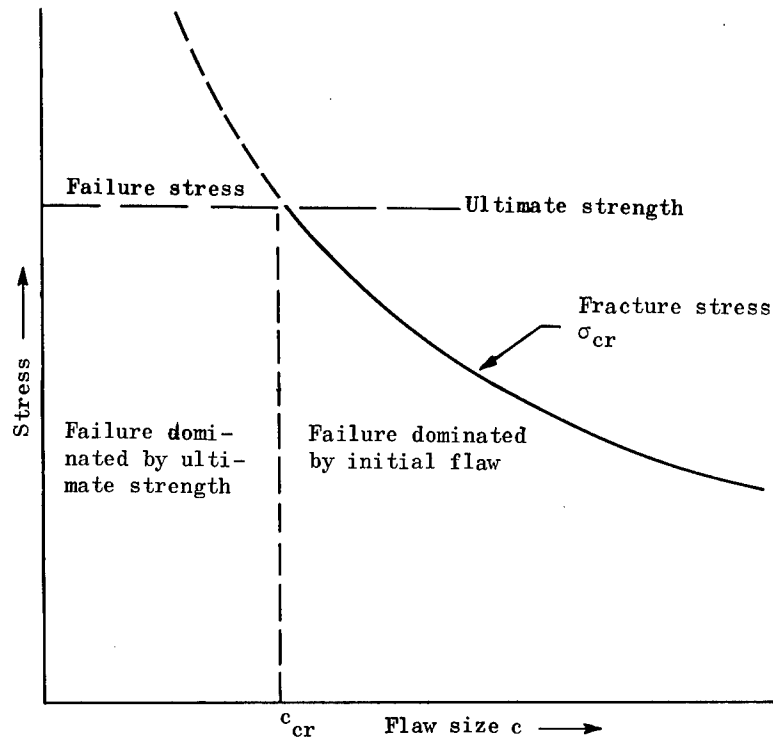
Figure 8. – Sketch of the conceptual relation between flaw size and
type of failure (adapted from ref. 23).

The use of the failure surface or failure envelope (fig. 9) for characterizing ultimate properties is a logical approach for materials whose properties are not functions of the loading history (ref. 84). Such logic is valid even if no analytical criterion can be correlated to the surface, since it is always possible to use the failure surface as a geometrical criterion or fit it with an arbitrary analytical equation. However, most solid propellant materials subjected to other than uniaxial states of stress (or strain) cannot be characterized by a simple failure envelope like that in figure 9, because their ultimate properties are strongly time-dependent. So if the failure surface is to be used to characterize the properties of such materials, it must be expected that the geometry of the surface will depend on the loading history. This condition immediately requires the definition of not one but many surfaces, since for each loading history a different set of failure conditions is appropriate. Therefore, a reasonably complete failure characterization presents major practical problems because of the large number of required experimental tests. On this account, certain empirical guides have been developed that, while not universal in nature, permit a comparison of the predicted and allowable motor response.

The first of these empirical guides recognizes that the time and temperature influences on failure can be interrelated by means of a shift factor, as is done for mechanical properties.
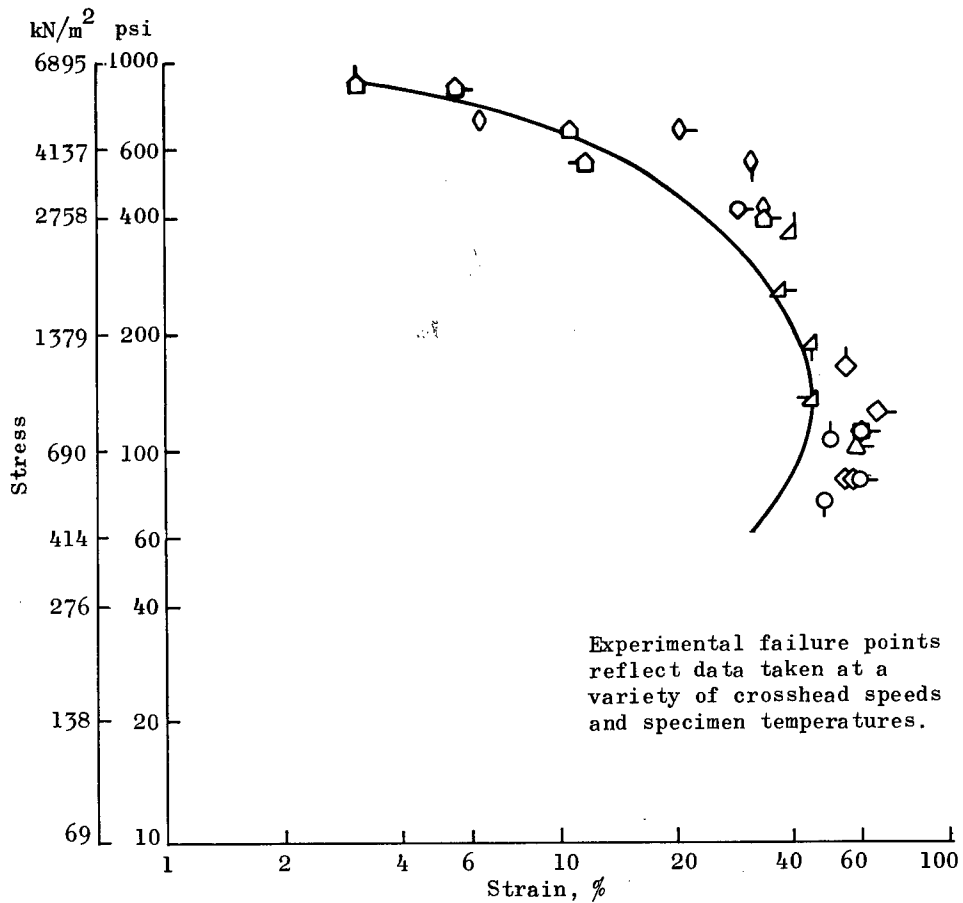
Figure 9. – Stress–strain failure envelope for a typical propellant, JANAF uniaxial specimen (adapted from ref. 52).

Tests thus can be performed at laboratory conditions and the results shifted to actual motor conditions. Figure 10 compares the predicted and experimental values for log a_T for shifting both the mechanical and the failure properties (ref. 85).

The subscript m on the variables in figure 10 indicates the maximum stress and the strain at the maximum stress during a constant-strain-rate test as described in reference 7. Typical data from such a test is shown in figure 11(a). Figure 11(b) shows the time dependence of typical failure data (in this instance, uniaxial data) for a propellant. The quantities are plotted against $\epsilon_m / (\dot{\epsilon}_o a_T)$ the reduced time required for the failure to occur.

The second empirical guide emphasizes the need to perform tests with specimens that duplicate the $\epsilon_m / (\dot{\epsilon}_o a_T)$ and state of stress at the point in the grain where failure is expected

48
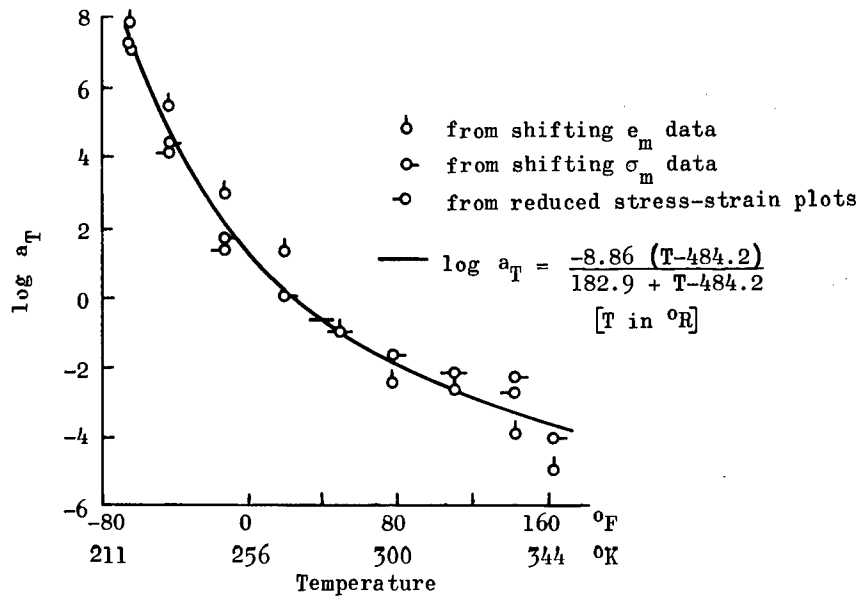
Figure 10. – Experimental values of log a_T compared with values predicted by the Williams–Landel–Ferry equation (adapted from ref. 85).

to originate. Further, the strain and temperature history that the motor element will experience should be duplicated as closely as possible. If the history and strain state were known in advance and could be exactly duplicated in the laboratory, a failure criterion would not be required. For solid propellants, the failure criterion can be used reliably only for small extrapolations from the test conditions. Following are examples of failure analyses based on tests duplicating the propellant condition of interest:

- Case-bonded propellant grains develop tensile stresses adjacent to the case bondline when they are exposed to temperatures lower than cure temperature. Near midlength of the grain, these stresses are hydrostatic tensile, and the strains are small. The failure analysis is conducted by comparing the predicted stresses with failure data from a triaxial tension (poker chip) test.

- Inner-bore grain surfaces experience biaxial stresses during restrained shrinkage (thermal cooldown) and triaxial (but not primarily hydrostatic) stresses during ignition pressurization. Failure analysis is performed by comparing bore strains with strain failure data on unpressurized and pressurized biaxial strips (or with pressurized tensile strain data corrected to the biaxial state).[1]

---

[1] Internal pressurization loads develop an interesting phenomenon. Failure from other types of loads usually is preceded by particle dewetting in the propellant, but an imposed pressure retards dewetting. So both the failure stresses and strains are increased when dewetting is impeded by the pressurization.

49
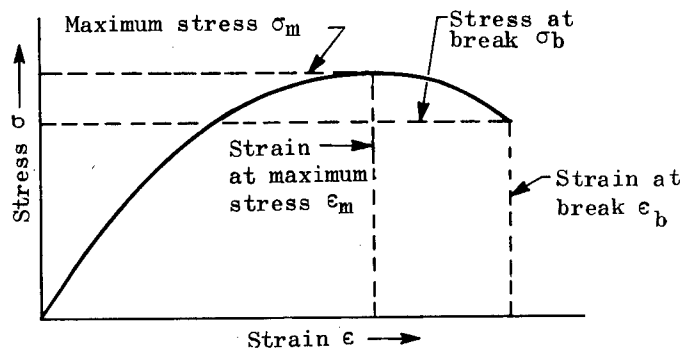
(a) Typical stress-strain curve for a
     composite propellant, constant
     strain rate
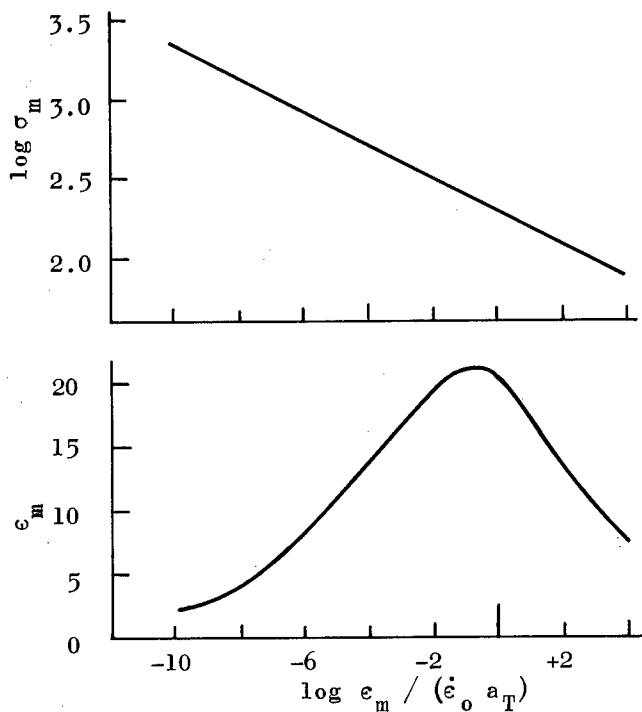
(b) Variation of σ_m and ϵ_m with time
     and temperature (data reduced to
     $77^{\circ}F$ $(298^{\circ}K)$).

Figure 11. – Typical uniaxial failure data (adapted from ref. 85).

50

The third empirical guideline is to base predictions on the variable one can calculate with the most confidence. If the strain state and history and, in turn, the stress state and history to be experienced by the grain are duplicated exactly by the laboratory test, then the only consideration would be: Which responses can be calculated with the greater accuracy? For thermal loads, the calculated strains at the port usually are more reliable than the calculated stresses; for acceleration loads, the calculated stresses are more reliable.

Significant flaws. – Propellant grains frequently have flaws that result either from processing or from prior loads. In such instances, it is appropriate to apply fracture-mechanics theory to determine whether the flaws will grow during subsequent loading (ref. 44, 86, and 87). This determination involves calculating the strain energy lost from the body as the crack propagates (body restraints are reduced) and comparing it to the work necessary to form new surface area. The latter is a property of the material established by laboratory tests (sec. 3.2.3) that is termed the characteristic strain-energy release rate γ. If the crack is internal in a given material, the subscript c is used to indicate the cohesive release rate γ_c; if it is a crack propagating along a bonded area between differing materials, the subscript a is used to indicate adhesive release rate γ_a.

For linearly elastic systems where kinetic contributions may be considered negligible, the energy-balance relation that describes fracture criticality is (ref. 88):

$$\left. \frac{\partial U}{\partial A} \right|_c = \gamma \tag{38}$$

where

γ = characteristic strain-energy release rate

U = strain energy

A = free surface area

and the subscript c implies that the boundary displacements are held constant for evaluation of the derivative, i.e., evaluation of the change in the strain energy as the free surface area increases with crack growth.

Therefore, to define criticality conditions for an arbitrary body and constant boundary displacements, it is necessary to equate the rate of change of the strain energy with the characteristic strain-energy density. The strain energy may be described as

$$U = \int_{volume} U_o \, dv \tag{39}$$

51

where v is the volume and U_0 is the strain-energy density defined as

$$U_o = \frac{1}{2} (\epsilon_{ij} - \alpha \Delta T \delta_{ij}) \sigma_{ij} \tag{40}$$

The release of strain energy due to crack growth can be calculated numerically (ref. 89) or, for a crack (or cracks) emanating radially from a circular port in a plane-stress or plane-strain body, analytically (ref. 90). The numerical calculations require an evaluation of the strain energy, element by element, for incremented crack lengths. The sums of the elemental strain energies give the total strain energies of the body as the crack extends.

2.5.2 Adhesive Bond Fracture

Under load, case-bonded propellant grains develop tensile and shear stresses at the propellant/liner/case interface bonds. These stresses are calculated by the techniques described in section 2.4.

If a liner is to be used in the motor, a bimaterial poker chip (or joint-in-tension) specimen including representative liner material is used to establish the failure stress. The specimen bond must be made identical to that of the motor because of the characteristic sensitivity of the tensile strength to the processing techniques (ref. 29). The maximum-principal-stress criterion is used to incorporate the influence of the shear.

When aerodynamic heating of the case is a critical loading condition, the tractions on the bond surfaces between the case and grain must be considered. To be conservative, the grain is held at the original temperature and the case temperature is allowed to rise. The temperatures expected at the bonds as determined by thermal analysis, are used to establish the value of the maximum stress.

Near bond-area terminations, another difficulty appears. When the stresses, both tensile and shear, along the interface between differing materials are calculated by use of infinitesimal elasticity, a singularity (mathematically infinite stresses) occurs at the edges of the bonded area. The presence of the singularity means that, even if an allowable stress at the separation line for the grain/case interface were known, a finite stress for comparison with it would not be predicted by classical analysis.

An alternative is to use fracture-mechanics theory to evaluate the tendency for such an interface crack to grow as the assumed crack size approaches zero (ref. 89). This procedure at least permits a quantitative comparison of termination designs. The fracture-mechanics approach to adhesive failures also is valuable when debond areas are discovered and one wishes to determine by analysis whether or not they will grow larger.

Determination of the strain distribution throughout the loaded body and subsequent integration or summation of the strain-energy densities over the volume frequently requires use of a finite-element computer program. The procedure is identical to that described in the previous section except that γ_a is used as the characteristic energy release rate. Inclusion of a routine for calculating the strain energy for each individual element is a relatively simple task, and the total strain energy is simply the sum of the elemental energies. The technique is described in reference 91.

2.5.3 Excessive Deformation

Ballistic performance of a motor, being dependent on propellant geometry, will change if the grain is deformed. Minor geometric changes such as those that occur during thermal cycling (except cracking) can be tolerated. Slump may occur during long-term storage (ref. 66) or as a result of vibration (refs. 5 and 92). In either event, slump may be such that it alters ballistic performance or even causes case rupture when the motor is fired. In certain applications, excessive deformations may arise during free-flight thrust and maneuvering acceleration. Cartridge-loaded grains are always checked for the possibility of nozzle choking when gas pressures can be exerted between the case and the grain. Deformations calculated in the stress analysis are evaluated for their effects on the ballistic performance to determine if the deformations are allowable.

2.5.4 Autoignition

Solid propellants may be ignited by exposure to hypergolic materials, static discharges, high temperatures, surface abrasions, or shock waves. Current safety measures have been effective against hypergolic reactions and static discharge; but the other environments, any of which may be encountered during the service life of solid propellant grains, still represent hazards.

High temperatures result from hot environments, from aerodynamic heating during flight, and from internal heat dissipation during vibration. Currently it is believed that autoignition depends not only on temperature but also on the time of exposure to that temperature. Ignition may occur at relatively high temperatures after only short exposure times and at lower temperatures after relatively long exposure times. The probability of autoignition is evaluated by calculating the grain temperature at various times under storages and service conditions, then comparing the calculated values with test data on ignition temperatures and time of exposure (ref. 93).

2.5.5 Cumulative Damage and Margin of Safety

Application of a load to a solid propellant results in mechanical damage, even though such damage may not be readily detectable. Subsequent loads cause additional damage, until failure finally occurs. Various approaches, including a modified linear-cumulative-damage theory (refs. 1 and 94), have been investigated for predicting propellant response to cumulative loads. All theories suffer from difficulties in evaluating cumulative damage that results from thermal excursions because it is not yet possible to accurately predict even single-excursion responses.

The classical Miner's law (ref. 95) has been more widely accepted than any other theory for predicting the accumulation of damage due to sequential or superposed loadings. This acceptance has resulted primarily from the ease with which it can be applied. This law, traditionally applied to metals subjected to repetitive (or fatigue) loads of differing magnitudes, is expressed as

$$\sum D_k = \sum \frac{n_k}{N_k} \qquad (41)$$

where

D_k = damage fraction added by the application of the kth load level

n_k = number of cycles at the kth load level

N_k = number of cycles measured for failure at the kth load level

When $\sum D_k$ becomes equal to 1.0, it is hypothesized that failure will occur.

For propellants, a more appropriate formulation for the law is based on time to failure under constant stress (ref. 92):

$$P \sum D_i = \sum_{i=1}^{n} \frac{\Delta t_i}{t_{fi}} \qquad (42)$$

where

P = probability distribution function observed during replicate laboratory failure tests

D_i = damage fraction added by the application of the ith stress level

Δt_i = time specimen is exposed to i^{th} stress level

$\overline{t_{fi}}$ = mean time to failure if specimen experienced only i^{th} stress level

To make equation (42) applicable to arbitrary stress histories, a continuous relationship between the time to failure and the applied stress must be determined. It is assumed to be of the form

$$\overline{t_f} = t_o \, a_T \left(\frac{\sigma_{ot} - C}{\sigma_t - C} \right)^B \tag{43}$$

where

$\overline{t_f}$ = mean time to failure at any stress σ_t

t_o = time to failure at a specified stress σ_{ot}

a_T = time-temperature shift factor

C = arbitrary constant to fit measured data (usually zero for propellant)

B = negative slope of the log/log plot of σ_t vs $\overline{t_f}$

This expression $(\sigma_t - C)$ is fitted to a plot of failure times observed for specimens subjected to a constant stress. The damage accumulated during other arbitrary stress and temperature histories is then evaluated from

$$\sum D_i = \frac{1}{P \, t_o \, (\sigma_{ot} - C)^B} \int_0^t \frac{(\sigma_T - C)^B}{a_T(\tau)} \, d\tau \tag{44}$$

When the sum $\sum D_i$ becomes equal to 1.0, it is predicted that failure will occur.

55

A similar approach is available when the maximum-principal-strain theory is used for comparison with the predicted strains. The equivalent of equation (42) is

$$P\sum D_i = \sum_{i=1}^{n} \Delta \epsilon_i \Big/ \overline{\epsilon}_{fi} \tag{45}$$

where

$\Delta \epsilon_i$ = increment of strain at i^{th} rate and temperature

$\overline{\epsilon}_{fi}$ = mean failure strain at i^{th} rate and temperature

The probability function P is simply a ratio of time (or strain) at failure for a particular probability of failure to the average time (or strain) to failure for the population; it thus represents the statistical spread of the failure data about the mean time (or strain).

Equation (45) can be used in combination with either equation (42) or (44) to account for the accumulation of damage due to acceleration stresses superposed onto the damage due to thermal strains.

Historically, the end result of the failure analysis has been calculation of a margin of safety MS defined as

$$MS = \frac{\overline{R}_a}{R} - 1.0 \tag{46}$$

where

$\overline{R}_a$ = average allowable response (e.g., failure stress or strain)

R = calculated response

The significance of the margin of safety calculated as shown, however, is clouded by several important influences for which equation (46) does not account; e.g., the accumulation of damage during sequential and simultaneous loading, phenomena that are not yet well understood. Moreover, the equation is based on the assumption that the distribution of failure times is independent of stress (strain) level. Further, there is scatter in both (1)

56

responses generated in the grain during service and (2) responses the grain is capable of surviving. Variations in the mechanical properties of the propellant lead to the first condition; cumulative damage from loadings, batch-to-batch differences, aging, and chemical changes lead to the second condition. These scatters are illustrated in figure 12. Figure 12(a) compares the distribution of actual service responses $f(R)$ and the cumulative probability of the material allowable responses $G(R)$ for a grain in which the scatter in each distribution is large; figure 12(b) presents a similar comparison for a grain wherein the scatter is small. If average values R_s and R_a of the actual and allowable responses are used to compute the margin of safety, the values will be the same for both distribution (a) and distribution (b). Yet the probability of failure (the cross-hatched area)

$$P_f = \int_{-\infty}^{+\infty} f(R) \, G(R) \, dR \tag{47}$$

is much greater for (a) than for (b).

Ideally, the probability of failure rather than the margin of safety would be calculated and reported. However, data required to generate meaningful, quantitative distribution curves are expensive to gather and are not collected during most motor development programs. Consequently, a compromise approach usually is taken. When possible, the variabilities in the allowables due to cumulative damage, aging, and processing are determined by tests and are accounted for by adjusting the calculations. The remaining scatter is assumed to be distributed in either a normal (Gaussian) or logarithmic-normal manner. Sufficient tests are performed to determine the standard deviation of the assumed distribution.

Specific test loads representative of the service life are prescribed to the designer. The statistical characteristics of the motor ignition pressures are assumed, the assumptions being based on experience and, as the program progresses, on results of actual firings. The scatter caused by errors in experimental values and in analytical techniques used to calculate test-load responses are disregarded. The compromise approach then calls for the calculation of a margin of safety using reduced allowables, the amount of the reduction from the average depending on the observed scatter. For pressure loadings, the calculated average response is similarly increased in accordance with the expected pressurization scatter. Responses to other test loads are treated as if there were no scatter.

A technique for data collection and evaluation that will permit realistic calculation of a probability of failure is presented in reference 24. The technique accounts for the variation observed during loading (from experience with the motor being studied or from prior experience); variations in the relaxation modulus (from a linear regression analysis of replicate tests); and variations in the failure data (from a probability function such as that in
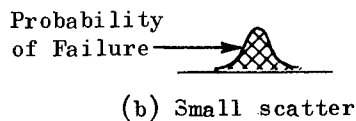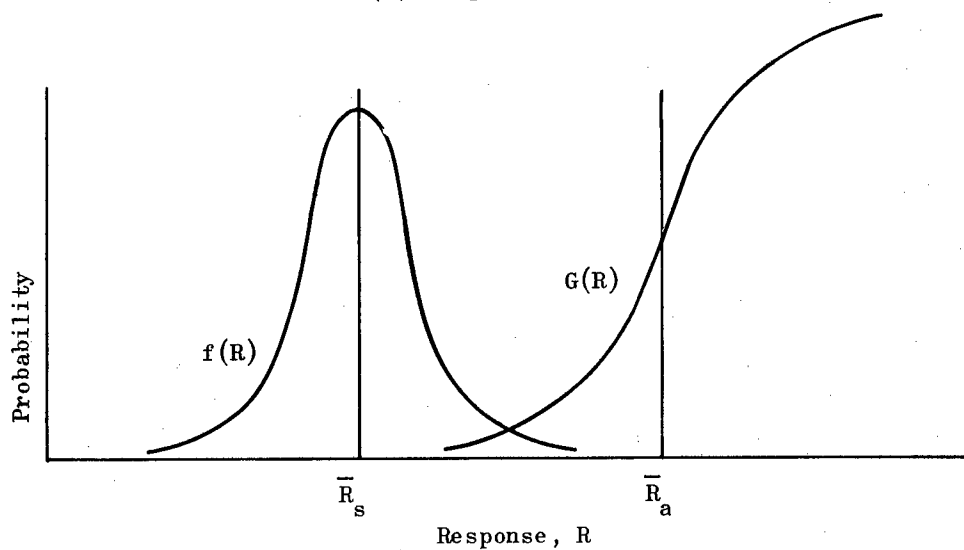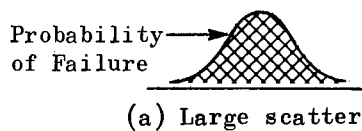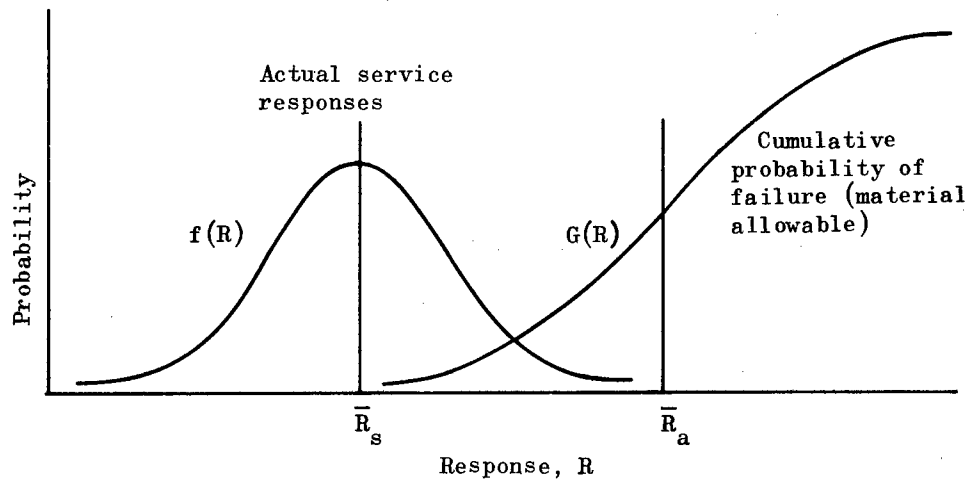
Figure 12. – Curves illustrating how response scatter influences the calculated probability of failure of a propellant grain.

58

equation (42)). From these distributions the analyst computes not only the mean margin of safety from

$$MS = \frac{1}{\Sigma D_i} - 1 \qquad (48)$$

but also a distribution of the margins of safety. That portion of the distribution having negative values is the probability of failure determined by the best parameters the analyst normally has available to him.

3. DESIGN CRITERIA and

Recommended Practices

3.1 GRAIN GEOMETRY

The grain geometry shall not violate the requirements for structural integrity.

The stress analyst should be familiar with the details of grain design (ref. 11). During the grain design procedure, the stress analyst should assist in selection of materials and optimization of the geometry. Initial and preliminary assessment of each candidate design (special attention usually is given to star valleys, end terminations, and similar geometrical features) should be based on experience supplemented with approximate calculations and parametric data such as that available in references 6, 48, 55, 88, and 96. Detailed and quantitative analyses should be performed after the material has been selected and geometric design has become relatively stable. These analyses should consider interrupted case bonding, stress-relief systems, internal grain supports, sharp corners (singularities), and similar features significant to the structural integrity.

3.2 PROPELLANT PROPERTY CHARACTERIZATION

Test procedures and methods of data reduction shall provide the propellant properties necessary to evaluate the grain response to all specified and predicted loads and verify grain structural integrity throughout the mission.

The tests selected for propellant characterization will depend on the application for which the results are to be used. The deviations from the basic analytical assumptions that have been observed in propellants force the prescription of laboratory tests reproducing what is expected or being studied in the grain. For example, vibration tests must be used to measure the properties necessary for a meaningful prediction of response to vibration. The conventional tests (constant strain rate, stress relaxation, etc.) give properties that probably are not valid for a vibratory load. Further, there is a lack of a universal failure criterion appropriate for all loading conditions and states of stress. So it is imperative the stress analyst participate in the planning, execution, and data-reduction phases of the characterization program in order to ensure that the types of tests and the testing procedures will produce data valid for the intended uses.

60

The specific procedures for the tests and use of the data are set forth in sections 3.2.1 through 3.2.4.

3.2.1 Thermal Properties

The thermal properties used for evaluating the stress/strain states shall be demonstrably characteristic of the propellant.

Test methods recommended for determining values for the basic thermal properties required for the stress-strain equations are listed in table IV.

Table IV. — Recommended Tests for Thermal Properties

Property	Recommended test	Remarks
Coefficient of thermal expansion α	Structural test motor (ref. 7, sec. 4.8.2)	This method is preferred because it gives an "effective" value for propellant under realistic motor conditions.
	Quartz-tube dilatometer (ref. 7, sec. 4.9.1)	Alternate method.
Mean specific heat c	Differential scanning calorimeter (ref. 18)	
Thermal conductivity k	Modified ASTM Method D2214 (ref. 19)	This test defines thermal conductivity k. Diffusivity is then computed from
Thermal diffusivity χ		$\chi = \dfrac{k}{\rho c}$ where ρ = density c = mean specific heat

61

3.2.2 Mechanical Properties

The mechanical properties used for evaluating the stresses, strains, and displacements shall be demonstrably characteristic of the propellant.

If the assumptions of linearity and thermorheological simplicity are valid for the material, there will be a unique relationship between the moduli and time-temperature shift derived from the cyclic tests and those determined by the relaxation tests, the creep tests, the constant-rate tests, or any other loading history. However, because the two assumptions are not valid for most solid propellants (indeed they have been shown to be far from it (ref. 20)), the derived relationships are not valid and should be used with caution.

The alternative is to use specimens and loading histories as representative as possible of the conditions for which the analysis is to be performed. The specimen geometry should be chosen to generate a state of stress (or strain) comparable to that the grain will experience, and the loading history should reproduce the temperature and other significant environments to which the propellant will be exposed.

The principal properties required for stress analyses are listed in table V, together with the tests recommended for their determination. Details of the tests are set forth in the text that follows.

Relaxation modulus. — The uniaxial constant-strain-rate test should be conducted exactly as prescribed in reference 7, section 4.3.6.1. The Class A JANAF specimen should be used. A sufficient variety of rates and temperatures must be run to define the relaxation curve completely, values for the rubbery and glassy moduli being included. Each individual test gives a curve of stress vs strain or the equivalent time as shown by the solid curve in figure 13. As illustrated in the figure, an initial toe of increasing slope sometimes is observed during these tests. For purposes of data reduction, this portion of the curve should be disregarded and the curve should be extrapolated back to zero stress with a slope proportional to t^{1-n} (n is the slope of the log/log plot of relaxation modulus vs time), which for practical purposes is a straight line. This extrapolation, also shown in figure 13, establishes the origin from which the secant modulus calculations are made, using

$$E_s(t,\epsilon) = \frac{\sigma(t)}{\epsilon(t)} \tag{49}$$

Such calculations will yield several modulus values corresponding to different strain rates and magnitudes. If a curve is drawn through the points representative of each strain level, a family of curves results. The vertical spacing of the curves is indicative of the degree of nonlinear behavior expected as a function of strain magnitude. These changes are reflected

62

Table V. — Recommended Tests for Mechanical Properties

Property	Recommended test	Remarks
Relaxation modulus $E_{rel}(t)$	Uniaxial constant strain rate (ref. 7, sec. 4.3.6)	
	Biaxial constant strain rate	Provides basis for assessing the influence of the state and magnitude of stress on the modulus.
	Simultaneous straining and cooling (biaxial specimen preferred; uniaxial specimen an alternate	Provides basis for assessing deviation from the assumptions of linearity and thermorheological simplicity.
Creep compliance $D_{crp}(t)$	Uniaxial constant stress (ref. 7, sec. 3.6.2) or constant stress rate	Methods similar to those described for finding the relaxation modulus may be used for the creep compliance if desired.
	Biaxial constant stress or constant stress rate	
Dynamic modulus $G^*(\omega)$	Double-lap shear vibration	Preferred.
	Vibrating plate (ref. 7, sec. 4.6.2.1)	
	Oscillating plate (ref. 7, sec. 4.6.2.2)	Any of the latter three can be used if necessary testing equipment is available.
	Fitzgerald transducer (ref. 7, sec. 4.6.2.3)	
Poisson's ratio ν	Structural test motor (STM)	ν can be used to compute K for tensile stresses.
Bulk modulus K	Large pressurized-block test (ref. 6)	Provides direct evaluation of K for compressive loadings.
Density ρ	Large-block density measurement	Primary method.
	ASTM D-297 (ref. 21)	Alternate method.

63
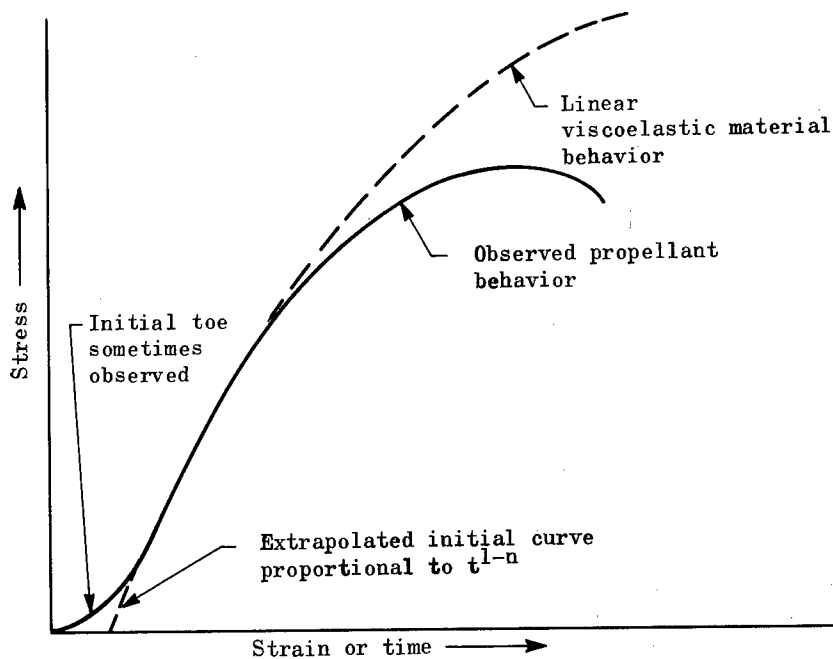
Figure 13. – Typical stress–strain curve resulting from a uniaxial constant rate test.

in figure 13 by the way the observed stress-strain curve falls away from that predicted by linear viscoelastic theory. However, the strain dependence of the secant modulus does not reflect all the nonlinearity the propellant may possess (e.g., the Mullins effect [ref. 98]) but can only be considered a warning of the inapplicability of linear analyses.

When the disparity between strain levels can be resolved, the relaxation modulus can be determined by the use of the secant modulus and the expression

$$E_{rel}(t) = E_s(t) \left(1 + \frac{d \log E_s(t)}{d \log t} \right) \qquad (50)$$

The shift factor required to cause the moduli at various temperatures to overlap and to coalesce into a single curve may be determined from either the secant or the relaxation modulus values.

64

Because the stiffness properties also may be dependent on the state of stress (refs. 37, 44, 52, 96, and 99), it is recommended that some tests be made with specimens having states of stress similar to those expected within the motor. For ported grains, the biaxial strip specimen (fig. 14) seems best suited for this purpose. The primary tensile strain ϵ_x on the
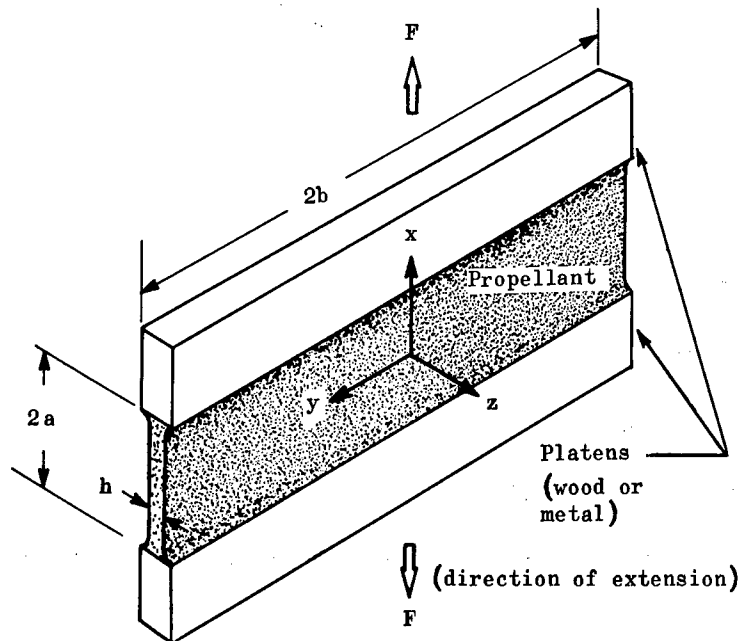
Figure 14. – Biaxial strip specimen.

specimen corresponds to the circumferential strain in the motor, and the lateral strain ϵ_y corresponds to the longitudinal strain in the motor. Because of the absence of constraint through the thickness of the specimen, the normal stress and strain in the z direction is different from the radial stress and strain in a motor except at the free port surface, where they are identical. So the properties measured with the biaxial strip are valid for the free surface at the port and also provide the best approximation available for the interior of the web.

Platen displacements, linkage forces, and specimen temperatures must be recorded as a function of time during the biaxial test. The platen displacements are divided by the initial platen spacing to compute the primary strains ϵ_x. (It would be preferable to measure independently the strain or relative displacements of points well within the test specimen itself; this kind of measurement is not usually made, and the resulting errors probably are small). To determine the distribution of the stresses, it is necessary to use tabulated solutions: analytical (ref. 100), numerical (ref. 101), or experimental (ref. 50). These

65

distributions are a function of the aspect ratio b/a and lead to expressions for the tensile modulus. For example, the modulus in an elastic specimen as shown in figure 14 can be expressed as

$$E = \frac{1}{k(b/a)} \left[\frac{Fa}{2bh\Delta a} \right] \qquad (51)$$

where

a = specimen half-height

b = specimen half-width

h = specimen thickness

F = total force on the specimen

Δa = one-half the total displacement of the platens with respect to each other

$k(b/a)$ = a factor obtained from the curve of figure 16 of reference 101

The influence of strain state should be evaluated by comparing the modulus determined for biaxial specimens with that determined for uniaxial specimens. Generally, this comparison will indicate that the moduli have the same shape when plotted against time on log/log scales, but that the biaxial modulus has slightly higher values. When such differences are observed, a correction to the small-strain uniaxial modulus should be incorporated into subsequent stress-strain calculations.

Another test supplementing the uniaxial modulus data should be made to establish the validity of the assumption of thermorheological simplicity, viz., simultaneous straining and cooling tests, preferably with the biaxial strip specimen (the alternative being the uniaxial specimen).This test should be performed at straining and cooling rates typical of those the motor is expected to experience. The linkage force necessary to impose a constant strain rate should be measured and compared with the force calculated by the use of the relaxation modulus $E_{rel}(t/a_T)$ [eq. (29)]. If there are significant differences, the relaxation modulus again should be shifted, vertically, before the thermal stresses for the grain are calculated.

Creep compliance. — If it is necessary to calculate strains resulting from given stresses, the creep compliance $D_{crp}(t)$ must be determined by tests. Specimens appropriate for this test

are the same as those for the relaxation modulus: JANAF uniaxial for primary data, and biaxial strips for supplementary and confirmatory data. Either a constant stress or a constant stress rate may be the prescribed loading. The constant-stress test is described in reference 7, section 4.3.6.2. When the constant-stress-rate test is used, the secant compliance D_s should be determined from

$$D_s(t,\epsilon) = \frac{\epsilon(t)}{\sigma(t)} \qquad (52)$$

and the creep compliance from

$$D_{crp}(t) = D_s \left(1 + \frac{d \log D_s}{d \log t} \right) \qquad (53)$$

Again, a shift factor to reflect the influence of temperature must be evaluated. The significance of nonlinearities due to both the state and magnitude of stress also should be evaluated.

Dynamic modulus. – For cyclic or vibratory loadings, the dynamic modulus must be determined. The recommended practice is to measure the dynamic shear modulus $G^*(\omega)$ directly, using a double-lap shear test, because values of the G^*'s derived from relaxation or compliance data have been found to be too small. Care should be taken during the shear test to maintain constant spacing of the platens and impose only small strains. The resulting data (linkage forces and displacements vs time) are used to calculate the real and imaginary parts of G^* from

$$G'(\omega) = \frac{\sigma_o}{\epsilon_o} \cos \delta \qquad (54a)$$

and

$$G''(\omega) = \frac{\sigma_o}{\epsilon_o} \sin \delta \qquad (54b)$$

where

σ_o = the amplitude of the shear stress

ϵ_o = the amplitude of shear strain

δ = arctan (G''/G')

Both G' and G'' change during a test, having high initial values that decay rapidly until they approach asymptotes after many cycles. For repetitive-type loads, it is recommended that both the initial and long-term properties be determined, so that calculations and judgments can be made for both conditions.

Bulk properties. – The direct method of determining the bulk modulus is to subject a large block of propellant to uniform pressure and measure dimensional changes, usually with electronic sensors. This technique has the benefit of giving K directly at constant temperature. However, the propellant is in compression, an unrealistic state of stress that rarely occurs in motor grains.

A better approach for the determination of K, and the one recommended, is to obtain values for ν and α by the use of STM's, as noted in section 2.4.3.1 in the presentation of equation (30). The value for K (appropriate for tensile stresses) then can be obtained by suitable rearrangement and solution of equations (6) and (7).

Density or specific gravity measurement must be made so that the forces involved when the propellant grain is subjected to acceleration loadings may be calculated. The method described in reference 21, wherein a small specimen of propellant is weighed when submerged in a fluid compatible with the propellant, is recommended. However, if the accurate measurements required in this method are impractical, a large-block density determination (ref. 6) is an acceptable procedure.

3.2.3 Failure Properties

The failure properties used for evaluating the margins of safety against failure shall be demonstrably characteristic of the propellant.

Since the primary mode of failure confronting the analyst is propellant fracture, that mode must be considered first. When the flaws are so small that they are not significant, a failure criterion must be evaluated; otherwise, a characteristic strain-energy release rate must be established. Table VI lists the laboratory tests recommended for determining propellant failure properties and relates the tests to the applicable kind of failure. Equipment required to perform most of the recommended tests is almost universally available in propellant company laboratories. Several of the tests can be run in conjunction with those for determining the mechanical properties simply by continuing the application of load until failure is observed.

Slump failures are dependent primarily on mechanical properties and no separate failure tests are recommended. The ignition temperature of a new propellant should be determined

68

Table VI. — Recommended Tests for Failure Properties

Failure criterion	Failure property	Test	Remarks
Ultimate strength (insignificant flaw)	Strain at maximum stress ϵ_m on free propellant surface	Uniaxial tensile or biaxial strip tensile	For long-term low-strain-rate motor loads, use constant strain test until failure. Generate data by continuing the constant-strain-rate tests for mechanical properties until failure.
	Strain at maximum stress ϵ_m on pressurized propellant surface	Pressurized (1) uniaxial tensile or (2) biaxial strip tensile	For use when the dilatational stress is primary compressive; e.g., ignition pressurization.
	Maximum failure stress σ_m, hydrostatic tensile field	Instrumented poker chip (refs. 99 and 102)	For use when dilatational stress is primarily tensile; e.g., near grain/case bond surfaces in ported grains.
	Bondline-termination failure strains (ϵ_m)	Structural test motors (ref. 37)	
Fracture (significant flaw)	The following tests provide data for determining the characteristic strain-energy release rate γ necessary to propagate an existing crack:		
	Cohesive-strain-energy release rate γ_c	Strip biaxial tension (with center precrack)	Reference 104 provides factors necessary to reduce the test results.
	Adhesive-strain-energy release rate γ_a	Pressurized bubble test (ref. 103)	Reference 103 provides analytical solutions for data reduction.
———	Maximum peeling force[1]	Peel test (ref. 7)	

[1]This test is recommended only for quality control and for product and processing selection guides (it does not give quantitative design values).

69

by test, as should the tendency for exothermal chemical reactions near (just below) the ignition temperature. The relationship of autoignition temperature and time of exposure should be defined as described in reference 93.

3.2.4 Property Variability

The statistical variability of the mechanical and failure properties shall be known to the extent necessary for the best possible prediction of the probability of failure.

Statistical variability of the loadings, mechanical properties, and failure properties of solid propellants are inherently large, and they influence the reliability of the calculated margin of safety. For this reason, it is recommended in section 3.5.5 that an estimate of the probable distribution of the margin of safety be computed if the required data are available. Hence, the variabilities of the loadings and properties must be either estimated or established. The variability of the modulus is the basic mechanical property that should be considered. The mean modulus and its variance should be established by linear regression. The procedure for performing the calculations, based on minimizing the sum of the squared errors, is given in reference 24. Judgment of the analyst is required to decide how many replicate tests are required, which moduli representation should be utilized, and how much use should be made of data from previous tests of similar propellants.

The variability of each of the failure properties should be assessed. Regardless of the failure theory employed, it is necessary to have some indication of the statistical variability inherent in its use. To make this assessment economically, assume the form of the statistical distribution. It is recommended, more for expediency than for data fit, that a normal (Gaussian) distribution be assumed. For a normal distribution, a minimum of 10 tests is sufficient to establish a mean $\overline{m}$ and the standard deviation S from the mean:

$$\overline{m} = \frac{1}{n} \sum_{i=1}^{n} m_i \quad \text{(for n tests)} \tag{55}$$

$$S = \left(\frac{1}{n-1} \sum_{i=1}^{n} (m_i - \overline{m})^2 \right)^{1/2} \tag{56}$$

where m_i is the data collected on the ith test.

70

3.2.4.1 PROCESSING EFFECTS

Any significant effects of processing on the propellant properties shall be isolated and evaluated.

Tests should identify and define any significant variations of the propellant properties resulting from production processing as opposed to the variations determined under laboratory conditions. Such tests should evaluate the influence of the processing variables, including batch size and cure conditions (ref. 25). Suitable tests are discussed in references 93 and 105.

3.2.4.2 ENVIRONMENTAL EFFECTS

Any significant effects of the fabrication, storage, test, and service environment on the propellant properties shall be isolated and evaluated.

The most significant of the environmental effects on the propellant are those resulting from aging, humidity, chemical contamination, and radiation (ref. 26). When any of these influences is expected (aging always is), tests of mechanical and failure properties must be repeated after the propellant has been exposed to the damaging environment. Typically, tests of propellant subjected to short periods at high temperature should be used to simulate the properties of propellant aged at normal (storage) temperatures for much longer periods of time.

A method for numerically predicting the accumulation of damage over the stress (strain) history and the resulting effect on the failure level is described in section 2.5.5.

3.3 LOAD ANALYSIS

Grain structural integrity analyses shall identify and consider all specified and predicted loads applied in sequences and combinations anticipated for the motor mission.

A survey of the details of the required loading sequences and combinations should be made early in the grain stress analysis. These requirements are dictated by the motor's function and frequently will be defined by standard specifications such as references 30 and 31. Loads characteristic of the given motor design will come from the system and ballistic analyses (ref. 11). These loads will change as the design evolves and the analyst must stay informed of these changes and the resulting impact on the structural integrity calculations.

3.4 STRESS, STRAIN, AND DISPLACEMENT ANALYSES

The method used for making the stress, strain, and displacement analyses shall be based on the grain geometry, material properties, loading conditions, and the application for which the solution is intended.

Alternate and complementary methods for predicting grain responses can be categorized as analytical, numerical, and experimental. Section 3.4.1 tells how to evaluate property characterization data and the influence the evaluation will have on the methods of analyses to be chosen. The characterization data must be evaluated for evidence of deviations from the key assumptions of classical methods of analyses and for indications of the magnitudes of any deviations. Section 3.4.2 treats the capabilities and limitations of theoretical stress analyses as applied to propellants. Section 3.4.3 guides the use of experimental methods of analyses. Finally, section 3.4.4 points up specific methods of analysis appropriate for particular loads and specific grain geometries.

3.4.1 Deviations from Assumptions

Laboratory characterization data shall be adequate to reveal deviations of the propellant from the assumptions of the analysis to be used.

Test results for the coefficient of thermal expansion of a given propellant over all temperatures to which the grain may be subjected should be examined to determine the variations that can be expected. Plot the change in specimen length (or volume) against temperature, both as the temperature slowly decreases and as it slowly increases. Deviations from a single, straight line (the slope being the coefficient of thermal expansion) give a quantitative measure of the variations of the coefficient of thermal expansion.

Next, as described in section 3.2.2, determine the instantaneous secant moduli at selected strain levels from tests at different rates and temperatures and evaluate the degree of nonlinearity due to strain level. Then check the validity of the assumption of thermorheological simplicity by performing simultaneous straining and cooling tests. Use equation (29) to calculate the forces required to maintain the prescribed strain on the specimen during the test; compare the calculated values with those measured. The differences indicate the extent of the deviation from thermorheological simplicity.

Finally, the results of tests with biaxial strip specimens subjected to similar loading histories should be used to evaluate the influence the state of stress or strain will have on the calculated predictions.

72

3.4.2 Theoretical Stress Analyses

3.4.2.1 ANALYSES BASED ON ELASTICITY

When time effects on propellant properties can be neglected, the relationships between stress and strain shall be based on constitutive equations for elastic materials.

The techniques for obtaining elasticity solutions are divided into two broad classes: analytical and numerical.

Analytical solutions. — During the early part of a motor design and development program, when ballistic requirements and structural integrity are being traded off to arrive at a satisfactory geometric design, rapid decisions based on minimal analyses are required. Closed-form solutions and the related supplementary charts and graphs provide suitable bases for these judgments. Solutions such as those tabulated in tables I, II, and III and equations (35), (36), and (37) can be used to evaluate the influence of the propellant properties, web fraction, and motor case on the grain responses to thermal, acceleration, spin, and pressurization loads.

For isothermal problems, the convolution integral (eq. (18)) should be used to determine the effective stiffnesses or compliances for most histories. For uniform cooling, the instantaneous value of the relaxation modulus $E_{rel}(t/a_T)$ can be used as the elastic modulus (as in eq. (29)). For points in a grain where a linear-strain-rate history can be assumed, the instantaneous values of an integral of the relaxation modulus can be used for the elastic modulus (as shown in eq. (27)).

When grains are only slightly confined or are subjected to loads where deviatoric stresses predominate, the bulk modulus may be assumed to be either infinitely large or constant. When dilatational components are significant, the bulk relaxation modulus (time-dependent) should be incorporated into the calculations, again using the convolution integral to account for the loading history.

The most important use the stress analyst has for the elasticity solutions is in making quasi-elastic calculations. Effective properties for given loading and temperature histories, computed as prescribed in the concluding paragraphs of section 2.4.2.2, should be used with the elastic analyses to calculate the viscoelastic responses at given points in time.

Numerical solutions. — Numerical methods, primarily finite-element stiffness programs for digital computers (refs. 62 and 106 through 109) should be used to (1) make elastic stress-strain analyses of grains with complex geometries or with nonhomogeneous or orthotropic material properties and (2) compute stored energy in support of fracture-mechanics studies.

Numerical solutions are approximate, and care should be taken with the element modeling to hold errors within acceptable limits. Special study must be given to problems involving anisotropic material properties and combined thermal loading situations. The ability to make sound judgments for improving the quality of numerical solutions comes through experience and a detailed understanding of both the theory and the computational routines.

Special rules almost always are dependent on the program being used and on the purposes of the analysis. Some general recommendations for element modeling can be made:

- Intersections at quadrilateral corner nodes should be as nearly perpendicular as possible.

- Lengths of the sides of quadrilateral elements should be as nearly equal as possible. It would be best if any side never exceeded twice the length of another side of the same element, but limited computer storage capacity frequently makes the observation of this rule impractical.

- Element dimensions in the direction of high stress or strain gradients should be kept small, the actual dimension being dependent on the detail and accuracy required of the solutions.

- Abrupt transitions between element sizes should be avoided.

Two-dimensional analyses are adequate for all but the more complex geometries. Two-dimensional programs such as those described in reference 110 can be used for plane-stress, plane-strain, and axially symmetric problems for both compressible and incompressible materials with nonhomogeneous and orthotropic properties. Three-dimensional analyses (ref. 108) should be used only on special problems, because current costs for these analyses are relatively high.

The technique recommended for calculation of total stored energy in a grain as a crack grows is presented in references 88 and 91.

3.4.2.2 ANALYSES BASED ON VISCOELASTICITY

When time effects on propellant properties cannot be neglected, the relationships between stress and strain shall be based on constitutive equations for viscoelastic materials.

It must be realized that the analytical approaches all require propellant behavior that is linearly viscoelastic and, if the temperature varies, thermorheologically simple. To the degree that the properties vary from these assumptions, the predicted stresses or strains will

be in error. Although most propellants exhibit significant variations from these assumptions, the approximate viscoelastic solutions will be adequate for most analyses. For example, for most practical pressurization and acceleration problems (except vibration), the quasi-elastic method (sec. 2.4.2.2) will be adequate. For slowly cooling grains (no thermal gradients in space), an elastic modulus having a value corresponding to t/a_T, taken from a curve like that in figure 3, can be used in equation (29) to calculate the stress. Typically, this method of calculating thermal stresses will be conservative even when space gradients are involved, but this is not a universal rule. Variations of this method accounting for case expansion should be employed in problems involving aerodynamic heating of a grain.

Analytical representations of viscoelastic moduli will be required for some classes of problems. For example, for steady-state vibration problems, the numerical method involving a dynamic modulus E^* evaluated by means of the Prony series should be employed (ref. 76); in problems where the conditions are not compatible with approximate solutions (e.g., wave propagation and shock problems), use the more rigorous convolution integral or Laplace inversion based on either the modified power law or the Prony series.

Four parameters are available for fitting the modified power law (eq. (9)) to the measured relaxation curve: the glassy modulus E_g, the rubbery modulus E_e, the time constant τ_o, and the maximum log/log slope n. First make a log/log plot of the measured (and shifted) $E_{rel}(t/a_T)$ against t/a_T; then pick E_g and E_e. Next measure the maximum log/log slope. This leaves τ_o, which shifts the curve right and left across the time scale, undefined. Choose τ_o to make the transition portion of the curve coincide with the laboratory data.

The modified power law with only four parameters is easier to fit to the test data and to use in many analytical calculations. However, the Prony series has an advantage over the modified power law in that it can be interrelated, term by term, with the real and imaginary parts of a dynamic modulus. Furthermore, it is particularly appropriate for three problem situations noted in section 2.4.2.2.

In fitting the terms of Prony series (eq. (11)) to the measured relaxation data, the first step is to select the values of the τ_k's; one for each decade of time, through the transition region of the relaxation curve, appears to be about optimum. If the spacing is greater (fewer τ_k's), the undulations in the representative curve are too great; if the spacing is less, the task of fitting the individual terms becomes excessive. Then the best E_g's are chosen, using collocation as suggested in reference 41. A better fit often can be achieved by estimating a value for each individual E_g, starting with the rubbery modulus, and then plotting the contribution of the resulting term to the sum of the series. This hand-fitting process permits judgment in the selection of each E_g and prevents oscillations that sometimes occur with the collocation procedure.

3.4.3 Experimental Stress Analyses

Experimental methods shall, as required, provide either primary or supplementary values for stresses, strains, and displacements.

Two basic experimental techniques are capable of providing either primary or supplementary stress analyses. When calculated predictions are believed to be valid, STM's provide a check or verification. But more often the motor geometry or the mechanical properties are such that the calculations must be considered only as approximations. In these instances, instrumented motors subjected to actual test loads should be considered the primary indicators of the stress-strain response. The analytical calculations then can be adjusted to provide the complete stress-strain fields and predict responses to other loads not included in the tests. The basic STM techniques are described in section 3.4.3.1. When visual modeling of the stress-strain field will assist the analyst in presenting his conclusions or recommendations, the photoelasticity (or brittle coating or Moire fringe) techniques are recommended (sec. 3.4.3.2). Because of the high cost of three-dimensional finite-element computations and because new developments in three-dimensional photoelasticity make photoelasticity studies simpler and easier to perform, such studies may be dictated for many three-dimensional problems. For quick preliminary stress calculations, the published strain (stress) concentration factors, derived with parametric studies using photoelasticity, almost always will be helpful.

3.4.3.1 STRUCTURAL TEST MOTORS

A structural test motor shall to the greatest extent possible duplicate the mechanical state in the motor being modeled, and the instrumentation on the test motor shall accurately reflect that state.

Structural test motors should be constructed from actual motor materials, preferably in full-scale configurations. The instrumentation should be carefully chosen and strategically placed so as to be most sensitive to the critical variables to be measured. The benefit of planning to match the instrument characteristics and locations to the quantities to be measured cannot be overemphasized. Reference 9 provides the best guidance available for these preliminary steps.

Selection of instrumentation depends on the specific application, but certain guidelines should be observed: (1) surface-displacement or strain-measuring instruments should be compliant enough that they do not reinforce the propellant; (2) instruments imbedded within the propellant should match propellant stiffness and compressibility, so that they will not disturb the stress-strain field; and (3) through-the-case "stress" transducers should be stiff enough to minimize propellant/gage interaction. It is always best to calibrate the transducer in place within or on the propellant. Propellant deflections resulting from slump

76

and acceleration may be measured using LVDT's and linear potentiometers; in some instances, the deflections may be derived better by integrating the output of accelerometers.

When either the radial or shear stresses adjacent to liner/case bondlines are apt to be large, data from normal or shear stress transducers will be informative (ref. 37). Both mechanical properties and time of failure may be inferred from data from these sensors.

Shown in figure 15 is a schematic of a carefully instrumented STM (ref. 52) employing several types of transducers; not shown are strain gages for monitoring strains on the free propellant surfaces. The complete load environment and history should be carefully monitored and well documented, since propellant behavior usually is sensitive to these factors. Reference 7 describes the use of small STM's for determining the effective Poisson's ratio and the failure strain for the inner port. However, with data from two (or more) such STM's with differing web fractions, both Poisson's ratio and the coefficient of thermal expansion can be evaluated (eq. (30)).

3.4.3.2 PHOTOELASTICITY

Photoelastic studies shall provide visual evidence of the strains and quantitative evaluation of stress-concentration factors.

Preliminary design calculations may be made from the published parametric photoelastic data used in the manner described in references 55 and 58. When a configuration is not axially symmetric, the effects of the grain ends lead to problems involving three-dimensional geometry. End effects may be evaluated approximately by use of the correction curves presented in reference 111, Appendix C.

To evaluate a distinctly different geometry, or to optimize a geometry that has been documented previously, a photoelasticity analysis like that described in reference 48 should be considered. When a three-dimensional stress analysis is required, the photoelastic techniques offer a definite alternative to the expensive finite-element computer programs. It is recommended that this alternative, using either the laser-beam technique or the frozen-stress technique, be considered in such instances.

3.4.4 Analyses for Specific Loads

The method of analysis for a specific load shall be consistent with the grain geometry, the kind of load, and the purpose of the analysis.
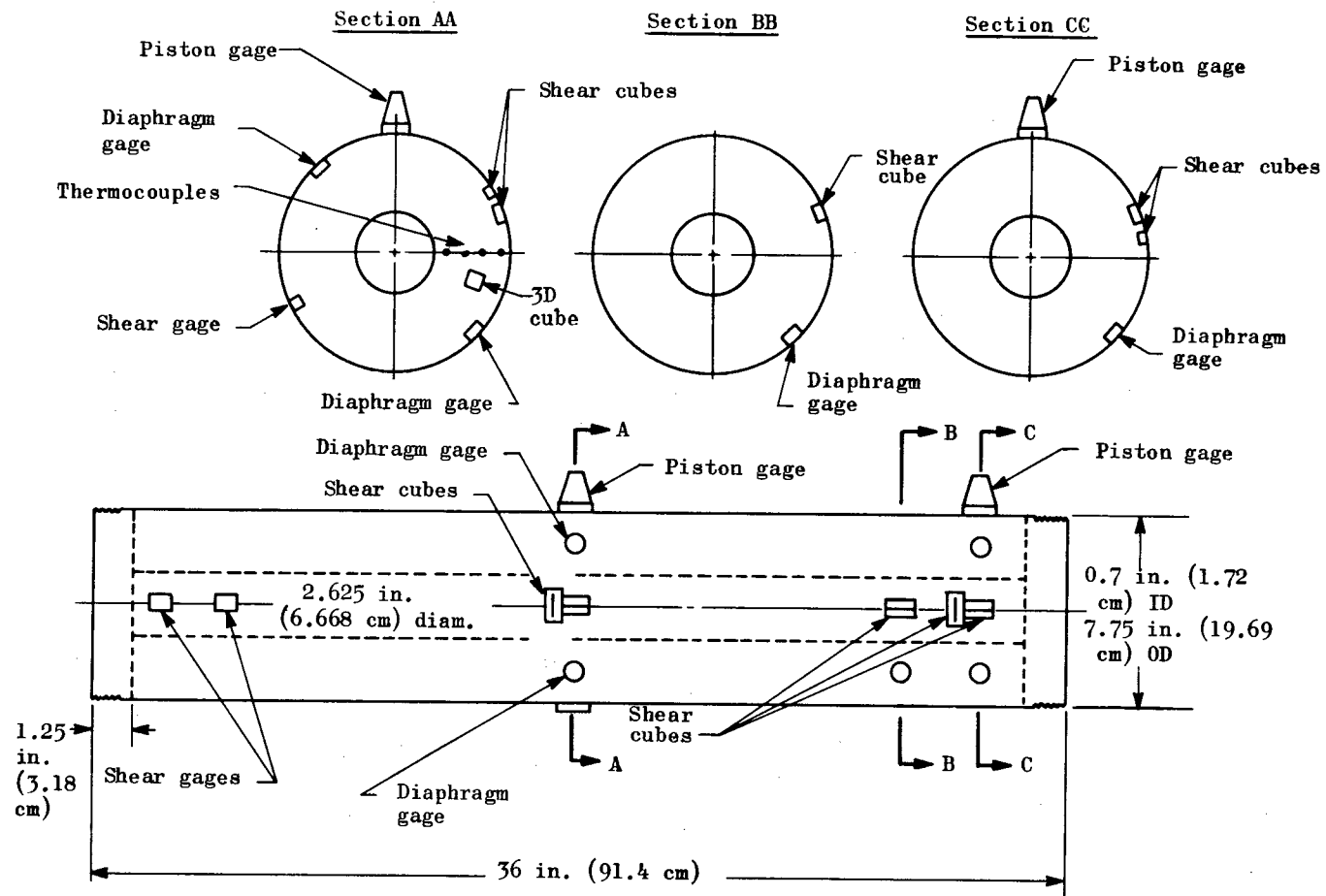
Figure 15. – Schematic of an STM (adapted from ref. 52).

The loads that should be considered are those resulting from uniform temperature changes; pressure loads on the boundaries; and inertial effects resulting from uniform acceleration, shock, spin, and vibration. Combinations of these loads must be taken into account when it is possible the loads will be applied simultaneously. The type of analysis and detail required will depend on the purpose for which the analytical results are to be used. For preliminary design and early geometric studies, "rough cut" calculations are more appropriate; after the design configuration becomes firmer, the detailed analyses are in order. Sections 3.4.4.1 through 3.4.4.3 provide descriptions of the recommended practices for analyzing typical loads on specific types of grain geometries.

3.4.4.1 UNIFORM COOLING

The analysis shall predict displacements, stresses, strains, and local temperatures resulting from thermal loads.

Before thermal stress problems can be analyzed, it must be determined that the assumption of uniform temperatures is realistic. This verification requires either very slow cooling rates or long times at given temperatures.

For preliminary calculations in an elastic analysis, the use of $E_{rel}(t/a_T)$ as an effective modulus (eq. (29)) is certainly satisfactory. Indeed the same effective modulus $E_{rel}(t/a_T)$ determined from simultaneous straining and cooling tests probably gives the most reliable analytical predictions of any method.

The finite-element computer programs should be used for evaluating the stress and strain fields in plane-strain cross sections with irregular ports and in or near axially symmetric features such as conocyls and free ends. For more sophisticated analyses, the convolution integral (eq. (18)) is necessary. Both numerical and analytical methods for its evaluation are available (ref. 47).

When the grain is severely constrained volumetrically (the usual situation for modern case-bonded motors), a finite rather than infinite value for the bulk modulus will result in more accurate predictions. A time-varying bulk modulus is preferable, but such data usually are not available.

As noted in section 3.4.1, an early check on the validity of assuming thermorheological simplicity is to compare the predicted force with the measured force required to strain a laboratory specimen while it is being cooled. If the discrepancies between predicted and measured values are large, alternative methods of analyses must be selected. One alternative is to use instrumented STM's, which may be qualification or preflight test motors. Care must be exercised to ensure that proper calibrations are made, the effects of both grain/gage interaction and temperature being evaluated (ref. 9).

When case heating due to atmospheric drag is a significant load, a simplified, conservative approach is in order. Grain/case interface tractions should be computed with the grain uniformly cool and the case uniformly hot. The hot temperature to assume for the case must be determined by thermal analysis coupled with judgment. The allowable magnitude of the propellant/liner and liner/case tractions must take into account the predicted temperature of the respective bond surface.

3.4.4.2 PRESSURIZATION

The analysis shall predict the mechanical response of the grain to pressurization loads.

Because motors are almost never fired at a strain-free temperature (near cure temperature), the pressurization stresses and strains usually have to be superposed on the thermally induced stresses and strains.

Primarily the quasi-elastic methods should be used. Ascertain by elastic analysis the time-dependent response to a step pressure loading. Use the methods of references 55, 56, and 58 or numerical methods to evaluate the responses of plane-strain or axially symmetric configurations. Then use the convolution integral (eq. (18)) to evaluate at critical points the responses to the anticipated variations in pressure with time. Grain ablation may be safely ignored except for extremely progressive pressure histories.

Because the high pressures inevitably force a metal case to assume the shape it would have without the presence of the grain, no matter what the shape just prior to ignition, a displacement boundary should be used for all pressurization analyses of case-bonded grains. For the more compliant cases, the significance of this approximation should be evaluated.

3.4.4.3 ACCELERATION

3.4.4.3.1 Uniform Acceleration

The analysis shall predict the mechanical response of the grain to uniform accelerations.

The approximate, closed-form, elastic equations in references 3, 63, and 64 should be used for early estimates of the vulnerability of a grain to specified lateral accelerations. If required, more precise finite-element analyses of plane-strain or plane-stress cross sections can be performed. Normally the propellant inertia forces in the transverse direction will be balanced by sinusoidal shear flows along the grain/case interface. If it is necessary to incorporate time effects into the elastic solution, use the convolution integral (eq. (18)).

Examination of the equation for the shear stress σ_{rz} in table III indicates that the shear stresses due to longitudinal accelerations are small except in very large motors or in those subjected to high accelerations (> 25 g). The influence the grain deformations will have on the ballistic performance of the motor also must be considered. The viscoelastic properties of the propellant must be incorporated into the calculations of these deformations; normally this can be done by use of the creep compliance and the convolution integral.

3.4.4.3.2 Shock

Analytical and experimental techniques shall demonstrate that the grain is not susceptible to failure from shock loads.

Judgment and good design practices based on previous experience should be used to arrive at a grain geometry that is not susceptible to failure from shock loads. If values for the stresses, strains, and displacements are necessary, they should be obtained from instrumented structural test motors. Stress calculations for uniform accelerations balanced by concentrated loads at the point of impact will prove useful in identifying potential problem areas due to shock. If a vulnerable geometry cannot be avoided by proper design, instrumented STM's (replicates of the motor geometry) should be tested to determine the local accelerations, stresses, and strains and the corresponding probability of survival. These data may be collected using free-surface strain sensors, bondline stress (force) transducers, LVDT's for displacements, and accelerometers. The calculations based on an equivalent uniform acceleration will assist in choosing locations for instrumentation that will provide the most useful data.

3.4.4.3.3 Vibration

The analysis of grain response to vibration shall determine points of high stress and strain, identify large deflections, and evaluate the possibility of excessive internal heat generation.

The overall response of grain, case, and related hardware to lateral vibrations normally should be analyzed by beam theory, vibrating supports being assumed. Propellant damping and stiffness can be neglected safely in such calculations.

Study the dynamic behavior at critical points within the grain by modeling the grain as a deformable continuum. To make practical problems tractable, use numerical analyses such as those reported in references 75 and 76. Points of high stress and strain concentration should be isolated and the magnitudes considered. The numerical analyses assume both idealized structures and loads (e.g., a perfectly axially symmetric structure with a perfectly axially symmetric oscillatory load). Slight deviations from these idealizations, nearly impossible to avoid in tests, may lead to large discrepancies in the predicted motor responses. Thus, the only satisfactory alternative is to conduct vibration tests using actual

81

motor and grain structure. Current practice is to include vibration tests in the qualification and preflight testing programs. However, the use of instrumentation for monitoring the behavior of the grain during these tests has been neglected to a great extent and the usable data accruing to the stress analyst for improving his predictive capability have been sparse. Therefore, it is recommended that appropriate sensors be installed on all qualification and preflight test motors in locations established by the stress analysis as being the most informative.

To determine the possibility of excess heat buildup, examine carefully points where the strains are apt to be large. To estimate the rate of internal heat generation, use approximate methods similar to those described in references 8 and 70.

Any possibility for rubbing or bumping between parts of the grain or between the grain and other hardware should not be tolerated.

3.4.4.3.4 Spin

The analysis shall predict stresses, strains, and displacements due to centrifugal body forces in grains subjected to spinning.

For the analysis of this kind of load, use the finite-element stiffness programs or, when applicable, the closed-form solutions. Body forces, based on the radial coordinate, angular velocity, and propellant density, should be applied to each element. Viscoelastic effects, normally small except where the case is very compliant, can be incorporated using the quasi-elastic approximation and the convolution integral (sec. 2.4.2.2).

3.5 FAILURE ANALYSES

3.5.1 Cohesive Fracture

The evaluation of the probability of grain survival through the mission shall be based on appropriate fracture criteria.

Cohesive fractures, those occurring within or through a homogeneous material, should be considered from two viewpoints. For fractures where initial flaw size does not influence crack initiation, one of the classical failure criteria should be used. The calculated motor stress or strain states judged to be most severe should be compared with corresponding failure stress or strain states evaluated by tests; recommended tests for several characteristic stress states are prescribed in table VI. For fractures where the geometry (initial flaw) is influential, an energy balance with the characteristic strain-energy release rate should be used.

Generalizations concerning the criterion and test appropriate for a given locale within a motor cannot be made. Usually the failure criterion is selected on the basis of which variable, stress or strain, can be predicted most reliably. However, when the three normal stress components are all in tension, it is recommended that the maximum-principal-stress criterion based on results of triaxial tensile poker chip tests be used. For failures in two-dimensional tensile stress fields, such as those at the inner port surface that result from thermal or spin loads, it is recommended that strip biaxial tensile test data (or appropriate corrections to uniaxial data) be used with the maximum-principal-strain criterion. The maximum-strain criterion also is appropriate when the loading results from pressurization; but the failure should be evaluated using a tension specimen subjected to external pressurization. The same shift factor $\log a_T$ used to effect the time-temperature shift for the mechanical properties also may be used with the failure properties.

For fractures when pre-existing flaws are significant, the rate of change of the strain energy with respect to the new surface area $\partial U/\partial A$ should be calculated with the use of finite-element computer programs. For simple geometries, similar to those for which theoretical solutions exist, the corresponding formulas can be used to great advantage.

The comparison of the response predicted with the response required to cause failure should be expressed in the form of a ratio. This ratio, the damage fraction for the given load, is written

$$D = \frac{\text{Predicted response}}{\text{Failure response}} \tag{57}$$

When more than one load must be considered, whether in sequence or combination (sec. 3.5.5), the damage fraction must be subscripted. For example, D_i indicates the damage fraction due to the ith load.

3.5.2 Adhesive Bond Fracture

The evaluation of the probability of a bond area survival through the mission shall be based on an appropriate fracture criterion.

For points away from flaws or terminations, the maximum-principal-tensile-stress criterion should be used. The maximum principal stress should be determined with bimaterial poker chip specimens carefully instrumented so that the initiation of bond failure can be detected.

To predict flaw growth, use energy-balance calculations (eq. (38)). Energy release rates for potential fracture areas should be calculated by methods given in references 88 and 91 and compared with the fracture energy of the adhesive interface.

83

The damage fraction D is calculated for adhesive bond failures in exactly the same manner as for cohesive failures (eq. (57)).

3.5.3 Excessive Deformation

The evaluation of the probability of failure from grain deformations shall be based on the effect of the deformation on internal ballistics.

Calculated deformations should be evaluated to determine whether motor performance will be impaired (refs. 11 and 12). Other deformations such as those reported by Tormey and Britton (ref. 92) are not currently amenable to analysis, and STM's must be used to obtain experimental data necessary to evaluate the effects.

3.5.4 Autoignition

An evaluation of the probability of failure due to autoignition shall be based on an analysis of the internal heat generation, temperature rise, and time of exposure.

Although no standard procedure seems prevalent in the rocket industry, the following steps suggest an approach for the evaluation of potential autoignition:

(1)   Autoignition temperature should be evaluated as described in reference 93.

(2)   Thermal conductivity for the propellant should be determined as recommended in table IV.

(3)   Heat-transfer analyses sufficient to specify adequate insulation for aeroheating exposures should be performed.

(4)   Heat energy generated within the motor should be estimated by methods described in references 8 and 70.

(5)   Thermal characterization or heat-transfer analysis of the motor should be made to evaluate the rate of heat dissipation and to estimate the maximum temperatures and length of exposure time. This temperature is then compared with the autoignition temperature, accounting for the time of exposure, to find whether the grain is vulnerable to this type of failure. If so, the geometry, dissipative properties, loading magnitudes, or the autoignition temperature must be changed to reduce the vulnerability.

3.5.5 Cumulative Damage and Margin of Safety

The margin of safety shall be based on an evaluation of the accumulated propellant damage.

The linear cumulative damage law should be used to account for sequences and superposition of the responses to loadings when evaluating the margin of safety. Under these conditions, the margin of safety is defined as

$$MS = \frac{1}{\Sigma D_i} - 1 \tag{58}$$

where the damage increments D_i may be either stress or strain ratios. Statistical data on the loads, mechanical properties, or failure properties available to the analyst should be incorporated into the calculations, and the probability of failure should be evaluated as indicated in figure 12.

REFERENCES

1. Williams, M. L.; Blatz, P. J.; and Schapery, R. A.: Fundamental Studies Relating to Systems Analysis of Solid Propellants. Rep. SM 61-5 (AD 256905), Guggenheim Aeron. Lab., Calif. Inst. Tech. (Pasadena, CA), Feb. 1961.

2. Anon.: Engineering Methods for Grain Structural Integrity Analysis. LPC Rep. 578-556-F-3, Lockheed Propulsion Co. (Redlands, CA), May 1963.

3. Hoekle, T.: The Structural Design of Solid Propellant Grains. Rep. 2123, Emerson Electric Co. (St. Louis, MO), Jan. 3, 1967.

4. Bollard, R. J. H.; and Dill, E. H.: Structural Integrity Analysis of Large Solid Propellant Motor Grains. MSC Rep. 65-21-2, Mathematical Sciences Corp. (Seattle, WA), July 1965.

5. Leeming, H.: The Structural Design of a Large Solid Rocket Motor Grain. Lead article in Solid Rocket Structural Integrity Abstracts (SRSIA), vol. 4, no. 3, July 1967, pp. 1-40.

6. Anon.: Study of Mechanical Properties of Solid Rocket Propellants. Rep. AGC-R-0411-10F with Apps. A-G (AD 281 852), Aerojet-General Corp. (Sacramento, CA), Mar. 1962.

7. Anon.: ICRPG Solid Propellant Mechanical Behavior Manual. CPIA Publ. 21, Chem. Prop. Information Agency (Johns Hopkins Univ., Silver Spring, MD), Sept. 1963.

8. Structures & Mechanical Behavior Working Group, CPIA: JANNAF Solid Propellant Structural Integrity Handbook. W. L. Hufferd and J. E. Fitzgerald, eds., CPIA Publ. 230, CPIA, Sept. 1972.

9. Leeming, H.: Techniques for Measuring Stress, Strain and Temperature in Solid Propellant Motors. Spec. Rep. AFRPL-TR-71-131, Lockheed Propulsion Company (Redlands, CA), Nov. 1971.

10. Anon.: Rocket Motor Manual (U). CPIA/M1, CPIA, Mar. 1969.

11. Anon.: Solid Propellant Grain Design and Internal Ballistics. NASA Space Vehicle Design Criteria Monograph. NASA SP-8076, March 1972.

12. Anon.: Solid Rocket Motor Performance Analysis and Prediction. NASA Space Vehicle Design Criteria Monograph, NASA SP-8039, May 1971.

13. Anon.: Coefficient of Linear Thermal Expansion of Plastics, Tests for. ASTM Method D 696-70, Part 27, Am. Soc. for Testing and Materials (Philadelphia, PA), July 1970.

14. Anon.: Mean Specific Heat of Thermal Insulation, Test for. ASTM Method C 351-61 (1967), Part 14, Nov. 1970.

15. Anon.: Thermal Conductivity of Materials by Means of the Guarded Hot Plate, Test for. ASTM Method C 177-63 (1968), Part 14, Nov. 1967 and Part 27, June 1968, p. 1.

16. Anon.: Thermal Conductivity of Materials by Means of the Heat Flow Meter, Test for. ASTM Method C 518-70, Part 14, Nov. 1970.

17. Anon.: Estimating the Thermal Conductivity of Leather with the Cenco-Finch Apparatus, Test for. ASTM Method D 2214, Part 15, Mar. 1970.

18. O'Neill, M. J.: Measurement of Specific Heat Functions by Differential Scanning Calorimetry. J. Anal. Chem, vol. 38(10), Aug. 1966, pp. 1331-1336.

19. Allen, E. L.; and Willoughby, D. A.: A Simple, Accurate Method for Determining Thermal Conductivity of Solid Propellants. Bulletin of 7th Meeting ICRPG Working Group on Mechanical Behavior, CPIA Publ. 177 (AD 393 228), Oct. 1968, pp. 47-53.

20. Farris, R. J.; and Herrmann, L. R.: Applications of Non-Linear Viscoelasticity and Cumulative Damage. Final Report NOSC 1565-26-F, vols. I and II, Aerojet Solid Propulsion Co. (Sacramento, CA), May 1971.

21. Anon.: Rubber Products, Chemical Analysis of. ASTM Method D 297-68, Part 28, July 1970, p. 113.

22. Williams, M. L.; and Jacobs, H. R.: The Study of Crack Criticality in Solid Propellant Rocket Motors. Final Rep. Contract FO-4611-70-c-0006 (Air Force Rocket Prop. Lab.), Univ. of Utah (Salt Lake City, UT), Jan. 1971.

23. Williams, M. L.: Some General Observations on Failure and Fracture. Lead article, SRSIA, vol. 7, no. 1, Jan. 1970, pp. 1-5.

24. Chappell, R. N.; Jenson, F. R.; and Burton, R. W.: Statistical Service Life Prediction: Minuteman Third-Stage Propellant Grain. J. Spacecraft Rockets, vol. 5, no. 1, Jan. 1968, pp. 42-46.

25. Kobbeman, D. D.; and Ratliff, O. D.: Solid Propellant Processing and Influence on Rheological and Mechanical Properties. Bulletin of 26th JANNAF Solid Propulsion Meeting, CPIA Publ. 196, vol. 1, May 1970, pp. 83-111.

26. Fishman, N.: Environmental Effects on Solid Propellants. Lead article, SRSIA, vol. 3, no. 1, Jan. 1966, pp. 1-22.

27. Bills, K. W.; et al.: Development of Criteria for Solid Propellant Screening and Preliminary Engineering Design. Rep. AGC-R-1159-81F, Aerojet-General Corp. (Sacramento, CA), Nov. 1968.

28. Saylak, D.; and Beckwith, S. W.: An Integrated Approach to Solid Propellant Cumulative Damage. Lead article, SRSIA, vol. 6, no. 3, July 1969, pp. 1-79.

29. Fulbright, J. L.; and Miller, W. H.: Failure Analysis of Solid Propellant Grains Based on Dissected Motor Properties. Bulletin of 6th Meeting ICRPG Working Group on Mechanical Behavior, CPIA Publ. 158, vol. I, Oct. 1967, pp. 377-392.

30. Anon.: Environmental Test Methods. Military Standard MIL-STD-810B, June 15, 1967.

31. Anon.: Mechanical Vibrations of Shipboard Equipment. Military Standard MIL-STD-167, Dept. of Defense, Dec. 1954.

32. Silver, I.: Naval Rocket Motors and Structural Integrity Considerations. Proceedings Fourth Symposium on Naval Structural Mechanics (also the International Conference on the Mechanics and Chemistry of Solid Propellants), Purdue Univ. (Lafayette, IN), Apr. 19-21, 1965, pp. 1-18.

33. Wagner, F. R.: Solid Load Definition Study: The Vibration Environment. AFRPL-TR-68-140, UTEC DO 68-055 (AD 851 093), Univ. of Utah (Salt Lake City, UT), Jan. 1969.

34. Schapery, R. A.: A Theory of Nonlinear Thermoviscoelasticity Based on Irreversible Thermodynamics. Proceedings 5th U.S. National Congress Applied Mechanics, Univ. of Minnesota (Minneapolis, MN), June 1966, pp. 511-530.

35. Huang, N. C.; and Lee, E. H.: Nonlinear Viscoelasticity for Short Time Ranges. J. Appl. Mech., Trans. ASME, Series E, vol. 88, 1966, pp. 313-321.

36. Fitzgerald, J. E.; and Farris, R. J.: Characterization and Analysis Methods for Nonlinear Viscoelastic Materials. PROJECT THEMIS Report, UTEC TH 70-204, Univ. of Utah (Salt Lake City, UT), Nov. 1970.

37. Leeming, H.; et al.: Solid Propellant Structural Test Vehicle and Systems Analysis. Final Report AFRPL-TR-70-10, LPC-FR-966-F, Lockheed Propulsion Co. (Redlands, CA), Mar. 1970.

38. Leeming, H.; and Gillis, T. W.: The Mechanics of Highly Filled Propellants. Bulletin of the 4th Meeting ICRPG Working Group on Mechanical Behavior, CPIA Publ. 94u, vol. I (AD 451 712), Oct. 1965, pp. 1-28.

39. Bornstein, G. A.: Transient Thermoviscoelastic Analysis of an Uniaxial Bar. Bulletin of Subcommittee on Numerical Analysis of Solid Rocket Systems, Bulletin of 8th Mechanical Behavior Working Group, vol. 1, CPIA Pub. 193, Mar. 1970.

40. Schapery, R. A.: Approximate Methods of Transform Inversion for Viscoelastic Stress Analysis. Proceedings 4th U.S. National Congress Applied Mechanics, vol. 2, 1962, p. 1075.

41. Schapery, R. A.: A Simple Collocation Method for Fitting Viscoelastic Models to Experimental Data. SM 61-23A, Guggenheim Aeron. Lab., Calif. Inst. Tech. (Pasadena, CA), revised Feb. 1962.

42. Bills, K. W.; Campbell, D. M.; et al: Applications of Cumulative Damage in the Preparation of Parametric Grain Design Curves and the Prediction of Grain Failures on Pressurization. Rep. 1341-26F, vols. I and II, Aerojet-General Corp. (Sacramento, CA), Aug. 1971.

43. Arenz, R. J.: Uniaxial Wave Propagation in Realistic Viscoelastic Materials. J. Appl. Mech., Trans. ASME, Series E, vol. 86, 1964, p. 17.

44. Noel, J. S.; Burton, J. D.; and Harbert, B. C.: Fracture Mechanics Approach to Cumulative Damage. Final Rep. AFRPL-TR-68-132, Rocketdyne, Solid Rocket Division (McGregor, TX), North American Rockwell Corp., Dec. 1968.

45. Farris, R. J.; and Fitzgerald, J. E.: Deficiencies of Viscoelastic Theories as Applied to Solid Propellants. Bulletin JANNAF Mechanical Behavior Working Group, 8th Meeting, 1969, SPIA Pub. no. 193, vol. 1, Mar. 1970, pp. 163-191.

46. Alfrey. T.: Non-homogeneous Stresses in Viscoelastic Media. Quart. Appl. Math., vol. II, no. 2, 1944, pp. 113-119.

47. Schapery, R. A.; Vogt, J. P.; and Clemmer, L. E.: Studies Related to Thermoviscoelastic Stress Analysis of Highly-Loaded Solid Propellant. Final Rep. AFRPL-TR-67-106 (AD 656 347), Purdue Univ., (Lafayette, IN), Feb. 1967.

48. Durelli, A. J.; Experimental Strain and Stress Analysis of Solid Propellant Rocket Motors. Proceedings Fourth Symposium on Naval Structural Mechanics (Intl. Conf. on Mechanics and Chemistry of Solid Propellants), Purdue Univ., (Lafayette, IN), Apr. 19-21, 1965, pp. 381-441.

49. Hetenyi, M.: Handbook of Experimental Stress Analysis. John Wiley & Sons, Inc. (New York), 1950.

50. Hart, W. D.: Moire Method for the Measurement of Strains in Solid Propellants. Bulletin of 3rd Meeting ICRPG Working Group on Mechanical Behavior, CPIA Publ. 61u, vol. 1 (AD 451 712), Oct. 1964, pp. 545-560.

51. Leeming, H.; et al: Solid Propellant Structural Test Vehicle Program. Final Report, May 70 – Sept. 71. AFRPL-TR-72-29 (AD 893 748L), Lockheed Propulsion Co. (Redlands, CA), Apr. 1972.

52. Leeming, H.; et al.: Solid Propellant Structural Test Vehicle, Cumulative Damage, and Systems Analysis. Final Report, AFRPL-TR-68-130, LPC Rep. 831-F, Lockheed Propulsion Co. (Redlands, CA), Oct. 1968.

53. Holman, J. P.: Experimental Methods for Engineers. McGraw-Hill Book Co. (New York), 1966

54. Anon.: Solid Propellant Structural Test Vehicle and Systems Analysis. Rep. R-4418, Rocketdyne, Solid Rocket Division (McGregor, TX), North American Rockwell Corp., Dec. 21, 1966.

55. Parmerter, R. R.; and Fourney, M. E.: Summary of Photoelastic Design Data for Rocket Grain Configurations. Bulletin of 5th Meeting ICRPG Mechanical Behavior Working Group, CPIA Publ. 119, vol. I, Oct. 1966, pp. 393-420.

56. Fourney, M. E.; and Schmidt, W. F.: Extension of Photoelastic Design Data to Case-Bonded Grains and Axisymmetric Geometries. AFSC Rep. AFRPL-TR-68-136, Mathematical Sciences Corp. (Seattle, WA), Sept. 1968.

57. Becker, E. B.; and Brisbane, J. J.: The Effect of Propellant-Case Interaction on Stress/Strain Concentration Factors in Solid Propellant Rocket Grains. Bulletin of 4th ICRPG Mechanical Behavior Working Group, CPIA Publ. 94u, vol. I (AD 472 050), Oct. 1965, pp. 509-516.

58. Sampson, R. C.; and Campbell, D. M.: Contribution of Photoelasticity to Evaluation of Solid Propellant Motor Integrity. J. Spacecraft Rockets, vol. 3, no. 4, Apr. 1966, pp. 477-483.

59. Weller, R.: Three-Dimensional Photoelasticity Using Scattered Light. J. Appl. Phys., vol. 12, no. 8, Aug. 1941, pp. 610-616.

60. Braswell, D. W.; Ranson, W. F.; and Swinson, W. F.: Scattered Light Photoelastic Thermal Stress Analysis of a Solid Propellant Rocket Motor. J. Spacecraft Rockets, vol. 5, no. 12, Dec. 1968, pp. 1411-1416.

61. Fitzgerald, J. E.: Propellant Grain Structural Integrity Problems: Engineering Status. Lead article, SRSIA, vol. 2, no. 3, July 1965, pp. 1-44.

62. Anderson, J. McKay: A Review of the Finite Element Stiffness Method As Applied to Propellant Grain Stress Analysis. Lead article, SRSIA, vol. 6, no. 4, Oct. 1969, pp. 1-54.

63. Parmerter, R. R.: Stresses in Case-bonded Solid-propellant Rocket Motors under Transverse Body-force Loading. Experimental Mechanics, vol. 9, no. 12, Dec. 1969, pp. 571-576.

64. Gillis, G. F.: Elastic Stresses and Displacements Induced in Solid Propellant Rocket Motors by Transverse Gravity Forces. Rep. P-62-13, Quart. Rep. Engrg. Res., Rohm and Haas (Huntsville, AL), July 1962.

65. Livi, G. D.; and Poesch, J. G.: Stress Analysis of the Solid Propellant in Sprint Rocket Motors (U). Bulletin of 7th Meeting ICRPG Mechanical Behavior Working Group, CPIA Publ. 117 (AD 393 228), Oct. 1968, pp. 103-117. (Confidential)

66. Lindsey, G.; and Williams, M. L.: The Structural Integrity of an Ablating Rocket Subjected to Axial Acceleration. AIAA J., vol. 3, no. 2, Feb. 1965, pp. 258-262.

67. Parr, C. H.: Deformations and Stresses in Axially Accelerated Case-Bonded Solid Propellant Grains of Finite Length. Rep. P-62-27, Quart. Rep. Engrg. Res., Rohm and Haas Co. (Huntsville, AL), Apr. 1963.

68. Achenback, J. D.: Dynamic Response Problems of Solid Propellant Rockets. Lead article, SRSIA, vol. 5, no. 1, Jan. 1968, pp. 1-34.

69. Baltrukonis, J. H.: The Dynamics of Solid Propellant Rocket Motors. Mechanics and Chemistry of Solid Propellants (A. C. Eringen, H. Liebowitz, S. L. Loh, and J. M. Crowley, eds.), Pergamon Press (New York, NY), 1967, pp. 297-332.

70. Anon.: Mk 38 Mod O Solid Propellant Rocket Motor Product Improvement Program Summary Report. Rep. R-4282, Rocketdyne, Solid Rocket Division (McGregor, TX), North American Rockwell Corp., May 1964.

71. Cantey, Dalton: Solid Propellant Structural Integrity Investigation. LPC-R-618-F, vol. I, Lockheed Propulsion Co. (Redlands, CA), Apr. 17, 1964.

72. Volterra, E.; and Zachmanoglow, E. C.: Dynamics of Vibrations. Charles E. Merrill Books, Inc. (Columbus, OH), 1965.

73. Gottenburg, W. G.: Experimental Study of the Vibrations of a Circular Cylindrical Shell. J. Acoust. Soc. Am., vol. 32, no. 8, Aug. 1960, p. 1002.

74. Leadbetter, S. A.; Alley, V. A.; Herr, R. W.; and Gerringer, A. H.: An Experimental and Analytical Investigation of the Natural Frequencies and Mode Shapes of a Four-Stage Solid Propellant Rocket Vehicle. NASA TN D-1354, 1962.

75. Baker, W. E.; and Daly, J. M.: Dynamic Analysis of Solid Propellant Grains Using the Finite Element Method (Direct Stiffness Method). Bulletin of 5th Meeting ICRPG Mechanical Behavior Working Group, CPIA Publ. 119, vol. I, Oct. 1966, pp. 319-338.

76. Anderson, J. M.: Adaptation of the Finite-Element Stiffness Method to Viscoelastic Steady-State Sinusoidal Vibration Solutions. Bulletin of 5th Meeting ICRPG Mechanical Behavior Working Group, CPIA Publ. 119, vol. I, Oct. 1966, pp. 297-318.

77. Schapery, R. A.: Thermomechanical Behavior of Viscoelastic Media with Variable Properties Subjected to Cyclic Loading. J. Appl. Mech., Trans. ASME, Series E, vol. 87, 1965, pp. 611-619.

78. Schapery, R. A.; and Cantey, D. E.: Thermomechanical Response Studies of Solid Propellants Subjected to Cyclic and Random Loading. AIAA J., vol. 4, no. 2, Feb. 1966, pp. 255-264.

79. Crandall, S. H.; and Mark, W. D.: Random Vibration in Mechanical Systems. Academic Press (New York, NY), 1963.

80. Landel, R. F.: Rupture of Elastomers and Propellants. SRSIA, vol. 2, no. 1, Jan. 1965, pp. 1-22.

81. Jones, J. W.; and Knauss, W. G.: Propellant Failure Criteria. Paper 65-157, AIAA 6th Solid Propellant Rocket Conference (Washington, DC), Feb. 1965.

82. Anderson, G. P.; and Bennett, S. J.: Fracture of Polymeric Materials in Multiaxial Stress Fields, Tech. Rep. AFRPL-TR-70-36, TCC Rep. 0370-27546, Thiokol Chemical Corp., (Brigham City, UT), Mar. 1970.

83. Majerus, J. N.; Briar, H. P.; and Wiegand, J. H.: Behavior and Variability of Solid Propellants and Criteria for Failure and for Rejection. J. Spacecraft Rockets, vol. 2, no. 6, Nov.-Dec. 1965, pp. 833-845.

84. Smith, T. L.: Characterization by a Time and Temperature Independent Failure Envelope. J. Polymer Sci., Part A, vol. 1, no. 12, Dec. 1963, pp. 3597-3615.

85. Landel, R. F.; and Smith, T. L.: Viscoelastic Properties of Rubber Like Composite Propellants and Filled Elastomers. J. Am. Rocket Soc., vol. 31, no. 5, May 1961, pp. 599-608.

86. Williams, M. L.: Stress Singularities, Adhesion, and Fracture. Proc. 5th U.S. Congress Appl. Mech., June 1966, pp. 451-462.

87. Burton, J. D.; and Harbert, B. C.: Application of Fracture Mechanics to Predicting Failures in Solid Propellants, Final Report — Period 1 Jan. 1969 to 27 Feb. 1970. Rep. R-4608, AFRPL-TR-70-62 (AD 870 735), Rocketdyne, Solid Rocket Division (McGregor, TX), North American Rockwell Corp., May 1970.

88. Noel, J. S.; and Webb, L. D.: The Role of Fracture Mechanics in the Design of Optimum Grain-Case Terminations. Bulletin of 5th Meeting ICRPG Mechanical Behavior Working Group, CPIA Publ. 119, vol. I, Oct. 1966, pp. 351-363.

89. Anon.: The Determination of the Optimum Length of End Relief for Case Bonded Solid Propellant Rocket Motors. Rep. R-4376, Rocketdyne, Solid Rocket Division (McGregor, TX), North American Rockwell Corp., May 2, 1966.

90. Bowie, O. L.: Analysis of an Infinite Plate Containing Radial Cracks Originating from the Boundary of an Internal Circular Hole. J. Math. and Phys., vol. 35, 1956, pp. 60-71.

91. Deverall, L. I.; and Lindsey, G. H.: A Comparison of Numerical Methods for Determining Stress Intensity Factors. JANNAF Mechanical Behavior Working Group 8th Meeting 1969, CPIA Publ. 193, vol. 1, Mar. 1970, pp. 559-565.

92. Tormey, J. F.; and Britton, S. C.: Effect of Cyclic Loading on Solid Propellant Grain Structures. AIAA J., vol. 12, no. 8, Aug. 1963, pp. 1763-1770.

93. Anon.: Solid Propellant Selection and Characterization. NASA Space Vehicle Design Criteria Monograph, NASA SP-8064, June 1971.

94. Bills, K. W., Jr.; Campbell, D. M.; Sampson, R. C.; and Steele, R. D.: Failures in Grains Exposed to Rapid Changes of Environmental Temperatures (An Application of Linear Cumulative Damage Concepts). Final Rep. AGC-TR-1236-81F, Aerojet-General Corp. (Sacramento, CA), Sept. 1969.

95. Miner, M. A.: Cumulative Damage in Fatigue. J. Appl. Mech., Trans. ASME, Series E, vol. 67, 1945, p. A-159.

96. Robinson, C. H.; Graham, P. H.; and Moore, F. C.: Effect of Grain End Shape on Stress Concentrations at the Case-Propellant Interface. Final Rep. AFRPL-TR-69-124, vol. I (AD 854 935), Atlantic Research Corp. (Alexandria, VA), May 1969.

97. Schapery, R. A.: Approximate Methods for Thermoviscoelastic Characterization and Analysis of Nonlinear Solid Rocket Grains. AIAA Paper 68-520, ICRPG/AIAA 3rd Solid Propulsion Conference (Atlantic City, NJ), June 4-6, 1968.

98. Mullins, L. J.: Effect of Stretching on the Properties of Rubber. J. Rubber Res., vol. 16, no. 12, Dec. 1947, pp. 275-289.

99. Harbert, B. C.: Triaxial Testing of Solid Propellants. Bulletin of 4th Meeting ICRPG Working Group on Mechanical Behavior, CPIA Publ. 94u, vol. I (AD 472 050), Oct. 1965, pp. 217-234.

100. Williams, M. L.; and Schapery, R. A.: Studies of Viscoelastic Media. Rep. ARL 62-366, Aeron. Res. Lab. (Dayton, OH), 1962.

101. Cost, T. L.; and Parr, C. H.: Analysis of the Biaxial Strip and Shear Lap Tests for Solid Propellant Characterization. Rep. S-73 (AD 813 719), Rohm and Haas Co. (Huntsville, AL), May 12, 1967.

102. Lindsey, G. H.; Shapery, R. A.; Williams, M. L.; and Zak, A. R.: The Triaxial Tension Failure of Viscoelastic Materials. Rep. ARL 63-152, Aeron. Res. Lab. (Dayton, OH), Sept. 1963.

103. Burton, J. D.; Jones, W. B.; and Williams, M. L.: Theoretical and Experimental Treatment of Fracture in an Adhesive Interlayer. Trans. Soc. Rheology, vol. 15, no. 1, 1971, pp. 39-50.

104. Bennett, S. J.; Anderson, G. P.; and Williams, M. L.: The Time Dependence of Surface Energy in Cohesive Fracture. J. Appl. Polymer Sci., vol. 14, no. 3, Mar. 1970, pp. 735-745.

105. Anon.: Solid Propellant Processing Factors in Rocket Motor Design. NASA Space Vehicle Design Criteria Monograph, NASA SP-8075, Oct. 1971.

106. Herrmann, L. R.: Elasticity Equations for Incompressible and Nearly Incompressible Materials by a Variational Theorem. AIAA J., vol. 3, no. 10, Oct. 1965, pp. 1896-1900.

107. Wilson, E. L.; and Jones, R. M.: Finite Element Stress Analysis of Two-Dimensional Structures with Orthotropic Temperature-Dependent Material Properties. Rep. SR 8111-300.2, Aerospace Corp. (San Bernardino, CA), Aug. 1968.

108. Rashid, Y.: Solution of Elasto-Static Boundary Value Problems by Finite Element Methods. PhD. Thesis, Dept. Civil Engrg., Univ. of Calif. (Berkeley, CA), Sept. 1964.

109. Herrmann, L. R.; and Peterson, F. E.: A Numerical Procedure for Viscoelastic Stress Analysis. Bulletin of 7th Meeting ICRPG Working Group on Mechanical Behavior, CPIA Publ. 177, Nov. 1968, pp.155-166.

110. Becker, E. B.; and Brisbane, J. J.: Application of the Finite Element Method to Stress Analysis of Solid Propellant Rocket Grains. Rep. S-76, Rohm and Haas Co., vol. I (AD 474031), Nov. 1965; vol. II, part 1 (AD 476515); vol. II part 2 (AD 476735), Jan. 1966.

111. Fitzgerald, J. E.; and Hufferd, W. L.: Handbook for the Engineering Structural Analysis of Solid Propellants. CPIA Publ. 214, CPIA, May 1971.

GLOSSARY

Symbol	Definition
A	area
a	(1) inside radius of cylindrical propellant grain (2) half-height (length) of biaxial test specimen
a_T	time-temperature shift factor, usually used as log a_T
B	slope of stress vs time-to-failure curve
b	(1) outside radius of cylindrical propellant grain (2) half-width of biaxial test specimen
C	(1) stress-concentration factor (2) arbitrary constant in equations (43) and (44)
c	(1) mean specific heat (2) flaw size (= ½ the characteristic dimension of a flaw)
c_{cr}	smallest dimension c that leads to a fracture-type failure
D	damage fraction
D_{crp}	tensile creep compliance
D_e	rubbery (long-term) compliance
D_g	glassy (instantaneous) compliance
D_k	k^{th} constant in Prony series representation of creep compliance
D_s	secant compliance
E	tensile modulus of elasticity
E*	dynamic tensile modulus, $E^* = E' + iE''$
E'	real part of E* (storage modulus)
E''	imaginary part of E* (loss modulus)
E_e	rubbery (long-time) modulus

95

Symbol	Definition
E_g	glassy (instantaneous) modulus
E_k	k^{th} constant in Prony series representation of relaxation modulus
E_{rel}	tensile relaxation modulus
E_s	secant tensile modulus of elasticity
e	sum of normal strains (change in volume per unit volume)
e_{ij}	components of the deviatoric strain tensor
F	force
$f(R)$	distribution of actual grain responses
G	shear modulus of elasticity
$G*$	dynamic shear modulus, $G* = G' + iG''$
G', G''	real and imaginary components of dynamic shear modulus
$G(\omega)$	input power spectral density
$G(R)$	cumulative probability of allowable grain responses
G_{rel}	shear relaxation modulus
$H(\omega)$	ratio of steady-state response amplitude to input amplitude
H_s	unit step function
h	thickness
I	input
I_k	k^{th} step input
I_o	constant input amplitude
I_s	step input
i	(1) imaginary number, $\sqrt{-1}$ (2) index number of a term in a series

96

Symbol	Definition
K	bulk modulus of elasticity
k	(1) thermal conductivity (2) index number of a term in a series (3) empirical constant
L	length
L_o	initial length
MS	margin of safety
$\bar{m}$	mean
m_i	datum collected on the ith test
N	number of g's of acceleration
N_k	number of cycles required for failure at the kth load level
n	(1) number of terms in a series (2) slope of the curve of a log/log plot of relaxation modulus vs time
n'	slope of the curve of a log/log plot of creep compliance vs time
n_k	actual number of cycles at the kth load level
P	probability distribution
P_f	probability of failure
p	(1) pressure (2) variable corresponding to time when transformed to Laplace plane
q	energy generated per cycle
R	calculated response
$\bar{R}_a$	average allowable response (e.g., failure stress or strain)
R_o	amplitude of constant response to a constant input
R_s	response to a unit step function
$\bar{R}_s$	average actual response

97

Symbol	Definition
$<R>$	root mean square of response to random vibrations
r, θ, z	cylindrical coordinates
S	standard deviation from the mean
STM	structural test motor
s_{ij}	components of the deviatoric stress tensor
T	temperature
T_g	glassy transition temperature
t	time
t/a_T	reduced time
$\overline{t_f}$	mean time to failure at σ_t, min
t_{fi}	mean time to failure for the ith stress level
t_o	time to failure at σ_{ot}, min
U	strain energy
U_o	strain-energy density
u, v, w	components of displacement in the r, θ, z directions, respectively
v	volume
x, y, z	Cartesian coordinates
( )	indicates the associated variable is a function of the parameter in the ( ).
α	coefficient of thermal expansion
γ	characteristic strain-energy release rate
γ_a	adhesive-strain-energy release rate
γ_c	cohesive-strain-energy release rate

98

Symbol	Definition
Δ	incremental change in a variable
δ	arctan (G''/G')
δ_{ij}	Kronecker delta: $\delta_{ij} = 0, i \neq j$ $\qquad\qquad\qquad = 1, i = j$
ϵ	strain
ϵ^*	steady-state cyclic strain
ϵ_{av}	average strain
ϵ_b	strain at break
ϵ_{fi}	failure strain at the ith rate and temperature
ϵ_{ii}	sum of the normal strains
ϵ_{ij}	components of the strain tensor
ϵ_m	strain at maximum stress
ϵ_o	amplitude of shear strain
$\dot{\epsilon}_o$	constant strain rate
$\epsilon_r, \epsilon_\theta, \epsilon_z$	normal strain components, cylindrical coordinates
$\epsilon_x, \epsilon_y, \epsilon_z$	normal strain components, Cartesian coordinates
ζ	reduced time variable accounting for varying temperature-time shift
Θ	sum of normal stress components
λ	Lamé's constant
ν	Poisson's ratio
ρ	density
Σ	summation symbol
σ	normal stress

99

Symbol	Definition
σ_b	stress at break
σ_{cr}	fracture stress
σ_i	i^{th} stress component
σ_{ii}	sum of the normal stresses
σ_{ij}	components of the stress tensor
σ_m	maximum stress
σ_o	(1) constant stress (2) amplitude of the shear stress
$\sigma_r, \sigma_\theta, \sigma_z$	normal stress components, cylindrical coordinates
$\sigma_x, \sigma_y, \sigma_z$	normal stress components, Cartesian coordinates
τ	dummy time variable
τ_k	k^{th} time constant in Prony series representation
τ_o	time constant in modified-power-law representation of relaxation
τ'_o	time constant in modified-power-law representation of compliance
χ	thermal diffusivity
ω	frequency, rad/min or rad/sec

Abbreviations	Identification
AFARL	Air Force Aerodynamic Research Laboratory
AFRPL	Air Force Rocket Propulsion Laboratory
AIAA	American Institute of Aeronautics and Astronautics
ARPA	Advanced Research Projects Agency
ASME	American Society of Mechanical Engineers
ASTM	American Society for Testing and Materials

Abbreviations	Identification
CPIA	Chemical Propulsion Information Agency
ICRPG	Interagency Chemical Rocket Propulsion Group
JANAF	Joint Army-Navy-Air Force
JANAFAN	JANAF-ARPA-NASA
JANNAF	Joint Army-Navy-NASA-Air Force
NOSC	Naval Ordnance Systems Command
SPIA	Solid Propellant Information Agency
SRSIA	Solid Rocket Structural Integrity Abstracts

NASA SPACE VEHICLE DESIGN CRITERIA
MONOGRAPHS ISSUED TO DATE

ENVIRONMENT

SP-8005	Solar Electromagnetic Radiation, Revised May 1971
SP-8010	Models of Mars Atmosphere (1967), May 1968
SP-8011	Models of Venus Atmosphere (1972), Revised September 1972
SP-8013	Meteoroid Environment Model—1969 (Near Earth to Lunar Surface), March 1969
SP-8017	Magnetic Fields—Earth and Extraterrestrial, March 1969
SP-8020	Mars Surface Models (1968), May 1969
SP-8021	Models of Earth's Atmosphere (90 to 2500 km), Revised March 1973
SP-8023	Lunar Surface Models, May 1969
SP-8037	Assessment and Control of Spacecraft Magnetic Fields, September 1970
SP-8038	Meteoroid Environment Model—1970 (Interplanetary and Planetary), October 1970
SP-8049	The Earth's Ionosphere, March 1971
SP-8067	Earth Albedo and Emitted Radiation, July 1971
SP-8069	The Planet Jupiter (1970), December 1971
SP-8084	Surface Atmospheric Extremes (Launch and Transportation Areas), May 1972
SP-8085	The Planet Mercury (1971), March 1972
SP-8091	The Planet Saturn (1970), June 1972
SP-8092	Assessment and Control of Spacecraft Electromagnetic Interference, June 1972
SP-8103	The Planets Uranus, Neptune, and Pluto (1971), November 1972
SP-8105	Spacecraft Thermal Control, May 1973

STRUCTURES

SP-8001	Buffeting During Atmospheric Ascent, Revised November 1970
SP-8002	Flight-Loads Measurements During Launch and Exit, December 1964
SP-8003	Flutter, Buzz, and Divergence, July 1964
SP-8004	Panel Flutter, Revised June 1972
SP-8006	Local Steady Aerodynamic Loads During Launch and Exit, May 1965
SP-8007	Buckling of Thin-Walled Circular Cylinders, Revised August 1968
SP-8008	Prelaunch Ground Wind Loads, November 1965
SP-8009	Propellant Slosh Loads, August 1968
SP-8012	Natural Vibration Modal Analysis, September 1968
SP-8014	Entry Thermal Protection, August 1968
SP-8019	Buckling of Thin-Walled Truncated Cones, September 1968
SP-8022	Staging Loads, February 1969
SP-8029	Aerodynamic and Rocket-Exhaust Heating During Launch and Ascent May 1969
SP-8030	Transient Loads From Thrust Excitation, February 1969
SP-8031	Slosh Suppression, May 1969
SP-8032	Buckling of Thin-Walled Doubly Curved Shells, August 1969
SP-8035	Wind Loads During Ascent, June 1970
SP-8040	Fracture Control of Metallic Pressure Vessels, May 1970
SP-8042	Meteoroid Damage Assessment, May 1970
SP-8043	Design-Development Testing, May 1970
SP-8044	Qualification Testing, May 1970
SP-8045	Acceptance Testing, April 1970

SP-8046	Landing Impact Attenuation for Non-Surface-Planing Landers, April 1970
SP-8050	Structural Vibration Prediction, June 1970
SP-8053	Nuclear and Space Radiation Effects on Materials, June 1970
SP-8054	Space Radiation Protection, June 1970
SP-8055	Prevention of Coupled Structure-Propulsion Instability (Pogo), October 1970
SP-8056	Flight Separation Mechanisms, October 1970
SP-8057	Structural Design Criteria Applicable to a Space Shuttle, Revised March 1972
SP-8060	Compartment Venting, November 1970
SP-8061	Interaction with Umbilicals and Launch Stand, August 1970
SP-8062	Entry Gasdynamic Heating, January 1971
SP-8063	Lubrication, Friction, and Wear, June 1971
SP-8066	Deployable Aerodynamic Deceleration Systems, June 1971
SP-8068	Buckling Strength of Structural Plates, June 1971
SP-8072	Acoustic Loads Generated by the Propulsion System, June 1971
SP-8077	Transportation and Handling Loads, September 1971
SP-8079	Structural Interaction with Control Systems, November 1971
SP-8082	Stress-Corrosion Cracking in Metals, August 1971
SP-8083	Discontinuity Stresses in Metallic Pressure Vessels, November 1971
SP-8095	Preliminary Criteria for the Fracture Control of Space Shuttle Structures, June 1971
SP-8099	Combining Ascent Loads, May 1972
SP-8104	Structural Interaction With Transportation and Handling Systems, January 1973

GUIDANCE AND CONTROL

SP-8015   Guidance and Navigation for Entry Vehicles, November 1968

SP-8016   Effects of Structural Flexibility on Spacecraft Control Systems, April 1969

SP-8018   Spacecraft Magnetic Torques, March 1969

SP-8024   Spacecraft Gravitational Torques, May 1969

SP-8026   Spacecraft Star Trackers, July 1970

SP-8027   Spacecraft Radiation Torques, October 1969

SP-8028   Entry Vehicle Control, November 1969

SP-8033   Spacecraft Earth Horizon Sensors, December 1969

SP-8034   Spacecraft Mass Expulsion Torques, December 1969

SP-8036   Effects of Structural Flexibility on Launch Vehicle Control Systems, February 1970

SP-8047   Spacecraft Sun Sensors, June 1970

SP-8058   Spacecraft Aerodynamic Torques, January 1971

SP-8059   Spacecraft Attitude Control During Thrusting Maneuvers, February 1971

SP-8065   Tubular Spacecraft Booms (Extendible, Reel Stored), February 1971

SP-8070   Spaceborne Digital Computer Systems, March 1971

SP-8071   Passive Gravity-Gradient Libration Dampers, February 1971

SP-8074   Spacecraft Solar Cell Arrays, May 1971

SP-8078   Spaceborne Electronic Imaging Systems, June 1971

SP-8086   Space Vehicle Displays Design Criteria, March 1972

SP-8096   Space Vehicle Gyroscope Sensor Applications, October 1972

SP-8098   Effects of Structural Flexibility on Entry Vehicle Control Systems, June 1972

SP-8102   Space Vehicle Accelerometer Applications, December 1972

CHEMICAL PROPULSION

SP-8087	Liquid Rocket Engine Fluid-Cooled Combustion Chambers, April 1972
SP-8081	Liquid Propellant Gas Generators, March 1972
SP-8052	Liquid Rocket Engine Turbopump Inducers, May 1971
SP-8048	Liquid Rocket Engine Turbopump Bearings, March 1971
SP-8101	Liquid Rocket Engine Turbopump Shafts and Couplings, September 1972
SP-8090	Liquid Rocket Actuators and Operators, May 1973
SP-8080	Liquid Rocket Pressure Regulators, Relief Valves, Check Valves, Burst Disks, and Explosive Valves, March 1973
SP-8064	Solid Propellant Selection and Characterization, June 1971
SP-8075	Solid Propellant Processing Factors in Rocket Motor Design, October 1971
SP-8076	Solid Propellant Grain Design and Internal Ballistics, March 1972
SP-8039	Solid Rocket Motor Performance Analysis and Prediction, May 1971
SP-8051	Solid Rocket Motor Igniters, March 1971
SP-8025	Solid Rocket Motor Metal Cases, April 1970
SP-8041	Captive-Fired Testing of Solid Rocket Motors, March 1971